

Natural Product Studies of Marine Organisms from the Western Atlantic Ocean

by

Andrew James Hall

*A Dissertation* Submitted to the Faculty of

The Charles E. Schmidt College of Science

In Partial Fulfillment of the Requirements for the Degree of

Doctor of Philosophy

Florida Atlantic University

Boca Raton, FL

August 2016

Copyright 2016 by Andrew Hall

Natural Product Studies of Marine Organisms from the Western Atlantic Ocean

by

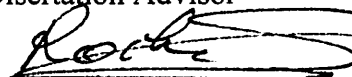
Andrew James Hall

This dissertation was prepared under the direction of the candidate's dissertation advisor, Dr. Lyndon West, Department of Chemistry and Biochemistry, and has been approved by the members of his supervisory committee. It was submitted to the faculty of the Charles E. Schmidt College of Science and was accepted in partial fulfillment of the requirements for the degree of Doctor of Philosophy.

SUPERVISORY COMMITTEE:



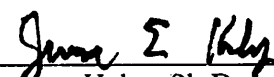
Lyndon West, Ph.D.  
Dissertation Advisor



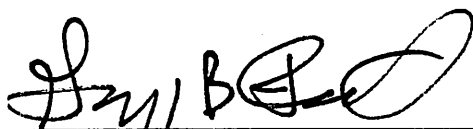
Stéphane P. Roche, Ph.D.



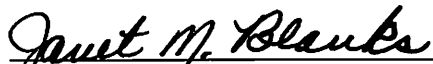
Ken Dawson-Scully, Ph.D.




Jerome Haky, Ph.D.



Gregg B. Fields, Ph.D.  
Chair, Department of Chemistry and  
Biochemistry



Janet M. Blanks, Ph.D.  
Interim Dean, Charles E. Schmidt College of  
Science



Deborah L. Floyd, Ed.D.  
Dean, Graduate College

07/20/2016  
Date

## Acknowledgements

For my father and mother; who have always served as an inspiration, have always stood by me and have supported me no matter the challenges. They are my rocks and I shall be forever grateful. I hope, one day, to one day become as compassionate and as wise as them.

For my brothers: Jon and Phil, who have always served as inspiration; for their intellect, immense kindness and ability to overcome so many obstacles. You remind me every day that the world is full of sweet adventures.

To my friends who I much consider my brothers Dan, Ford, Kyle, Andy, Ross, Bobby, Cliff, and Dr. Evan J Hasson™ who have been there to support me through this whole process. Your continued encouragement and support have stayed me through this journey. You have all shaped me into who I am today and I would have been unable to complete this journey without you. That said, without you I may have completed the journey two years earlier. I truly want to thank all of you from the bottom of my heart and will be forever in your debt.

For Joseph Maese, who truly showed me the meaning of generosity and humbleness; and without whom I would likely not be here. I thank him most of all for his support and encouragement and for demonstrating the true meaning of family. R.I.P. Uncle Joe.

I would like to thank Dr. West for the years put in for this degree and his contributions to its successful completion. I would also like to thank my committee

members, in particular Dr. Stéphane Roche without whose influence and encouragement I would neither be where I am, nor what I shall become. You have all truly shown me what it means to work hard and what true achievement requires.

In particular this work has taught me the true meaning of “Steels Forged Under Fire.” The path to true achievement is neither linear nor easy. My endeavors have taught me to never give up, but rather to keep pushing forward and the importance of getting back up until you succeed.

## Abstract

Author: Andrew Hall

Title: Natural Product Studies of Marine Organisms from the Western Atlantic

Institution: Florida Atlantic University

Dissertation Advisor: Dr. Lyndon West

Degree: Doctor of Philosophy

Year: 2016

The projects described in this dissertation are focused on compounds derived from marine organisms collected from the western Atlantic marine environment.

Chapter 1 provides an introduction to the study of natural products chemistry, marine natural products, and overview of the research undertaken from natural product chemists.

Chapter 2 describes the isolation and structure elucidation of a series of rare diterpenoids from the gorgonian *Briareum asbestinum*, together with their conformational analysis and biosynthetic interconversions. These rare diterpenes from *Briareum asbestinum* are linked by an unusual transannular oxa-6 $\pi$  electrocyclization which is described in detail and this work demonstrates the biomimetic hemisynthesis of briareolate esters L (**19**) to B (**22**) achieved via an intermediary, briareolate ester G (**2**), through a controlled set of photoinduced isomerizations and a unique photochromic transannular oxa-6 $\pi$  electrocyclization. This work focuses largely on the mechanistic

understanding of the photochemical production of these briarane diterpenoids and illustrates a unique UVA/UVC, photochromic switch which induces a transannular oxa- $6\pi$  electrocyclization.

Chapter 3 describes the assay-guided isolation of marine antioxidants. This chapter focuses on the screening of marine organism extracts using the Ferric Reducing Antioxidant Power (FRAP) assay for antioxidant activity guided isolation of marine natural products. The chapter concludes with the activity guided isolation and structural elucidation of 1-O-palmitoyl-2-O-myristoyl-3-O-(6-sulfo- $\alpha$ -D-quinovopyranosyl)-glycerol (**40**) to show direct antioxidant potential through FRAP analysis.

Chapter 4 describes the isolation, structural elucidation and pharmacological evaluation of the novel secondary metabolites iso-PsA(**45**), Iso-PsC (**46**), iso-PsD (**47**) as well as known Pseudopterosins A(**41**), B(**42**), C(**43**), D(**44**), K(**48**), K2'OAc(**49**), K2'OAc(**50**). These secondary metabolites were evaluated for both cytotoxicity. The chapter concludes with the screening of these compounds as  $\alpha\beta$ -amyloid fibril modulators utilizing atomic force microscopy (AFM).

## Natural Product Studies of Marine Organisms from the Western Atlantic Ocean

List of Tables .....	xii
List of Figures .....	xii
Chapter 1: Introduction .....	1
Natural Products.....	1
Marine Natural Products .....	3
Statement of purpose.....	5
Chapter 2: Biosynthetic Production of Marine Secondary Metabolites from	
Briareum Asbestinum. ....	7
Chemistry from Briarium asbestinum .....	7
Diterpenes produced by Caribbean Briareum asbestinum.....	7
Cladiellane-Type.....	8
Briarane-Type .....	9
Biosynthetic Study .....	10
Pericyclic reactions .....	12
Electrocyclic reactions .....	13
Photochromisim. ....	16
Isolation of Briareolate ester L(19), Ester G(20), and ester B (22) .....	18
Conformational analysis of the dienone (19) and (20) .....	18



Biosynthetic mechanism .....	19
Absorption Spectroscopy .....	21
Photochemical Transformations .....	23
Photochemical Interconversion and Kinetics.....	25
Photochemical reactions with UVC light .....	27
Photochemical reactions with UVAight .....	28
Retro-6 $\pi$ electro-cyclization with UVC light.....	31
Ground state interconversion.. .....	32
Structural elucidation of spiroketal $\gamma$ lactone (33).....	32
Mechanism and speculation on spiroketal $\gamma$ lactone (33) and ground state chemisry .....	36
Conclusion .....	38
Chapter 3: Isolation and phamacological evaluation of Marine Natural Products	
Protective against neurogengerative Oxidative Stress.....	42
Introduction.....	42
oxidative stress.....	43
Antioxidants .....	44
$\alpha\beta$ -Amyloid plaque and Alzheimer's Disease .....	46
Marine Antioxidants .....	47
Antioxidant Assays .....	47
Ferric Reducing Antioxidant Power (FRAP) Assay .....	49

Pseudopterosin Chemistry from Caribbean octocoral <i>P. elisabethae</i> .....	50
Isolation and screening of Marine extract for antioxidant activity .....	52
FRAP experimental verification .....	53
Activity screening of marine extracts .....	54
Isolation of Glycolipid (44) .....	56
Structural elucidation of glycolipid (44).....	57
Conclusion. ....	59
Isolation and Pharmacological Evaluation of Pseudopterosin terpenes from Gorgonian Octocoral Pseudopterogorgia.....	62
Collection of Pseudoterogorgia.....	62
Spectroscopic confirmation of iso-Pseudopterosins .....	64
Cell toxicity data .....	66
AFM imaging Assay for measuring A $\beta$ <sub>40</sub> plaque formation.....	69
conclusion .....	74
Chapter 5: Methods and Materials.....	76
Collection and Identification of Marine Material .....	76
<i>Pseudopterogorgia spp</i> .....	76
<i>Briareum asbesinum</i> .....	76
Small Scale Solid-Phase Extraction.....	76
Large Scale Extraction.....	77
Semi-Preparative HPLC Separation .....	77

Instrumentation .....	78
Structural elucidation .....	79
Thermal transformation procedures for Briareolate esters.....	79
Acid catalysis transformation procedures for Briareolate esters.....	80
Nucleophilic assisted isomerization for Briareolate esters .....	80
FRAP Assay .....	82
Acid hydrolysis of pseudopterosins A-D to pseudopterosin aglycone. ....	83
Base hydrolysis of pseudopterosins A-D to pseudopterosin aglycone. ....	83
Acetylation pseudopterosins A-D to pseudopterosin .....	83
MTS cell cytotoxicity Assay .....	84

## List of Tables

Table 1: NMR tables for spiroketal $\gamma$ lactone ( <b>33</b> ), in (CDCl <sub>3</sub> , 400 MHz)..	35
Table 2: MR tables for 1-O-palmitoyl-2-O-myristoyl-3-O-(6-sulfo- $\alpha$ -D-quinovopyranosyl)-glycerol( <b>40</b> ), Recorded in (CD <sub>3</sub> OD, 400 MHz),	59
Table 3: Summary of Results from Thermal and Acid Methods..	81

## List of Figures

Figure 1. Structures of tetrahydrocannabinidiol ( <b>1</b> ), cannabidiol ( <b>2</b> ), and Nabilone ( <b>3</b> ).....	3
Figure 2. Structures of of spongothymidine ( <b>4</b> ) and spongouridine ( <b>5</b> ), Prostaglandin (15 R)-PGA 2 ( <b>6</b> ) .....	4
Figure 3. Structures of Halichondrin B ( <b>7</b> ) and Eribulin ( <b>8</b> ).....	5
Figure 4. The proposed biosynthetic pathway from cembrane ( <b>9</b> ) to eunicellin ( <b>10</b> ), briarellin( <b>11</b> ), asbestinane( <b>12</b> ), and briarane-type carbon( <b>13</b> ).....	9
Figure 5. Structural differences within the Briarane C19 methyl esters.....	10
Figure 6. Biosynthetic analysis of briareolate esters.. .....	12
Figure 7. example of a typical oxa-6 $\pi$ electrocyclization. ....	14
Figure 8. Synthesis of Smenochromomene D through a transannular oxa- 6 $\pi$ electrocyclization. ....	15
Figure 9. photochromic interconversion of fungides.....	17
Figure 10. Revised biosynthetic analysis of briareolate esters.. .....	20
Figure 11. (a): Deconvoluted UV/Vis spectra of ( <b>19</b> ); (b): Deconvoluted UV/Vis spectra of ( <b>20</b> ).. .....	22
Figure 12 (a): Overlay of absorbance spectra of ( <b>19,20,22</b> ) with the normalized UVA and UVC emission spectra.....	24
Figure 13. <sup>1</sup> H NMR Chemical shift of H6 and H7 olfinic protons of Briareolate ester L ( <b>19</b> ), ester G ( <b>20</b> ), and ester B ( <b>22</b> ) .....	26
Figure 14. Photoirradiation of ( <b>19</b> ) under UVC light after 20 mins. ....	27

Figure 15. Photoirradiation of <b>(19)</b> under UVA light after 3h.....	29
Figure 16. Photoirradiation of <b>(19)</b> under UVA Photostationary state .....	29
Figure 17. Stacked overlay of selected <sup>1</sup> H NMR under UVA irradiation .....	30
Figure 18. Photoirradiation of <b>(22)</b> under UVC light after 40 min.....	31
Figure 19. COSY and HMBC correlation spiroketal $\gamma$ lactone <b>(33)</b> .....	34
Figure 20. NOE correlations observed on spiroketal $\gamma$ lactone <b>(33)</b> .....	34
Figure 21. Proposed mechanism for spiroketal $\gamma$ lactone <b>(33)</b> .....	37
Figure 22. Proposed biosynthetic sequence for formation of briarane containing lactone .....	38
Figure 23. Map of the hydrography collections region in Islamorada.....	52
Figure 24. small scale extraction and extract enrichment procedure.....	53
Figure 25. Standard curve generated using concentrations of Trolox. ....	54
Figure 26. Comparison of antioxidant potential of marine extracts. ....	55
Figure 27. Picture of Specimen LJ-14 used for large scale extraction.. ....	56
Figure 28. key COSY correlation for compound <b>(40)</b> .....	58
Figure 29. Key HMBC correlations for compound <b>(40)</b> .....	58
Figure 30. GC Fame coromatagram comparing unkown to standards... ..	60
Figure 31. ezymatics method for structural confirmation of compound <b>(40)</b> .....	61
Figure 32. chromatogram from the isolation of Ps- (A-D) <b>(41-44)</b> .....	63
Figure 33. chromatogram from the isolation of iso-Ps-(A,C,D) <b>(45-47)</b> .....	63
Figure 34. Structure of isolated pseudopterosins .....	64
Figure 35. Structure of iso-pseudopterosins structural skeleton.....	64
Figure 36. Structures of Iso-pseudopterosins (A,C,D) <b>(45-47)</b> .. ....	66

Figure 37. Cytotoxicity data for pseudopterosins Iso-PsA( <b>45</b> ), PsA( <b>41</b> ), and PsK( <b>48</b> ) .....	67
Figure 38. Cell cytotoxicity data for Iso-PsA( <b>45</b> ), PsA( <b>41</b> ), and PsK( <b>48</b> ) .....	68
Figure 39. Dose response cytotoxicity for Iso-PsA( <b>45</b> ).....	68
Figure 40. Tapping mode AFM images of A $\beta$ <sub>40</sub> amyloidogenesis (A) 0 days, (B) 3 days, and (C) 6 days.....	71
Figure 41. Tapping mode AFM images of A $\beta$ <sub>40</sub> with both glycoylated pseudopterosins Iso- PsA( <b>45</b> ), and PsA( <b>41</b> ) showing amyloidogenesis (A) PsA 3 days, (C)PsA 6 days B) iso-PsA( <b>45</b> ) 3 days, (C)iso-PsA( <b>45</b> ) 6 days.....	72
Figure 42. Tapping mode AFM images of A $\beta$ <sub>40</sub> with Ps-aglycone ( <b>51</b> ) showing amyloidogenesis (A) 0 days, (A) 3 days, and (B) 6 days. ....	73

## Chapter 1: Introduction

### Natural Products

Evolution has generated the immensely rich, and organically diverse planet that we know today<sup>1</sup>. It is through evolution that organisms attain advantages which allows them to thrive<sup>2</sup>. It is increasingly evident that evolutionary development is not restricted to physiological developments but includes evolutionary chemical advantages that organisms develop and exploit. As a result of the isolation and study of these molecules, the biomedical community increasingly finds growing and diverse therapeutic applications for these natural products.

A natural product is a chemical compound or substance produced and found in nature, these compounds differ from primary metabolites in that it is not required for survival but rather provides an evolutionary benefit to promote survival<sup>2a, 3</sup>. Natural products come from a variety of sources including terrestrial and marine-based plants, microorganisms and animals<sup>3a, 4</sup>. The diversity of organisms found in nature is unmatched only by the even greater diversity and structural complexity of natural products. Commercial use of natural products exploits beneficial, chemical evolutionary developments in one or more species to provide similar survivability benefits to humans<sup>3a, 5</sup>.

Natural products have long been recognized as a fundamental source of therapeutic agents. Today, nearly 49% of the most prevalent drugs originate from natural products<sup>6</sup> but through most of our history, natural products were the sole means



to\ treat disease and injury. It is a growing understanding of molecular biology and combinatorial chemistry, which has enabled the era of rational design of chemical compounds which target specific molecules <sup>7</sup>. In recent decades the growing capabilities in synthesis has changed the role of natural products in drug discovery and development where they are now regarded as a precursor. However the identification and study of natural products, where researchers may now create synthetic analogs of increasingly complex, natural products, has fueled studies within the biomedical community which offer pharmacological improvements in both efficacy and safety <sup>8</sup>.

The exploitation of natural products is seen throughout history where one of the world's oldest documented medicinal plants, marijuana, has been used for both recreational and medicinal purposes for centuries; and, in recent years, *Cannabis sativa* L. has undergone a medical research renaissance <sup>9</sup>. The Cannabis plant comprises a variety of chemicals, the most widely used being the 60+ cannabinoids which are C-21 terpenophenolic compounds and are found exclusively in this genus<sup>9a, 10</sup>. The most commonly studied cannabinoids, and the most widely and publically known within medicinal studies, are the bioactive tetrahydrocannabinol (THC) (**1**) and canibidiol (**2**) <sup>10</sup>. However, despite the pharmacological, though illegal, benefits of the direct natural compounds themselves, semi synthetic cannabinoid's such as Nabilone (**3**) were developed and approved in 1985 by the U.S. Food and Drug Administration for treatment of chemotherapy-induced nausea and vomiting, thereby giving testament to the use of natural products themselves being used as medically beneficial and also offering scaffolds as a basis to improve pharmacological benefits (Figure 1)<sup>11</sup>.

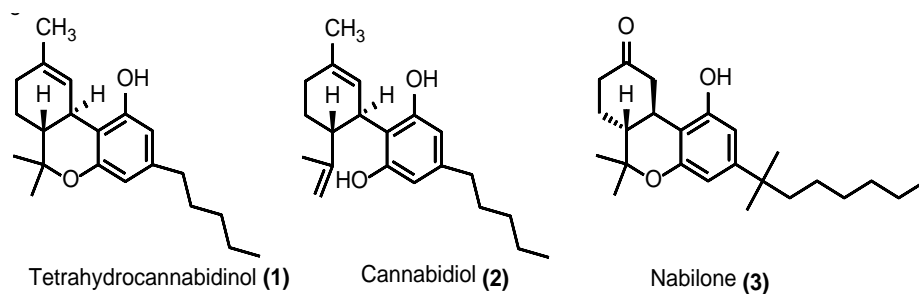
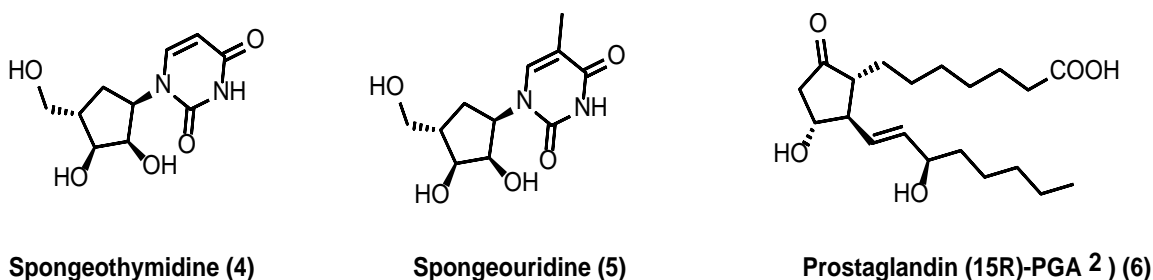


**Figure 1.** Structures of tetrahydrocannabininol (1), cannabidiol (2), and Nabilone (3).

## Marine Natural Products

Because marine environments exhibit some of the most biodiverse ecosystems on the planet they provide an excellent opportunity to find new chemistry. Marine invertebrates which include, the octocorals, or Octocorallia, are among the most diverse in the marine environment<sup>12</sup>. This diverse group of marine invertebrates which includes soft corals, blue corals, sea pens, sea whips and sea fans, comprises over 11,000 species<sup>13</sup> and are one of the richest sources of bioactive natural products which have found their way to market<sup>13</sup>. It is only within the past 60 years that advances have enabled marine natural products research and, as a consequence, the study of natural products continues to have renewed impact<sup>14</sup>. The start of marine natural products research can be dated back to the discovery of spongothymidine for anticancer (4) and spongouridine (5) for antiviral purposes both isolated from *Cryptotethia crypt*<sup>15</sup>. Through intensive biological testing upon initial isolation followed by synthesis of structural analogues led to the development of cytosine arabinoside (Ara-C) as a clinical anticancer agent approved of in June 1969 (figure 2)<sup>16</sup>. Possibly the most famous is Prostaglandin (15 R)-PGA 2 (6) which is derived from *Plexaura homomalla*, described in 1968, and which led to the common class of birth control (figure 2)<sup>3b, 17</sup>. Since then therapeutic value has been

found in the area of pain management with the discovery and approval of Zinconotide a  $\alpha$ -Conotoxin from a marine snail *Conus Magus*<sup>15</sup>.



**Spongothymidine (4)**                      **Spongouridine (5)**                      **Prostaglandin (15R)-PGA 2 (6)**  
**Figure 2.** Structures of of spongothymidine (4) and spongouridine (5), Prostaglandin (15 R)-PGA 2 (6)

Halichondrin B (7), was isolated from the western Pacific marine sponge *Axinella*, and which showed growth inhibitory activity towards multiple cancer cell lines<sup>18</sup>(figure 3). Halichondrin B (7) was studied intensely but, due to its structural complexity, proved too costly for commercial use from a synthetic, harvesting, or aquaculture standpoint<sup>18</sup>. To overcome these problems these natural products can serve as an important inspiration for drug discovery allowing synthetic chemist in collaboration with biologist to develop structurally similar frame work which can allow for the development of safer and more effective drugs and at the same time develop synthetic strategies that are practical with respect to commercial use of these compounds. Eribulin(8) exemplifies this importance and more specifically in the area of marine natural products for use as a framework for the development of therapeutic drugs(figure 3)<sup>15, 19</sup>. It was synthetic and structure relationship studies which resulted in the ability to commercially produce the synthetic analog eribulin (8) used for the treatment of metastatic breast cancer (Figure 1.2)<sup>15, 19</sup>. While there is not yet an abundance of marine-derived drugs, the sheer diversity of oceanic bio-environments all but dictate future successes in the quest for novel chemical structures and the subsequent development of new drugs and commercial products<sup>15</sup>.

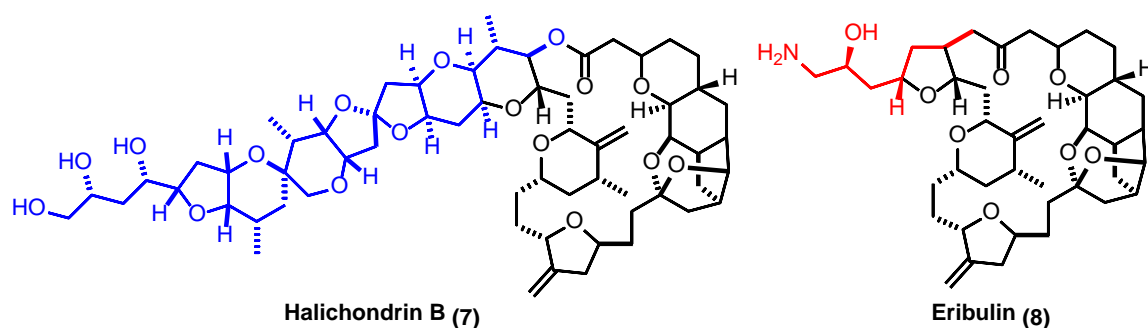


**Figure 3.** Structures of halichondrin B (7) and eribulin (8). Key structural difference are highlighted in blue and red

**Statement of purpose:**

Natural products often exhibit pharmacological activity and, as such, can have a significant impact in drug design. Natural products chemistry research emphasizes the study of the chemistry and biochemistry of naturally occurring compounds in the context of the biology of the living systems from which they are obtained. The study of natural products offers the opportunity for scientists to study the role, relationship, purpose, and synthesis of these compounds and their pharmacological potential<sup>3b</sup>. It is the goal of natural product chemists to not only explain the nature of these compounds but, more importantly, to determine how and why these natural compounds are produced and to specifically assess their potential to be utilized in new ways<sup>3b</sup>. As such, the isolation and understanding of both the structure and mechanisms of natural products has, and will continue to, significantly impact the scientific community. This thesis covers multiple subcategories within the area of marine natural products. Specifically it offers research focused on biosynthetic understanding, activity guided isolation, structural elucidation, and pharmacological evaluation of natural products from the western Atlantic Ocean.

Chapter 2 provides biosynthetic scrutiny of a set of bio transformations in *Briarium asbestinum*. This hemisynthetic work features rare, forward and retro

transannular  $6\pi$  electrocyclizations in which both the photochemical and the traditional, ground state synthetic parameters on which these pivotal transformations are predicated. As this is only the second, demonstrated example of a transannular electrocyclization we paid particular attention to the macrocyclic chemistry and to the constraints imposed by this system in order to achieve interconversion. Chapter 3 focuses on the isolation of marine natural products that may serve as novel chemical entities for protection against oxidative stress. Activity-guided isolation protocols are utilized for the isolation of these products from our collection of marine organisms harvested in Islamorada Florida. Chapter 4 covers the isolation and pharmacological evaluation of marine natural products from collections made in various locations throughout the Caribbean - specifically octocoral *Pseudopterosin elisabethae*. Pseudopterosins isolated during the course of this study were subjected to various biological assays in order to better assess their therapeutic potential and their utility as biomedical probes on specific targets.

## Chapter 2: Biosynthetic Production of Marine Secondary Metabolites from *Briareum*

### *Asbestinum*

#### **Introduction:**

The project outlined in chapter two revolves around the hemisynthetic study of Briareolate esters from *Briarium asbestinum*. *B. asbestinum* is a soft gorgonian octocoral found on coral reefs in tropical and subtropical areas. *B. asbestinum* is typically located in the western Atlantic Ocean, the Caribbean Sea, off the coast of Florida, and in the Gulf of Mexico although many species of *Briareum* are found worldwide <sup>12, 20</sup>. Natural product studies from *B. asbestinum* began in the late 1960s with the discovery of crystalline terpenoid lactones and taurobetanine, both isolated from *B. asbestinum* harvested from the Bahamas <sup>21</sup>. The *Briareum* genus has since provided a plethora of biologically active natural products including sterols, alkaloids, and terpenoids <sup>21a-c, 22</sup>. Natural products from *B. asbestinum* have exhibited numerous biological properties and have shown to be cytotoxic, antimicrobial, anti-inflammatory, antiviral, immunomodulatory, antifouling, ichthotoxic, and pesticidal <sup>21a-c, 22</sup>.

#### **Diterpenoids produced by Caribbean *Briareum asbestinum***

Some of the most interesting natural products from *B. asbestinum* are the cembranoids (**9**) which are prenyl diphosphates forming diterpenes and which, through cyclization and coupling, form the parent Cembranoid skeleton <sup>23</sup>. Cembranoid-based natural products found in *B. asbestinum* exhibit immense structural diversity as a result of a variety of cyclization events (via 3-8 or 2-11), followed by

bio-transformations which include oxidation, various types of ether linkage and, more specifically, pericyclic reactions that result in differing ring systems and substitutions (see Figure 4).

The 2,11-cyclized and 3,8-cyclized cembranoids have been classified into five main categories: the cladiellins (also known as eunicellins) (**10**), the briarellins (**11**), the asbestinins(**12**), the briarane type with or without the  $\gamma$ -lactone ring<sup>24</sup>. The cladiellane- and briarane-type metabolites are produced through different cembranoid terpene cyclizations and, as first proposed by Faulkner, are both bicyclic, fused, 6 and 10 membered rings (see Figure 4) <sup>24-25</sup>.

### **Cladiellane-Type**

The cladiellins (eunicellins) (**10**) represent the most abundant class of 2,11-cyclized, cembranoid natural products. These secondary metabolites represent a class of natural products with a common oxatricyclopentadecane core. To date, 23 briarellins (**11**) and 34 asbestinins (**12**) have been isolated exclusively from *B. asbestinum* <sup>24, 26</sup>.

Eunicellin (**10**), a cladiellin and the first 2,11-cyclized cembranoid (**9**), was first isolated in 1968 <sup>27</sup>. It is believed that briarellins and asbestinins are derived from this cladiellin-type scaffold through subsequent bio-transformations which generate the tetracyclic briarellin (**11**) scaffold. Asbestinins are derived from the briarellins where they undergo a very unfavorable, suprafacial 1,2-methyl shift which yields the asbestinin-type scaffold(**12**) <sup>24, 26</sup> (see Figure 4).

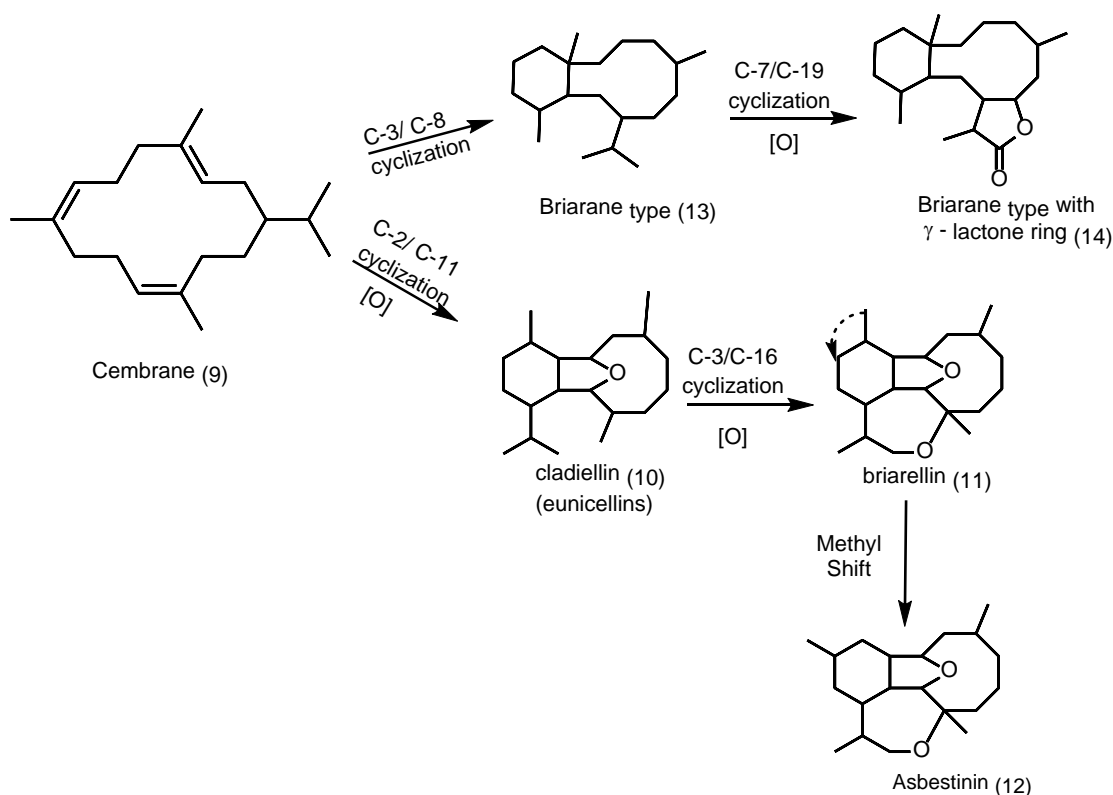


**Figure 4.** The proposed biosynthetic pathway from cembrane to sarcodictyins. eunicellin, briarellin, asbestinin, and briarane-type carbon skeletons<sup>28</sup>.

### Briarane-Type

In 1977, the first Briarane-type natural product, Briarein A, was isolated from the Caribbean gorgonian, *B. asbestinum*<sup>28</sup>. This briarane type represents the group of octocorallian 3,8-cyclized cembranoids, which exhibit a common 6 and 10 membered bicyclic system. *B. asbestinum* has yielded 34 briarane-type compounds that contain the  $\gamma$ -lactone ring (**14**) and a total of 14 briarane types which contain the C19-methyl ester in lieu of the  $\gamma$ -lactone ring(**13**)<sup>28</sup>. Briarane-type C19-briareolate esters (**13**) are a small group of briarane-types which contain an unusual C-19 methyl ester in lieu of the  $\gamma$ -lactone ring and which are typically found in gorgonian coral. The exact mechanism of the biosynthetic pathways however, is still not fully understood<sup>28</sup>.



This thesis concentrates on the biosynthetic study of a relatively small group of Briarane-type diterpenoids, specifically those which contain the C19-methyl ester in lieu of the  $\gamma$ -lactone ring and which were isolated exclusively from Caribbean *B. asbestinum*. These particular Briarane-type diterpenoids represent a small subset of compounds which account for less than 4% of all the diterpenoids produced by *Briareum* worldwide<sup>29</sup>. There are four main structural differences within this Briareolate ester subset, the (5*E*,7*Z*)-dienone moiety; the (5*Z*,7*Z*)-dienone, the 2*H* Pyran, and the (7*R*,8*S*) epoxide (Figure 5)<sup>28</sup>.

The biosynthetic study of secondary metabolites is often complex and is usually a multi-step, enzyme-catalyzed process with subsequent bio-transformations which result in a structurally rich class of natural products<sup>30</sup>; While these biosynthetic pathways are predominantly enzymatic in nature, several examples have been shown to occur spontaneously in nature through photochemical or thermal transformations.

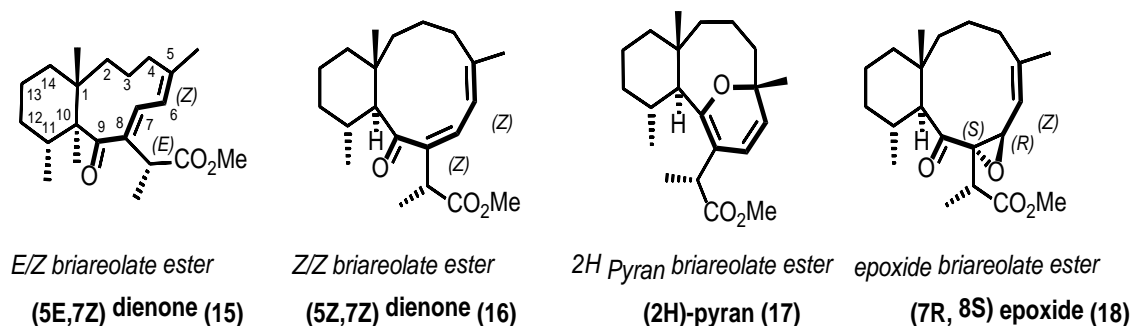


**Figure 5.** Key core structural differences within the Briarane-type C19 methyl esters

Many attempts to synthesize the chemistry from *Briareum* have been made, but with little progress in those Briarane types which contain the C19-methyl ester in lieu of the  $\gamma$ -lactone ring<sup>31</sup>. Recently, the photochemical production has been shown to be responsible for many marine secondary metabolites as a result, research in this field has enjoyed increased attention<sup>32</sup>. At it is already well known that natural, chemical

synthesis by both terrestrial and marine organisms often requires light-induced transformations such as isomerization, fragmentation, and pericyclic reaction<sup>33</sup>, it was the goal of the project outlined in chapter to study these interconversions, in particular the rare, transannular electrocyclization and the unique constraint's imposed by the macrocyclic ring found in the briareolate esters.

We recently isolated the briarane-type cembranoid briareolate ester L (**19**) - the first natural product to possess a 10-membered macrocyclic ring with a (*5E,7Z*)-dienone moiety. This cembranoid was isolated, along with its known isomer briareolate ester G (**20**), and was found to differ only in the (*5Z,7Z*)-dienone configuration. Two years prior to this isolation, Trauner had intuitively advanced (speculated) a proposed biosynthetic pathway in which briareolate ester G (**20**) “appeared correlated” and in equilibrium with its tricyclic isomer ester B (**22**)<sup>25</sup>. This attracted our attention for two reasons: a) oxa-6 $\pi$  electrocyclizations are known as fast and reversible reactions and one would imagine that a steady equilibrium between (**19**), (**20**) and (**22**) would be challenging to resolve and b) transannular oxa-6 $\pi$  electrocyclizations have rarely been studied. Previous studies concluded that alkyl substitutions on both  $\alpha$  positions induce steric interactions in which the *s-cis* conformer is destabilized and produces only the *s-trans* dienones<sup>34</sup>. The possibility of a transannular 6 $\pi$ -electrocyclization (TAPE) hinged on the ability of this unique E,Z-dienone system (**19**) to isomerize to the corresponding Z,Z-dienone (**20**) while overcoming the conformational constraints imposed by the macrocyclic ring structure to reach the puckered inside space.

In view of our ability to not only access these rare natural products, but to do so in relevant quantities, and more importantly with Transannular oxa 6 $\pi$  electrocyclization being extremely rare and only one published report, by the Trauner research group, is in evidence with

the synthesis of smenochromene D. Our system is therefore unique and we believe that, with the Trauner group having speculated this proposed biosynthetic pathway, the study of transannular oxa  $6\pi$  electrocyclization is of significant value to both synthetic and natural product chemists. This work appeared to be a means by which to better understand this unique macrocyclic chemistry and to determine the parameters required to overcome the (*s-trans* to *s-cis*) rotamer interconversion and thereby generate the unfavored *s-cis* cyclic transition state required for interconversion to (**22**).

The goals of this project were to fully study the proposed biosynthetic interconversion between (**19**), (**20**), and (**22**) and it almost seemed that we were destined to fully study this biosynthetic interconversion. Our goal was, upon isolation, to establish the full structure in respect of this unique macrocycle and to determine the constraints it may impose and the thermal and photochemical conditions required to achieve these interconversions.

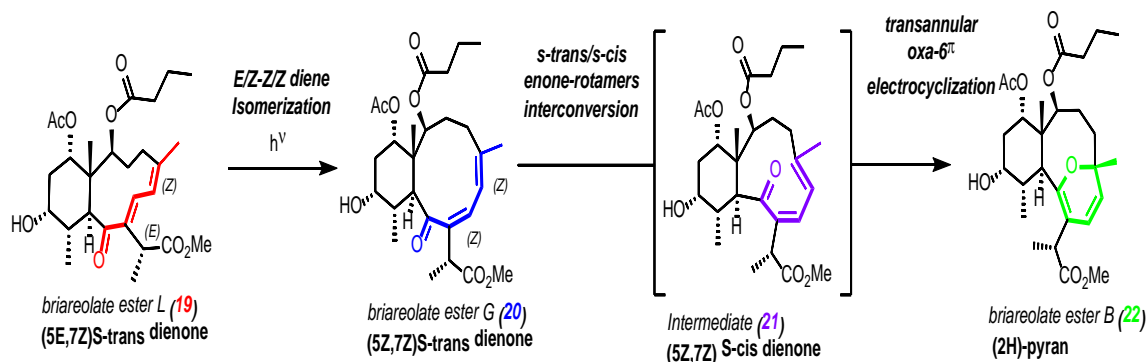


**Figure 6.** Biosynthetic analysis of Briarolate esters.

## Pericyclic Reactions

Pericyclic reactions are effective strategies for creating structurally complex molecules from simple precursors and are increasingly recognized for their role in the biosynthesis of natural products<sup>35</sup>. Pericyclic reactions represent an important body of chemical transformations that enables facile ring formation and skeletal rearrangements

(e.g. sigmatropic rearrangements, cycloadditions and electrocyclizations). Indeed a significant number of pericyclic reactions are shown to occur frequently in the formation of natural products <sup>36</sup>. A pericyclic reaction comprises a single step in which the transition state has a cyclic geometry and a bond formation occurs. In particular, transannular reactions are extremely efficient in the synthesis of complex polycyclic natural products which possess multiple stereocenters. A number of impressive precedents exist for transannular Diels–Alder <sup>37</sup> and hetero-Diels–Alder <sup>37a, 38</sup> reactions with electron-poor enones to achieve synthesis of complex molecules. An important subset of these reactions is the electrocyclic reactions and it is only in recent years that sufficient examples have been demonstrated for acceptance among synthetic and natural product chemists.

### Electrocyclic Reactions

Electrocyclic reactions represent a type of pericyclic rearrangement in which a pi bond is converted into a sigma bond <sup>39</sup>. Electrocyclizations, which include Oxa-6 $\pi$  electrocyclizations, are categorized by being either photochemical or thermal and can be either ring-opening or ring-closing in nature<sup>40</sup>. Depending on the type of reaction, (photochemical or thermal), these reactions occur specifically through either a conrotatory or disrotatory mechanism which dictates the predominant product with high stereospecificity <sup>36e, 39a, 40-41</sup>. Interestingly, examples of molecules presenting a conjugated (Z,Z)-dienone are extremely rare as a result of facile conformational rotation of the carbonyl moiety (*s-trans* to *s-cis* enone) which spontaneously induces a rapid thermal oxa-6 $\pi$  electrocyclization to afford the corresponding (2H)-pyran products (Figure 7)<sup>42</sup>. In fact, the equilibrium shift between dienone (or dienal(**23**)(**24**)) and their (2H)-

pyran(**25**) counterparts does not usually depend on conformational restrictions but rather incorporates electronic factors to either stabilize or destabilize the  $6\pi$  electron conjugation<sup>36e, 42d, 43</sup>. Although electrocyclizations of this type are common, simple (2H)-pyrans that are not masked by further transformations, of which are not fused to aromatic systems, are particularly rare<sup>36e</sup>.

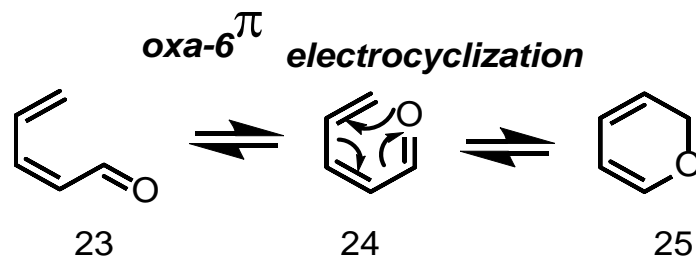


**Figure 7.** Example of a typical oxa-6 $\pi$ electrocyclization

While many, naturally-occurring, electrocyclic reactions have been explored in biomimetic syntheses, examples of transannular electrocyclization ( $6\pi$ ,  $8\pi$  or  $12\pi$ ) are sparse in scientific literature<sup>44</sup>. Transannular interactions, in particular electrocyclizations involving these same chemical interactions, typically take place in a large macrocycle to form the new molecules. These, in particular, are considered extremely rare and, to date, there has been just one biomimetic total synthesis which demonstrated a transannular oxa-6 $\pi$  electrocyclization. This study was undertaken by Trauner in the synthesis of smenochromene D (**29**)(Figure 8)<sup>45</sup>. The reactions involved a quinone-based terpene that, through boric acid, mediated alkylation (**26**) and subsequently formed a cyclicborate intermediate (**27**) which in turn, and through subsequent elimination, formed the vinyl orthoquinonemethide (**28**) which itself subsequently underwent a thermal oxa-6 $\pi$  electrocyclization in order to install the chromene system (**29**)(Figure 8). Dienones are rare and are typically not isolated as they undergo oxa-6 $\pi$  electrocyclization as in the case of chromenes. These pyrans occur in

many natural products but typically undergo further pericyclic transformations such as [2 + 2] cycloadditions or oxidations followed by [4 + 2] cycloadditions to produce further derivatives. Our system is therefore unique in that all three isomers are stable and reaction stops at the 2H pyran with no further transformations. Many 2H pyran formations have already been shown to exhibit photochromic properties and therefore additional goals of this study were to investigate both thermal and photochemical parameters and to determine the photochromic properties of the system in order to fully elucidate the mechanism behind these unusual transformations <sup>46</sup>.

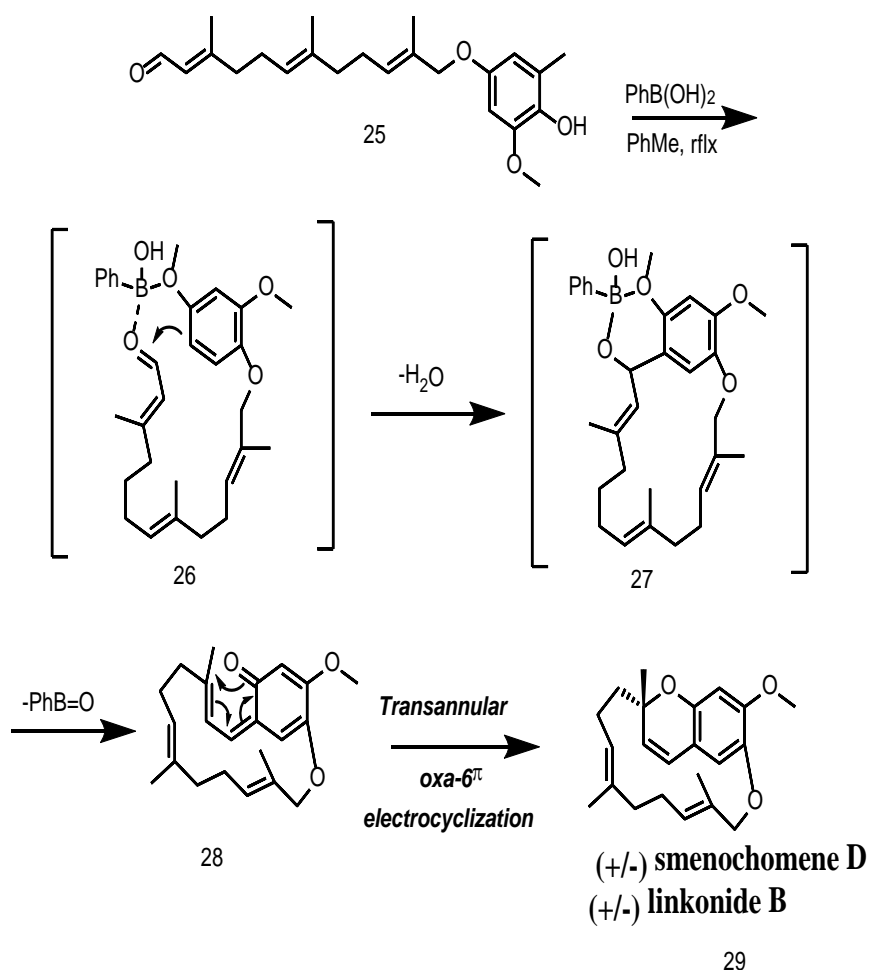


**Figure 8.** Synthesis of smenochomene D through a transannular oxa-6 $\pi$ electrocyclization <sup>45</sup>

## Photochromism

Photochromic material refers to the reversible transformation of chemical species, induced in one or both directions by electromagnetic radiation, between two states having observable variation in light absorptions in different regions.”<sup>46b, 47</sup>. Photochromism was first discovered by Fritzsche in 1867 with the study of the reversible color change of 2,3,4,4-tetrachloronaphthalen-1(4H)-one<sup>46</sup>. Photochromic materials can serve as ultraviolet protective shields<sup>47c-f</sup> and the use of light to trigger reactions is particularly attractive, for example, the photoisomerization of non-toxic E -combretastatins to the clinically active Z provides a phototherapeutic method to overcome nondiscriminative systemic toxicity of Z- combretastatins to allow accurate, remotely controlled cancer therapy<sup>48</sup>.

Photochromic compounds have many industrial applications such as optical molecular switches, biological sensors, and many more<sup>47c-f</sup>. The study of photochromic compounds involves the study of photochromism, the mechanism of the photoprocesses, the development of synthetic pathways, the investigation of the properties and their potential applications<sup>46b, 49</sup>.

All photochromic compounds have at least have two different forms which exhibit different absorption spectra of either the intensity or the wavelength. Fulgides, are one of the most intensely studied class of photochromic systems featuring both an isomerization and an electrocyclization similar to the system we are studying it is their ability to interconvert between the cyclized form (**33**) and un-cyclized (**30 & 31**) form upon exposure to certain wavelengths of light that is of particular interest (figure 9). Fulgides were first synthesized and discovered by Strobb in the 1905<sup>50</sup>. Various fulgides,





### Isolation of Briareolate esters

In order to study the biosynthetic pathway of these briarane type diterpenoids the first step was the isolation of **(19)** to **(22)** in order to test our hypothesis. The gorgonian *Briareum asbestinum* was collected by hand using SCUBA at a depth of 15 m from Hillsboro Ledge, Boca Raton in Florida (BR02-002). The sample of *B. asbestinum* (2 kg wet wt.) was extracted with methanol for 24 h. Extracts were then passed through a column of HP-20 resin equilibrated with methanol. The combined eluents were diluted with water and passed again through the column. The column was eluted with fractions of H<sub>2</sub>O, a) H<sub>2</sub>O, (b) 40% (CH<sub>3</sub>)<sub>2</sub>CO, (c) 75% (CH<sub>3</sub>)<sub>2</sub>CO: H<sub>2</sub>O and (d) (CH<sub>3</sub>)<sub>2</sub>CO. The 75% fraction was subjected to further column chromatography on HP-20SS resin, eluting with increasing concentrations of CH<sub>3</sub>CN in H<sub>2</sub>O / CH<sub>3</sub>CN (40-100%). Selected fractions based on TLC and NMR we combined and subjected to repetitive injections of purification on preparative PRP-1 column for clean up to give briareolate ester L (**19**; 200 mg), briareolate ester G (**20**; 10 mg), and briareolate ester B (**22**; 5 mg).

### Conformational analysis of the dienone

Having established the stereochemistry with our initial structural assignment of both **(19)** and **(20)** we felt it crucial to confirm the exact geometry of the dienone system with particular emphasis to the orientation of the C9 carbonyl of the dieneone fragment. The stereochemistry of the diene was easily distinguished through NOSEY correlations **(20)** showed correlations observed through the H6 and H7 established **(22)** as (5Z,6Z). However **(19)** showed a correlation of the H7 to H2 which indicated the proton was inside the ring establishing a $\Delta$ <sub>6,7</sub> for **(19)** as (5E,6Z). To assign the geometry of the carbonyl we undertook a closer inspection of spectroscopic data NMR analysis which,

most notably, showed a downfield shift ( $^1\text{H}$  NMR  $\text{CDCl}_3$ ) of the  $\Delta 7,8$  olefinic proton in **2**  $\delta_{\text{H}7}$  6.62 ppm,  $\delta_{\text{C}7}$  138.1 ppm versus  $\delta_{\text{H}7}$  7.64 ppm,  $\delta_{\text{C}7}$  145.2 ppm,  $\delta_{\text{H}2}$  5.52 ppm. ( $^1\text{H}$  NMR  $\text{CD}_3\text{OD}$ ) of the  $\Delta 7,8$  olefinic proton in **2**  $\delta_{\text{H}7}$  6.71 ppm, versus  $\delta_{\text{H}7}$  7.71 ppm,  $\delta_{\text{H}2}$  5.13 ppm. The large deshielding of both the H7 in (**19**) as compared to (**20**) indicates the carbonyl in closer proximity to the H7 proton compared to (**20**)<sup>53</sup>. Similarly the H2 proton in (**19**), which is directly across the macrocycle, shows a similar increase of about 0.5 ppm compared to (**20**) which suggests an isotropic from the carbonyl which could, in turn, suggest that the C9 carbonyl in (**19**) is placed inside the ring in *s-cis* conformation<sup>34</sup>. However the epoxide (**18**), which was determined through x-ray crystallography and which shows a near identical pattern of shift exhibits the same  $\delta_{\text{H}2}$  5.52 ppm to indicate that the carbonyl is outside the ring and in the E,Z-*s-trans*-dienone geometry<sup>54</sup>. With IR stretching of the carbonyl  $\lambda_{\text{vmax}}$  = 1640 (**19**) and 1650 (**20**), both indicate *s-trans* conformation as this shift would be expected to be higher around  $\lambda_{\text{vmax}}$  = 1700 if the *s-cis* conformer was present<sup>34</sup>. However, more importantly with only one carbonyl stretch strongly indicates this locked geometry and with evidence pointing indicating E,Z-*s-trans*-dienone geometry for (**19**) this would also support (**20**) is also in fact *s-trans* conformation<sup>34</sup>. Establishing (**20**) is also in fact (Z,Z-*s-trans*-dienone).

### **Mechanism**

Having assigned the conformation of both dienone's in both briareolate ester L (**19**) (E,Z-*s-trans*-dienone moiety) and G (**20**) (Z,Z-*s-trans*-dienone moiety), we could further expand on the proposed biosynthetic mechanism knowing that upon isomerization of briareolate ester L (**19**) yielded (**20**). Briareolate G (**20**), with the Z,Z-*s-trans*-dienone moiety, would need to undergo the sterically unfavored *s-trans* to *s-cis* rotamer

interconversion in order to generate the cyclic transition state required for the oxa-6 $\pi$  electrocyclization to occur and, from (22) (Figure 10), we anticipated that under the correct synthetic parameters these compounds could be selectively interconverted and thereby undergo either isomerization or oxa-6 $\pi$  electrocyclization, through traditional photochemical, thermal or acid catalysis protocols<sup>36e, 39a, 41, 43, 55</sup>.

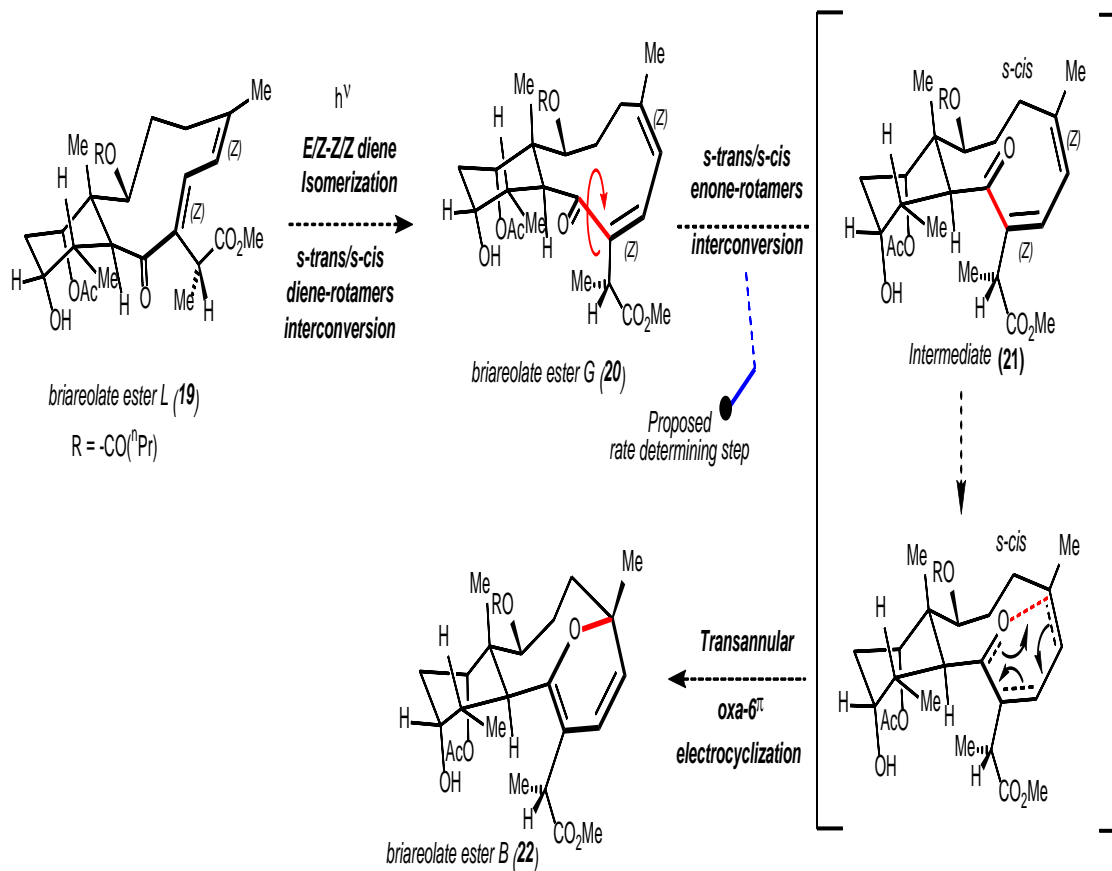


**Figure 10.** Revised biosynthetic pathway for a plausible conversion of briareolate esters L and/or G to briareolate ester B.

## Absorption Spectroscopy

To better understand the photochemical properties we undertook a closer inspection of the UV absorption spectra (figure 11). **(19)** UV (MeOH) showed absorption maxima  $\lambda_{\text{max}} = 237 \text{ nm}$  ( $\epsilon = 2075$ ),  $284 \text{ nm}$  ( $\epsilon = 1276$ ) compared to **(20)** UV (MeOH) which showed absorption maxima  $232 \text{ nm}$  ( $\epsilon = 5626$ ) and  $288 \text{ nm}$  ( $\epsilon = 4677$ ) and **(22)** UV (MeOH)  $\lambda_{\text{max}} = 284 \text{ nm}$  ( $\epsilon = 3800$ ). As no  $n\text{-}\pi^*$  association with the carbonyl in **(19)** was directly observable, we used Origin™ software to deconvolute the spectra of both dienones **(19)** and **(20)** in solutions of EtOH which resulted in three, specific bands. Spectra of **(19)** showed  $\lambda_{\text{max}} = 234 \text{ nm}$  ( $\epsilon = 2055$ ),  $284 \text{ nm}$  ( $\epsilon = 1306$ )  $\lambda = 314 \text{ nm}$  ( $\epsilon = 138$ ) and spectra of **(20)** showed  $\lambda_{\text{max}} = 221 \text{ nm}$  ( $\epsilon = 5867$ ),  $284 \text{ nm}$  ( $\epsilon = 2140$ )  $\lambda = 324 \text{ nm}$  ( $\epsilon = 394$ ) (Figure 11). The first band correlates to the primary  $\pi\text{-}\pi^*$  transitions. The second band correlates to the secondary  $\pi\text{-}\pi^*$  transition of the diene; and the third band correlates to the  $n\text{-}\pi^*$  transition associated with the carbonyl. We noted an increased overall absorption intensity of **(20)** compared to **(19)** together with a slight shift to a longer wavelength through this analysis we believed we could selectively target both the  $n\text{-}\pi^*$  through UVA light and the  $\pi\text{-}\pi^*$  through UVC light.

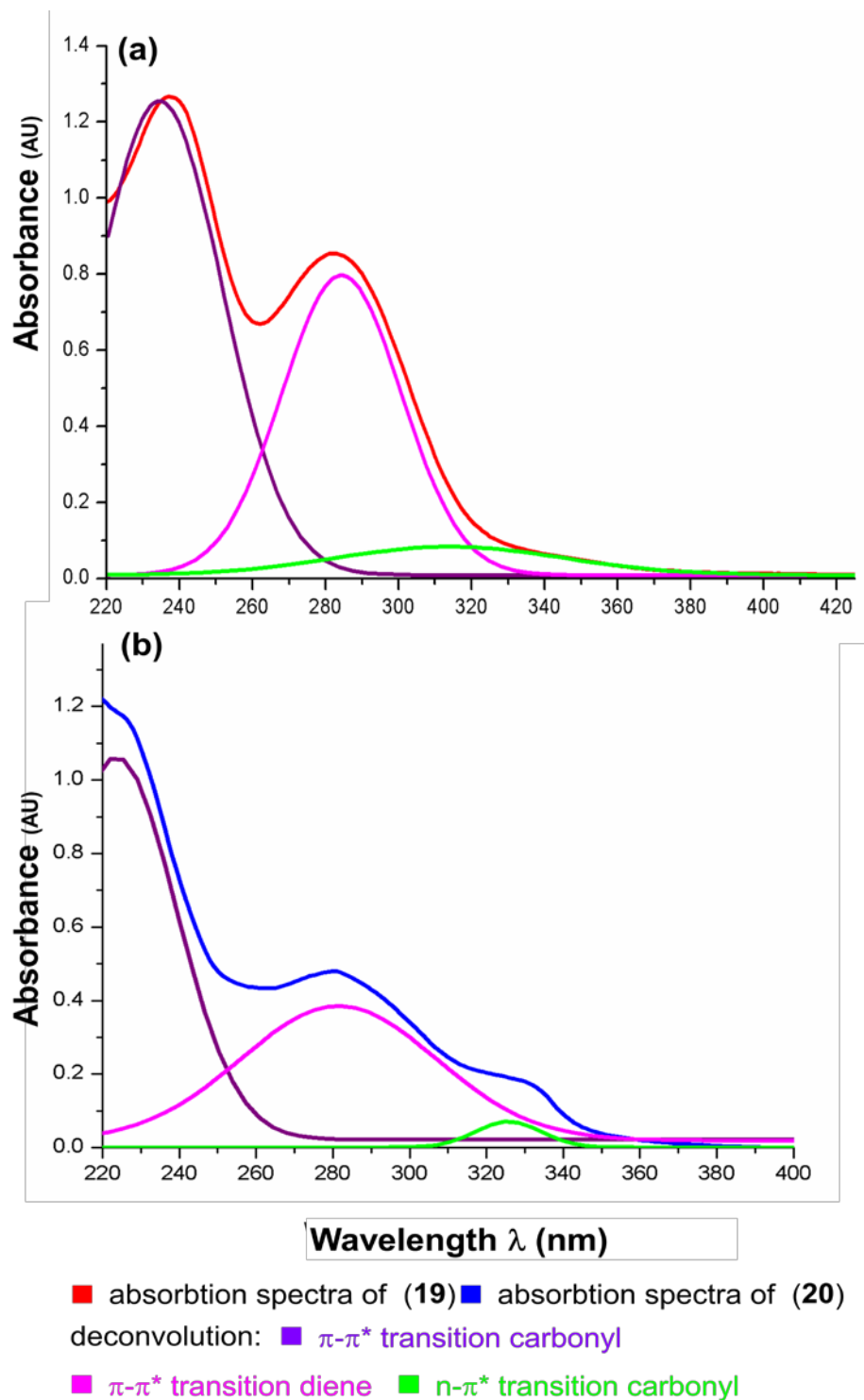


**Figure 11.** Normalized UV absorptions spectrum of (19) (610 $\mu$ M) and (20) (180 $\mu$ M) in EtOH(a): Deconvoluted UV/Vis spectra of (19); (b): Deconvoluted spectra of (20)

## Photochemical Transformations

To further assess the photo-physical properties of Briareolate (**19**), (**20**) and (**22**) we took measurements of the emission spectra of both UVA and UVC lights used in the experiments and compared these to the absorption spectra (Figure 12).

The photochemistry experiments were carried out using a RAYONET Model RMR-600 photochemical reaction chamber. Reactions using UVC light utilized the 2537Å bulb, and UVA light experiments were conducted with the 3500 Å series bulb. The UVA 3500 Å light has a single strong emission band  $\lambda = 350\text{nm}$  with a range of (315-400 nm). The UVC light 2537Å bulb had a strong emission band at  $\lambda = 253.4$ , with weaker spectral emission bands corresponding to with  $\lambda_{\text{max}} = 265.2, 280.4, 289.4, 296.7, 302.2, 312.9, 365.4, 404.7$ . Under UVA emission a slight overlap presents with the  $n-\pi^*$  transition of (**19**) and (**20**). The UVA emission from the Rayonnet Photoreactor omits spectral overlap with (**22**) as the  $n-\pi^*$  is significantly decreased due to a lone pair being in conjugation with the  $\pi$  system. This causes a shift to a lower wavelength and reduced intensity (figure 12 Panel c). These results indicate that compound (**22**) would not undergo photochemical reactions under UVA. Both dieneones show an increase in the absorption band intensity and a shift to a longer wavelength as seen with (**19**) and (**20**). Direct comparison of the dieneone's (**19**) and (**20**) show a decrease in absorption intensity of (**19**) compared to (**20**) which suggests that (**20**) would likely undergo more photochemical reactions compared to (**19**) when photochemically excited under these parameters. As previously mentioned, the slight shift in spectra (**19**)  $\lambda_{\text{max}} = 284\text{nm}$  compared to (**20**)  $\lambda_{\text{max}} = 288\text{ nm}$  in MeOH suggests greater spectral overlap with UVA and provides evidence to support a greater quantum yield. The UVC emission from the

Rayonnet Photoreactor contains spectral overlap with (19), (20) and (22), specifically with  $\pi$ - $\pi^*$ , which confirms that photochemical excitation can occur and that photochemical reactions can proceed.

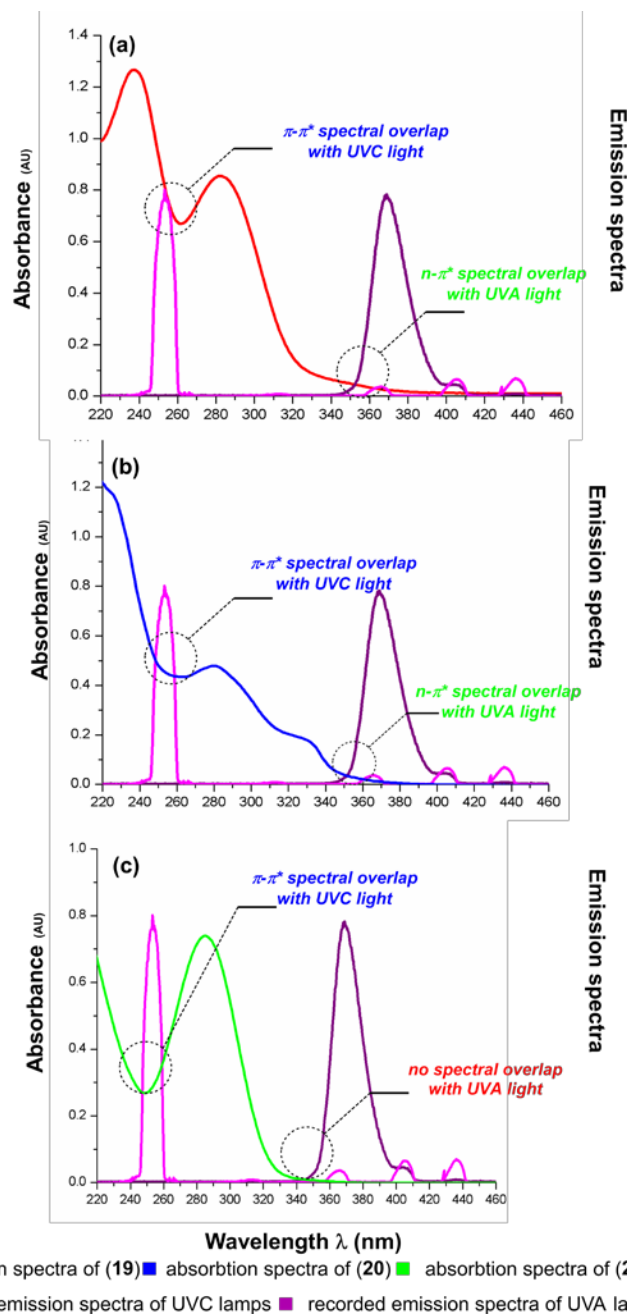


**Figure 12.** (a): Overlay of absorbance spectra of (19) with the normalized UVA and UVC emission spectra in the Rayonnet Photochemical Reactor. (b): Overlay of absorbance spectra of (20) (c): Overlay of absorbance spectra of (22).

## Photochemical interconversion and kinetics

The photoreaction experiments were followed by standard  $^1\text{H}$  NMR and irradiation for set time intervals. As the isomers **(19)**, **(20)** and **(22)** are present in measurable concentrations during the reactions, we used standard  $^1\text{H}$  NMR to follow the photoreactions and the reaction kinetics. Kinetics data for the interconversion of briareolate esters was achieved using Origin <sup>TM</sup> and ACD NMR software, monitoring the integration intensities of the corresponding 6H and 7H olefinic protons within the vinylic region ( $\delta$  5.6 – 7.8 ppm) of briareolate ester L **(19)** and G **(20)** and 2H pyran briareolate ester B **(22)** to determine the component distribution. The average of the olefinic proton integration (H6 and H7), which patterns do not overlap, enabled precise measurement of isomer ratios over time (Figure 13). The conversion (%) vs. time (min) data was plotted and “best-fit” equations determined to assess the kinetic profiles of the reactions. Best fit equations were determined with starting values chosen at random and refined by trial and error to obtain the best fit equations using the least squares method. All equations had a  $<0.999\%$   $R^2$  value (see Appendix A1 for supporting data).

Photochemical reactions with briareolate ester L **(19)** were performed in a solution containing 10mg/ml of briareolate ester L **(19)** in  $\text{CD}_3\text{OD}$ . For photochemical procedures with briareolate ester B **(22)** a vial containing (7.2mg/ 20mM) briareolate ester L **(19)**: briareolate ester G **(20)**: Briareolate ester B **(22)** (12:18:70) was dissolved in 720  $\mu\text{l}$  of  $\text{CD}_3\text{OD}$ .

Photochemical reactions under UVA irradiation were performed in a standard NMR tube with a solution containing (7.2mg/ml / 20mM) of briareolate ester L **(19)** or briareolate ester B **(22)** prepared in  $\text{CD}_3\text{OD}$  and placed directly in the spectrometer for



monitoring. All solutions were secluded from ambient light until time of use. UVC photochemical reactions were similarly prepared but were performed in quartz reaction vessels with aliquots transferred to NMR tubes for analysis. Samples were irradiated for set time intervals before NMR recording was performed.

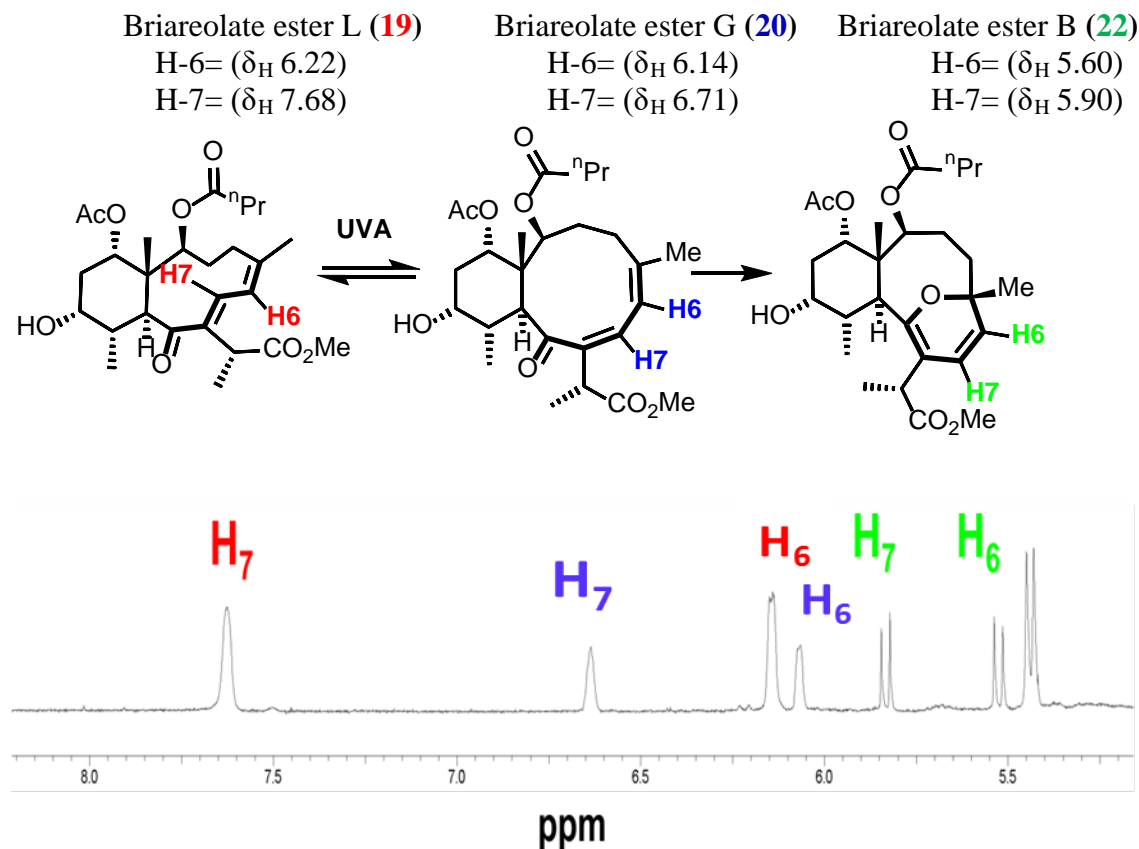


**Figure 13.**  $^1\text{H}$  NMR Chemical shift of H6 and H7 olfinic protons of briareolate ester L (**19**), briareolate ester G (**20**), and briareolate ester B (**22**) in ( $\text{CD}_3\text{OD}$ , 400 MHz).

### Photochemical Interconversion with UVC light

Under typical irradiation conditions to promote oxa-6 $\pi$  electrocyclization (UVC), we were unable to achieve the desired transannular, photoinduced electrocyclization (Figure 14). Instead, under UVC irradiation, briareolate (**19**) readily underwent isomerization to (**20**). Irradiation of a methanolic solution of (**19**) in a quartz reaction vessel delivered a mixture of the E,Z-dienone (**19**) and Z,Z-dienone (**20**) and reached a steady state equilibrium after 15 minutes. Interestingly, under UVC irradiation, the double bond isomerization was obtained with no obvious formation of (**22**). (Steady state ratio for 1:2:3 of 38:62:0). With the lack of spectral overlap of briareolate (**22**), we speculate that (**22**) is likely too labile under these conditions, and that the strongly absorbent dienolether chromophore may be also be photo excited under ( $\pi$ - $\pi^*$  transition) thereby enabling a rapid, facile retro-electrocyclization to deliver the mixture of (**19**) and (**22**) in a 37:63 ratio.

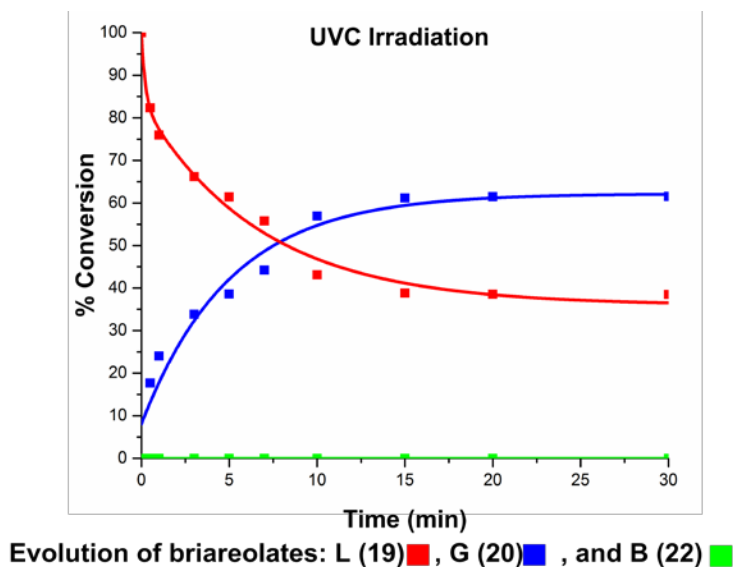


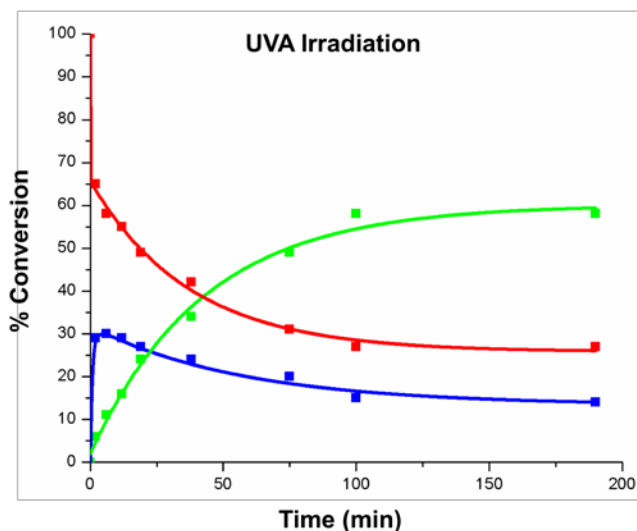
**Figure 14.** Photoirradiation of (**19**) in CD<sub>3</sub>OD [20 mM] under UVC light (254 nm) afforded a photostationary state of (**19**) and (**20**) (38:62 ratio) after 20 mins.

#### Photochemical Interconversion with UVA light

We next turned our attention to the photo-irradiation of **1** under UVA (Figure 15, 16, and 17). Irradiation of a methanolic solution of **1** in a Pyrex (or flint glass) reaction vessel delivered a mixture of dienones (**19**) and (**20**) as well as the desired (2H)-pyran **3** as the major product after 3 hours. (Steady state ratio for **19**:**20**:**22** of 27:14:57). Extended irradiation times did not result in full conversion in (**22**) as larger amounts of decomposition occurred over time. Under UVA irradiation, the isomerization of (**19**) to (**20**) takes place in minutes - rapidly reaching a novel, photostationary state (Figure 15, 16). This implies that the rate determination step of the cascade is likely the carbonyl C19 isomerization.

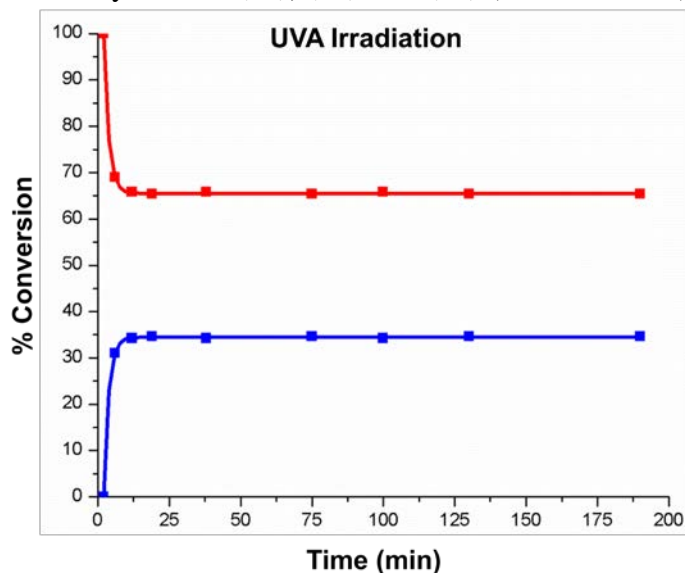
Interestingly, it was observed that isomerization between (**19**) and (**20**) under UVC conditions lead to a photostationary state (**19**) and (**20**) (37:63 ratio), whereas under UVA conditions, (**19**) is preferred to (**20**) achieving a photostationary state of (**19**), (**20**) (65:35) after 2 min, despite it being the thermodynamically less favored product. We attribute this to the intensity differences of both the molar absorptivity coefficient ( $\epsilon$ ) and the much more distinct  $n\text{-}\pi^*$  transitions observed. These intensity differences clearly generate differences in the photochemical reactions to cause wavelength-dependent quantum yield variations between all three species. This leads in turn, to the occurrence of significantly more photochemical reactions in (**20**) than in (**19**) to generate the experimentally observed photostationary state. As alluded to earlier, it is the  $n\text{-}\pi^*$  excitation which is responsible for pyramidalization which itself causes the rotation of the C19 carbonyl for placement inside the puckered macrocyclic space and enables the final step in which the thermal transannular  $6\text{-}\pi$  electrocyclization takes place. These results are unique in that a specific

n to  $\pi^*$  excitation mode was used to promote enone photo-isomerization and transannular oxa-6 $\pi$  electrocyclization.



Evolution of briareolates: L (19) ■, G (20) ■, and B (22) ■

**Figure 15.** Photoirradiation of (19) in CD<sub>3</sub>OD [20 mM] under UVA light (315-400 nm) afforded a photostationary state of (19), (20) and (22) (27:14:57 ratio) after 3 h.



Evolution of briareolates: L (19) ■, G (20) ■

**Figure 16.** Photoirradiation of (19) in CD<sub>3</sub>OD [20 mM] under UVA light (315-400 nm) afforded a photostationary state of (19), (20) (65:35) after 2 min.

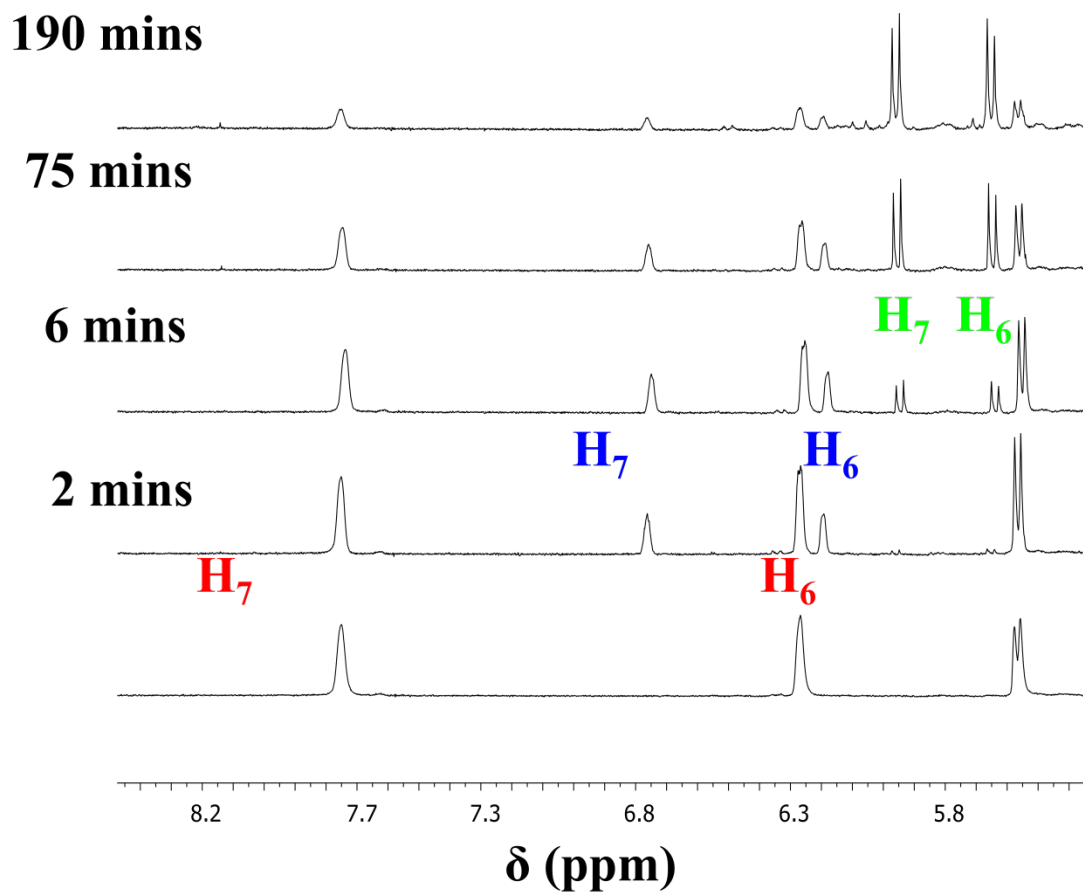
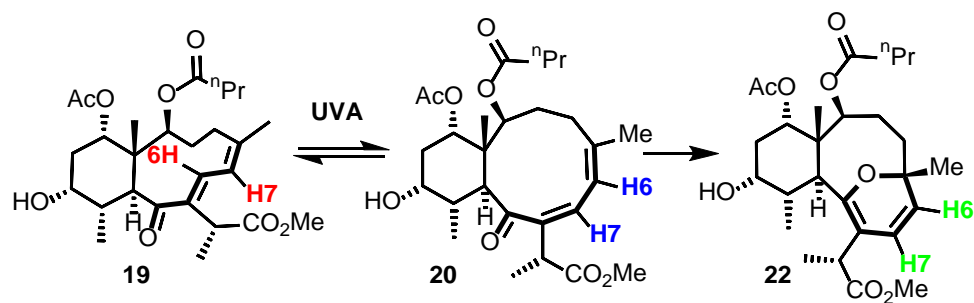


**Figure 17.** <sup>a</sup>Stacked overlay of selected <sup>1</sup>H NMR to monitor the photochemical reaction of **(19)** under UVA irradiation in an NMR tube;  $\delta$  values in CD<sub>3</sub>OD are reported. <sup>b</sup> After 3 hours, measurable decomposition can be observed.

### Retro-6 $\pi$ electro-cyclization with UVC light

Irradiation of pure briareolate ester B (**22**) under UVA showed neither reaction, nor degradation over the course of several hours. We therefore turned our attention to the photochemistry of (**22**) under UVC irradiation to evaluate the potential reversibility of the 6 $\pi$  electrocyclization. Under similar methanolic conditions, (**22**) underwent complete retro-6 $\pi$  electro-cyclization in 40 minutes to reach a photostationary state identical to that of the forward reaction from (**19**) also leading to the matching ratio between (**19**), (**20**) and (**22**) of 37:63:0 (see Figure 18). We attribute the lack of retro-6 $\pi$  electro-cyclization under UVA light to the lack of spectral overlap which itself would dictate an absence of photochemical reactions.

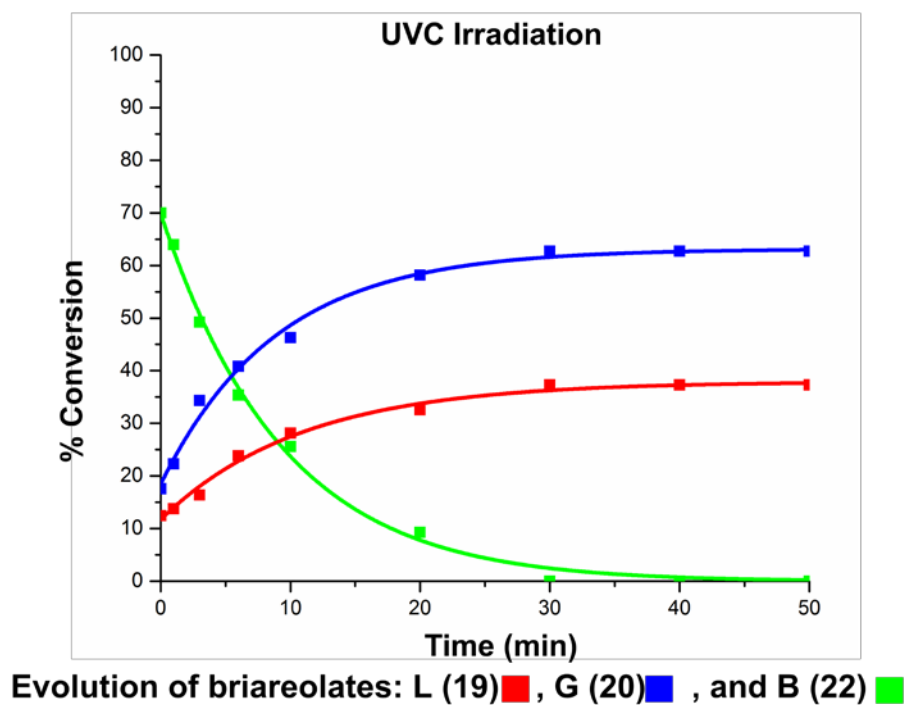


**Figure 18.** Photoirradiation of (**22**) in CD<sub>3</sub>OD [20 mM] under UVC light (254 nm) afforded a photostationary state of (**19**), (**20**) (37:63) after 40 min.

## Ground state interconversion

In order to assess the possibility of a ground-state, acid-mediated or thermal isomerization and  $6\pi$  electrocyclization sequence, we evaluated numerous conditions<sup>36e</sup>. Both natural products (**19**) and (**20**) were found to be thermally stable up to 150 °C as monitored through  $^1\text{H}$  NMR in  $\text{C}_6\text{D}_5\text{CD}_3$ , methanol,  $\text{CD}_3\text{OD}$  and  $\text{CDCl}_3$  (sealed tube; See materials and methods). Over time, decomposition was observed prior to any isomerization. As we reported previously, 1,4-conjugated additions can be achieved on (**19**) with various Lewis bases. With the addition of thiophenol this was readily achieved and stereoselectively delivered the macrocyclic enol<sup>56</sup>. Additions of Lewis or Brønsted acids to thioether did not promote the formation of (Z,Z)-isomer (**20**). Under acid-catalysis with TFA or PTSA, (**19**) remained untouched. However, in the presence of a large excess of these acids, (**19**) was slowly converted to (**20**) without ever generating the 2*H*-pyran (**22**). Instead, product (**33**) was cleanly delivered (Figure 21).

## Structural Elucidation of spiroketal $\gamma$ lactone (**33**) through Acid Catalysis.

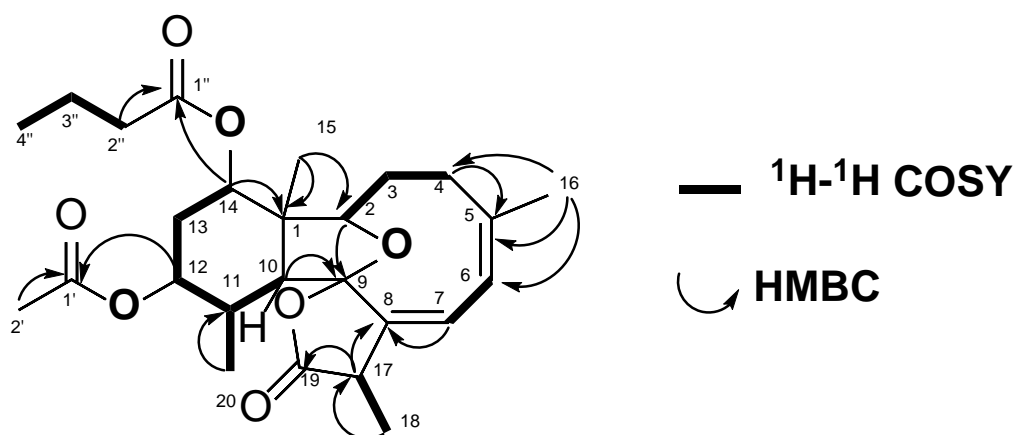
The HRMS of synthetic acid product (**33**) consisted of a mass HRESIMS  $m/z$  461.2532  $[\text{M} + \text{H}]^+$  (calcd. for  $\text{C}_{26}\text{H}_{37}\text{O}_7$ , 461.2539). Corresponding to the loss of 1 carbon, 4 hydrogen atom from the starting material (**19**) mass of 492.272, Briareolate ester L (**33**). Resonances attributable to all 26 carbons and 37 of the 37 hydrogens were observed in the  $^1\text{H}$  and  $^{13}\text{C}$  NMR spectra. A close inspection of the NMR spectra of Briareolate ester L (**19**) and synthetic product (**33**) revealed the similar nature of the two compounds, as expected, and allowed most carbons and hydrogens to be assigned by direct comparison of chemical shifts. These assignments were confirmed by HSQC, HMBC, and COSY correlations similar to those recorded on (**19**) and are summarized in

Table 2. Spectra analysis showed significant spectroscopic changes associated with C-1, C-2, C-6, C-7, C-8, C-9, C-10, and that the most significant changes were observed on C-2 ( $\delta_H$  4.5,  $\delta_C$  89.7), C5 ( $\delta_H$  5.8,  $\delta_C$  124.8), C8 ( $\delta_C$  139.3), and C9 ( $\delta_C$  112.7). Key HMBC correlation of C-9 to both H-2 and H-10, in addition to the diagnostic C-2( $\delta_H$  4.5,  $\delta_C$  89.7), provides evidence to support this acetyl/ hemiacetyl link in this position. This is consistent with clandelin-type molecules found in Briarium Asbestinin (**5**)<sup>22b, 57</sup> [42, 118-120] [42, 118-120] [42, 118-120] [42, 118-120] [42, 118-120] [42, 118-120] [42, 118-120] [42, 118-120] [42, 118-120] [42, 118-120] [41, 117-119]. Assignment of both the butonic ester and acetate were confirmed through long range HMBC correlations placing the acetate ( $\delta_C$  170.6) to C-14 ( $\delta_H$  5.07) and respectively the carbonyl present on the butanoic group ( $\delta_C$  173.6) to C-12 ( $\delta_H$  5.18). Changes to C-20 ( $\delta_C$  177.4) from ( $\delta_C$  173.2) and IR  $\lambda_{\text{vmax}}$  = 1738 respectively, is consistent with both lactone formation and the loss of the methyl ester from the starting material Briareolate ester L(**19**).

These results indicate that both the methyl ester and the C-2 Butanoic ester were hydrolyzed and the ester subsequently transferred to the C-12 position. The relative configuration of C-1, C-2, C-10, C-11, C-12, and C-14 were determined from coupling patterns in the  $^1\text{H}$  NMR spectrum. NOE correlations observed from H-6 to H-7 and H-16 established the geometry of  $\Delta^{6,7}$  Double bond. Correlations between H-18 and H-20 established the geometry of the spiroketal  $\gamma$  lactone which is in conjunction with the stereochemistry observed by the Ketal group assigned by the correlations of H-2 and H20 all of which provided confirmation of isomerization and lactone stereochemistry of the spiroketal  $\gamma$  lactone.

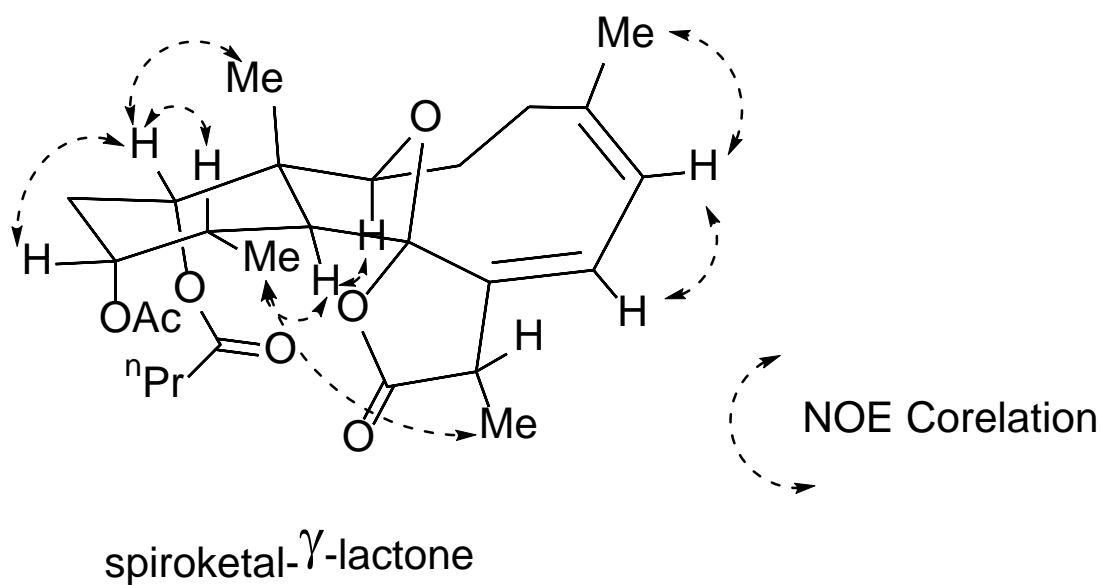


**spiroketal  $\gamma$  lactone (4):** isolated as colorless oil  $\lambda_{\text{max}} = 234 \text{ nm}$  ( $\epsilon$  3500) MeOH, 287 ( $\epsilon$  1713 HRESIMS  $m/z$  461.2532  $[\text{M} + \text{H}]^+$  (calcd. for  $\text{C}_{26}\text{H}_{37}\text{O}_7$ , 461.2539). IR  $\lambda_{\text{vmax}} = 2960, 2874, 1738, 1464, 1365, 1227, 1063, 103, 950, 738$ , Optical rotation  $[\alpha]_{\text{D}}^{18} -181.9$  ( $c$  0.008, MeOH)



spiroketal- $\gamma$ -lactone (33)

**Figure 19.** Observed COSY and HMBC correlation spiroketal  $\gamma$  lactone (4).



spiroketal- $\gamma$ -lactone

**Figure 20.** NOE correlations observed.

**Table 1:** NMR tables for spiroketal  $\gamma$  lactone (**33**), in (CDCl<sub>3</sub>, 400 MHz)

Pos.	$\delta_{\text{H}}$ (mult., $J$ in Hz)	$\delta_{\text{C}}$	COSY	HMBC	ROSEY
1	-	46.6 qC	-	-	-
2	4.45 (d10.7)	89.6 CH	3	1, 3, 9, 15	10
3 <i>a</i>	2.21 (m)	25.6 CH <sub>2</sub>	2, 4	1, 4	-
3 <i>b</i>	2.21 (m)	-	-	1, 4	-
4 <i>a</i>	3.16 (t, 12.1)	29.6 CH <sub>2</sub>	3	2, 3, 16	-
4 <i>b</i>	1.74(m)	-	3	2, 3, 5, 16	-
5	-	143.8 qC	-	-	-
6	5.7 (br s)	123.5 CH	7	5, 7, 16	7, 16
7	5.8 (br s)	124.8 CH	6	6, 8	6, 16, 18
8	-	139.3 qC	-	-	-
9	-	112.3 qC	-	-	-
10	4.10(d, 11.7)	39.2 CH	11	1, 9, 11, 20	2, 20
11	2.10 (m)	31.5 CH	10,12,20	10, 12, 20	12,14, 15
12	5.07 (br s)	73.5 CH	13	13,20 1'	15
13a	2.23 (m)	32.6 CH <sub>2</sub>	12,14	12, 14	-
13b	2.23 (m)	-	-	12, 14	-
14	5.18 (br s)	73.2 CH	13	15, 13, 1''	11,14 15
15	1.28, (s)	24.6 CH <sub>3</sub>	-	1, 2	11, 14
16	1.94 (s)	27.1 CH <sub>3</sub>	-	4, 5, 6	4, 6
17	3.52 (q, 6.0)	38.8 CH	18	8, 18, 19	-
18	1.37 (d, 6.7)	14.8	17	17	20
19	-	177.1 qC	-	-	-
20	0.71 (d, 6.7)	15.1 CH <sub>3</sub>	11	11	10, 12
Ester at C-12	-	-	-	-	-
1'	-	170.6 qC	-	-	-
2'	2.05 (m)	21.6 CH <sub>3</sub>	-	1'	-
Ester at C-14	-	-	-	-	-
1''	-	173.8 qC	-	-	-
2 ''	2.20 (m)	37.0 CH <sub>2</sub>	-	1'', 3''	-
3''	1.68 (m)	18.5 CH <sub>2</sub>	-	2'', 4''	-
4''	0.95(t, 7.0)	13.5 CH <sub>3</sub>	-	3''	-

### Mechanism and speculation on spiroketal $\gamma$ lactone (33) and ground state chemistry

Formation of the resulting product indicates that under strong acidic conditions isomerization does occur, and subsequent ester hydrolysis results in the formation of (33). The proposed mechanism occurs through first acid catalyzed acetate transfer from the C14 to the C12 position forming (34). This newly formed will subsequently undergo further ester transfer transferring the butanoic ester from the C2 to the C14 position forming (35). This newly formed C2 alcohol will undergo a transannular attack on the C9 carbonyl to generate the hemiacetyl (36). Subsequent hydroxyl formation in this hemiacetal will result in in hydroxyl mediated reduction of the methyl ester from this C9 position resulting in spiroketal  $\gamma$  lactone formation to form (37) the resulting spiroketal  $\gamma$  lactone (figure 21). It is unclear why both esters subsequently stereoselectively transfer to both the C12 and C14 positions however this was confirmed through HMBC correlations and thought to occur through subsequent steps(figure 19). The ease at which lactone formation occurs under acid conditions strongly indicates the epoxide methyl esters (18) are precursors to this lactone class of briarane (38). We speculate that through stereoselective dihydroxylation of epoxide (18) leads to (38) which can subsequently undergo hydroxyl-directed reduction to yield the commonly found briarane containing (7S, 8R) lactones (39) seen in figure 22.

It is clear from the ground state chemistry that isomerization is possible but the conformational restrictions imposed by the steric interactions of the carbonyl prevent it from entering inside the ring to form the s-cis cyclic transition state (21) required for electrocyclization which lead us to believe that photochemical parameters are the only way

of overcoming these energy requirements of generating this cyclic transition state with the carbonyl inside the ring (**22**).

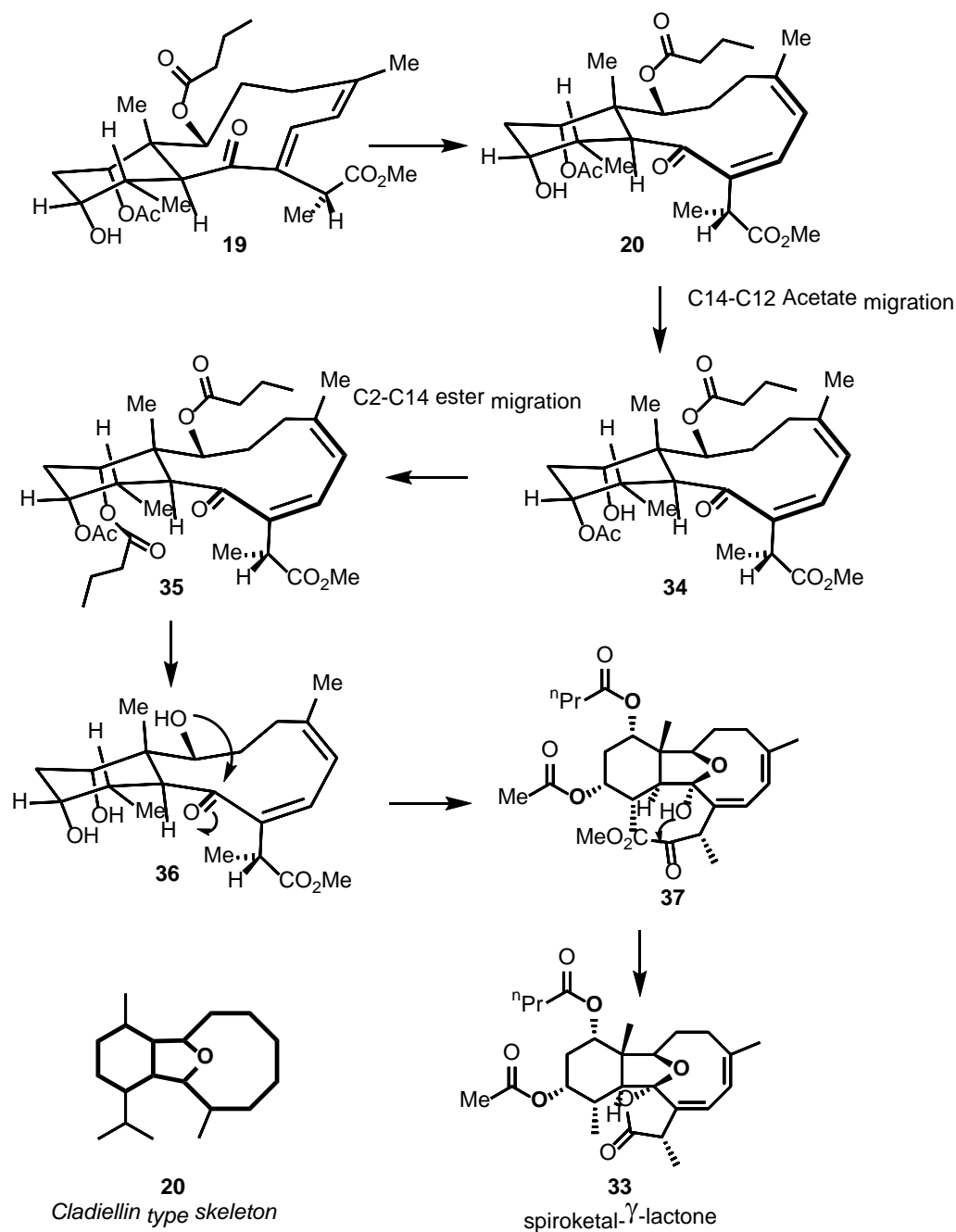


**Figure 21.** Proposed mechanism for acid product.

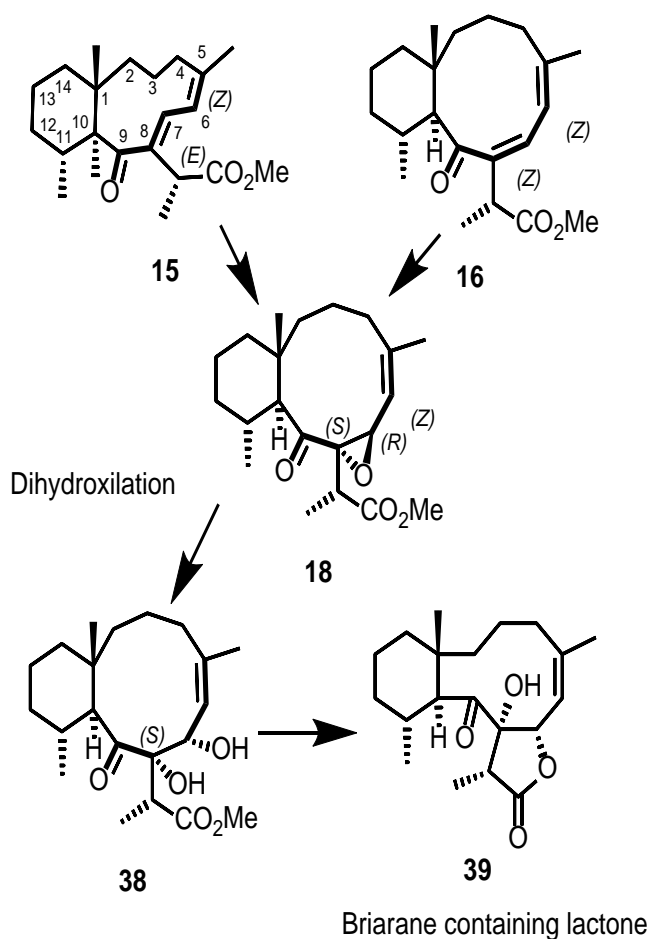


**Figure 22.** Proposed biosynthetic sequence for formation of briarane containing lactone.

**Conclusion:**

Through this work we successfully isolated these unique macrocyclic systems (19), (20), and (22). We believe that the macrocyclic chemistry on the dieneone (19) and (20) imparts a high strain to the system which facilitates the forward electrocyclization formation of the typical pyran product as is usually the case of both macrocyclic examples and typical dieneone systems<sup>34, 36e, 58</sup>. It is also believed that the steric strain and lack of free rotation imposed by the macrocycle inhibits free rotation thereby inhibiting the potential for the nucleophilic assisted methods of isomerization which are typical of enzyme based methods<sup>56b, 59</sup>. Ground-state acid catalysis also failed to achieve

a similar sequence of isomerization from **(19)**, but instead enabled the synthesis of a new acid scaffold **(33)** related to the cladielin natural product. This offers interesting insight into the biosynthetic steps involved, but further supports the likelihood that electrocyclization is inhibited due to the lack of free rotation of the carbonyl.

It is believed that the alkyl substitutions on both  $\alpha$  positions of the dieneone induce steric interactions making interconversion between these species rather high as is typically the case making these particular macrocyclic dieneones stable in the absence of light<sup>34</sup>. The results of the conformation are consistent with destabilization of the s-cis conformer **(21)** and only the s-trans dienones **(20)** are produced. These are stable and therefore inhibit electrocyclization<sup>34</sup>.

Under the correct photochemical parameters however, we easily overcame the energy requirements for this unique macrocycle with regards to the isomerization and rotation of the carbonyl (s-trans or s-cis) by putting it inside the ring puckered thereby facilitating electrocyclization - specifically under UVA light.

Through this work we identified a novel, UV-selective, photochromic switch that transforms briareolate esters L **(19)** to B **(22)** and vice versa via the intermediate Briareolate G **(20)**. For the first time a UVA/UVC photochromic switch has been shown to enable both forward and retro  $6\pi$  electro-cyclizations on demand in a transannular fashion and represents the first photochemical, transannular  $6\pi$  electro-cyclizations demonstrated. The unusual excitation of the  $n-\pi^*$  transition from **(19)** or **(20)** with selective UVA light was determined as critical in facilitating the forward electrocyclization. It is believed the  $n-\pi^*$  transition is responsible for putting the carbonyl in sufficiently close proximity inside the ring to facilitate the electrocyclization. As the

forward and retro electrocyclization both occur under UVC, due to spectral leakage in the UVA region under UVC light parameters, it is believed that the high energy postulated intermediate (Z,Z)-s-cis-dienone rotamer (**21**) is unfavored with respect to the rate at which it is created and is able to undergo the forward electrocyclization at a comparable rate to the retro electrocyclization which occurs with (**23**). Under these UVA conditions, we show (**23**) does not absorb light and thus switches off the competing retro electrocyclization – allowing for a kinetic sink and the observable formation of (**23**). Our work provides significant evidence of the unique photochemical properties associated with the exclusive excitation of the n- $\pi^*$  spectral band which enables carbonyl rotation inside the macrocyclic ring to facilitate the oxa-6 $\pi$  electrocyclization<sup>60</sup>. Our results strongly imply that these briareolate esters are produced entirely photochemically in their natural habitat and are the only methods by which the large energy requirements for these transformations can be overcome<sup>36e</sup>. In light of the effectiveness of this novel UVA/UVC photochromic switch approach, this work likely revises the original biosynthetic proposal of briarane diterpenes and provides a unique strategy for laboratory preparation of medium-sized ring macrocycles through photo-induced retro-6 $\pi$  electrocyclization of bridged (2H)-pyrans<sup>31b</sup>. The work offers significant mechanistic insight into photochemical oxa-6 $\pi$ -electrocyclization of macrocyclic dienone systems which will assist with the development of numerous applications in organic chemistry, photo pharmacology, optigenetics, and a variety of industrial applications<sup>47c-f</sup>.

### Chapter 3: Isolation of Marine Natural Products Protective against Oxidative Stress

#### **Introduction**

Oxidative stress and reactive oxygenative species have been implicated in a variety of neurological disorders such as amyloid lateral sclerosis, heart attack, stroke, Alzheimer's disease and a variety of other neurological disorders<sup>61</sup> and novel antioxidants are now being used as potential therapeutic agents to treat and manage such disorders<sup>62</sup>. Marine organisms, such as microalgae and other invertebrates have been shown to produce completely novel antioxidants<sup>63</sup>. However, research in this field has largely focused on the antioxidant effects of crude extracts<sup>64</sup>. The premise of this work was to use activity-guided isolation protocols to identify new chemical entities from marine organisms which can be subsequently subjected to pharmacological evaluation. To isolate marine natural products with strictly antioxidant potential we chose a standard assay guided isolation protocol, specifically the ferric reducing ability (FRAP) assay. The FRAP assay was attractive for two reasons (1) it was simple, fast and efficient which enables activity-guided isolation of a large library of extracts attainable in a reasonable amount of time and eschews the need for expensive robotics. (2) The FRAP assay allowed direct analysis of the extracts<sup>65</sup>. This assay therefore, serve as an ideal platform for activity-guided isolation from our marine organism collection.

The work covered in this chapter largely concentrates on the bioassay guided isolation of marine extracts from our marine organism's collection from the western



Atlantic. These organisms were extracted using a developed cyclic loading technique in order to generate a library of enriched crude extracts for bio-activity screening. Fractions were then assayed using the ferric reducing ability of plasma (FRAP) assay in order to measure "antioxidant power" and to develop a putative index of antioxidant potential, the results of which enabled selection and prioritization of organisms thereby allowing us to focus on the isolation of marine natural products that are actively antioxidant <sup>66</sup>. Additionally through previous work we were able to identify that Pseudopterosins from *Pseudopterogorgia elisabethae* showed potent antioxidant activity, with that our goals were to isolate and confirm these compounds as well as subject these compounds to further pharmacological scrutiny surrounding neurological disorders.

### **Oxidative Stress**

Oxidative stress is a term used to describe small molecules, containing oxygen, that are free radicals or are oxidizing agents that are easily converted into radicals<sup>67</sup>. They represent any molecule containing oxygen with an unpaired electron. These species are high energy and seek equilibrium by oxidizing the nearest molecule/biomolecule <sup>67</sup>. The radicals are produced as a byproduct from many common biological processes like membranous enzymes, hemo-enzymes containing  $\text{Fe}^{2+}$ , and enzymes containing  $\text{Cu}^{2+}$  atoms <sup>68</sup>. In the body, the largest production of these ROS occurs from mitochondrial respiration, mainly in the form of superoxide and  $\text{H}_2\text{O}_2$  <sup>69</sup>. These free radicals are also naturally generated in other ways such as from high temperatures, UV light exposure and other ionizing radiation which, in turn, generates these highly charged reactive species. Free radicals contribute to protein and deoxyribonucleic acid (DNA) injury, inflammation, tissue damage, and consequently to cellular apoptosis <sup>61b-g</sup>. ROS's are not

universally harmful and can have important beneficial roles such as in cellular signaling, neuronal synaptic transmission <sup>67, 70</sup> and cellular protection from ischemic preconditioning <sup>71</sup>.

Oxidative stress/ reactive oxygen species (ROS) has however, been implicated in a number of neurological disorders such as Parkinson's disease, aging, amyotrophic laterals sclerosis (ALS), dementia, and Alzheimer's disease (AD) <sup>61a, 72</sup>. Phenolic compounds like, flavonoids, quinons, coumarins, lignans, stilbenes, tannins and nitrogen-containing compounds such as alkaloids, betalains and many others, have been identified as rich sources of antioxidant activity<sup>73</sup>. Some of these novel antioxidants are now regarded as persuasive therapeutic agents against ROS and related diseases <sup>73-74</sup>.

### **Antioxidants**

An antioxidant is any substance, present at low concentrations, that can significantly prevent oxidation by neutralizing radicals through either direct radical scavenging or by evoking a complex biological response <sup>75</sup>. Since free radical production is an inevitable function of metabolic activity, we have evolved a complex system for the defense against their damaging effects <sup>61e, 67, 76</sup>. We have complex biological systems, such as the Nrf 2 pathway, which when activated promotes the release phase II detoxifying enzymes that can quickly neutralize free radicals by increasing production of detoxifying enzymes that neutralize ROS effectively and efficiently when compared to conventional radical scavenging <sup>77</sup>. There are two main types of antioxidants: Those that prevent the generation of ROS, and those that intercept and neutralize them <sup>78</sup>. Recognition of upstream and downstream antioxidant therapies for oxidative stress have proven effective tools against the alteration of any neuronal damage <sup>73, 79</sup>.

An area of significant focus in antioxidant research surrounds the treatment and evaluation of a broad, terrestrial-based, phenolic flavonoids, a variety of ROS related neurological disorder, which has yield promising results <sup>80</sup>. Catechols, and phenols in general, have the ability to act as direct radical scavenger. Furthermore, there have been several examples, such as in the case of ECGC and curcuminoids that have been shown to provide protection against oxidative stress by evoking unique, biological mechanisms such as the Nrf2 pathway, by increasing the production of detoxifying enzymes. As such, they serve as unique therapeutics for neuronal protection and treatment of neurologically-related diseases <sup>81</sup>. Catechol-based curcuminoids and ECGC have been intensely studied with regard to their antioxidant potential and ability to counter a variety of neurological disorders by exhibiting unique mechanisms of action which play dual roles in the therapeutic research of Alzheimers <sup>82</sup>. Both phenols show neurological protection from oxidative stress induced by amyloid beta plaque formation and also an ability to inhibit plaque formation; thereby inhibiting the development of oxidative stress <sup>61c, 83</sup>. Vitamin E has also proven beneficial in combating neurodegenerative diseases in clinical trials and is now used in most treatments of neurodegenerative disease <sup>84</sup>. Currently, natural products such as Curcumin and Resveratrol, which contain phenols, have been shown to have neuroprotective properties and appear extremely effective against oxidative stress in neuronal related disease models <sup>85</sup>. The results of these studies clearly imply that the study of antioxidant marine natural products, and their evaluation as therapeutic probes for a variety of neurological disorders related to oxidative stress and related diseases, is promising area of research to pursue <sup>61b, c, 86</sup>. As many terrestrial-based antioxidants have been able to show dual roles as novel antioxidants protective against neurotoxic ROS and

an ability to modulate Alzheimer's amyloid plaque our goal was to screen the compounds isolated during the course of this study on various neurologically related disease to give preliminary justification to warrant further pharmacological exploration.

### **$\alpha\beta$ -Amyloid plaque and Alzheimer's Disease**

Alzheimer's disease (AD) is neurodegenerative disease which exhibits disease-specific neuropathological changes. According to the CDC in 2013, as many as 5 million Americans were living with AD and worldwide, it is currently thought to afflict as many as 20 to 30 million people<sup>43, 87</sup>. Scientists do not yet fully understand the causes of AD and there is little to no effective treatment<sup>88</sup>. The Amyloid Cascade Hypothesis however, is now considered a major pathology for the disease<sup>89</sup>. It involves the formation of oligomers of amyloid-beta, which subsequently polymerize to form plaque deposits on the brain. The formation of these plaques creates a neurotoxic environment through the generation of toxic species; specifically with the generation of ROS through mitochondrial dysfunction which causes neuronal cell death. The formation of these plaques is now thought to be one of the most critical factors in the development of AD and therapeutics that effectively inhibit  $\alpha\beta_{40}$  plaque formation and/or reduce the levels of consequent neurotoxic effects would be of significant help in combating this widespread and growing disease<sup>90</sup>. Through this work our goals were to isolate these marine natural products and determine if their was potential therapeutic applications for these small molecules and to provide preliminary, structural studies with the purpose to justify further experimentation and evaluation with regard to neural degeneration related disease.

## Marine Antioxidants

Marine organisms are exposed to some of the harshest environments on the planet and experience relatively high levels of ROS as a result. Photosynthesis, symbiotic oxygen production, and intense levels of sunlight all lead to free radical production<sup>91</sup>. In the ocean, a strong and clear correlation is evident between those organisms that undergo high levels of exposure to ROS and the effectiveness of the antioxidants produced by that organism<sup>92</sup>.

As with all evolutionary processes, if an organism is exposed to particularly high levels of ROS they will almost certainly evolve effective, antioxidant mechanisms<sup>64, 93</sup> and research development in the marine antioxidant field has recently enabled antioxidant screening of pure compounds and semi pure fractions, as opposed the screening of crude extracts that was typical in earlier antioxidant research<sup>64</sup>. Marine organisms, such as microalgae and other invertebrates, have been shown to produce completely novel antioxidants<sup>94</sup> which underscores the potential for marine natural product compounds in treating oxidative stress- related, neurodegenerative diseases. The goal of this project was to screen these compounds in various pharmacological assays in order to evaluate their therapeutic potential<sup>95</sup>.

## Antioxidant Assays

For the success of this project measurement of antioxidant capacity was of critical importance. The assays used may be categorized into two main groups: (1) those that measure *direct* antioxidant abilities on a specific substrate and, (2) those that measure these compounds in a biological setting (*in- vivo* and *in- vitro*). Both categories have value, but each has its own advantages and disadvantages. The intent of the project was

to identify a simple assay that would enable the quick identification of antioxidant bio-activity and the purification of the identified leads.

Most direct methods measure the extent of inhibition of free radical generation by the antioxidants present in the sample and are predominantly based on different free radical generators, a target molecule, endpoints and comparison to a known standard such as Trolox <sup>96</sup>. Consequently, response to the antioxidants will depend on the specific assay chosen. There are however, relative advantages and disadvantages inherent in each assay and these will vary according to the situation and the type of study undertaken.

The Total Radical Trapping Antioxidant Parameter (TRAP) assay was one of the first antioxidant capacity assays developed and since its introduction numerous assays have become available <sup>97</sup>. While TRAP is fast and convenient, it is of limited value in determining fat soluble antioxidants. The Chemiluminescence Antioxidant Capacity (AOC) assay provides an ability to distinguish between the effectiveness of certain antioxidants, however, it is not truly representative of oxidative stress in an actual biological setting <sup>96,98</sup>. The Oxygen Radical Absorbance Capacity (ORAC) assay offers high specificity using a physiologically important radical but the various extraction techniques required in ORAC assay is cumbersome when trying to screen a large library of compounds <sup>99</sup>. In addition, the ORAC index is unclear when evaluating antioxidant potential as the results will vary as they are dependent on the specific free radical used. The results of other methods correlate better for reactive ROS. The Trolox Equivalent Antioxidant Capacity (TEAC) assay assesses the degree of free-radical inhibition at set time intervals in order to standardize the antioxidant capacity. This is a limiting factor when evaluating potential antioxidants that may work at a slower rate or may work in a

unique mechanistic way<sup>100</sup>. The TEAC assay can be used to measure antioxidant capacity of both hydrophilic and hydrophobic substances, but suffer from nonlinear results with sample dilution.

Several other assays exist, each having its own, particular advantages and disadvantages. Many of them have been widely used and are accepted for their specific applications<sup>97b</sup>. The FRAP assay in particular was attractive due to the fact that it is simple, fast, reliable, rugged and offers the ability to screen extracts directly and it was this ease of use which made it ideal for the purpose of our study on assay-guided isolation.

### **Ferric Reducing Antioxidant Power (FRAP) Assay**

Total antioxidant activity is measured by the Ferric Reducing Antioxidant Power (FRAP) assay. FRAP uses antioxidants as reductants in a redox-linked colorimetric method which involves Fe III to Fe II reduction/oxidation<sup>97b</sup>. At low pH, the ferric tripyridyl triazine (Fe III TPTZ) complex reduces to the ferrous form and is monitored through absorbance at 593 nm. The relevant chemical reaction of the FRAP method involves a single electron reaction between Fe (TPTZ)<sub>2</sub> (III) and an antioxidant (electron donor) such as Trolox<sup>97b, 101</sup>. The FRAP assay can be performed on a wide range of complex biological fluids, including aqueous and methanolic extracts from plants and marine organisms, as well as solutions of purified antioxidants<sup>66a</sup>.

## **Pseudopterosin Chemistry from the Caribbean octocoral *P. elisabethae*.**

Through previous research in the West laboratory pseudopterosins from the Caribbean octocoral *P. elisabethae* were shown to show antioxidant activity on the FRAP assay as well as the ability to cross the blood brain barrier through pharmacokinetic data we believed this presented an excellent area of study for these natural products in which we were to isolate pseudopterosins in sufficient quantity and from specific geographic locations to enable pharmacological evaluation across multiple assays, in order to assess potential therapeutic applications for these compounds <sup>102</sup>. Although the overall aim of this research was to find compounds that could counteract the detrimental effects of ROS/RNS to promote neuronal survival, however many human clinical studies involving direct radical scavengers has proven to be ineffective <sup>103</sup>. Caribbean gorgonian octocorals of the genus *Pseudopterogorgia* are both abundant and chemically rich. Many of the compounds isolated from these marine invertebrates are of great interest because of their structural complexity and pharmacological potential [92]. Pseudopterosins, a class of secondary metabolite compounds, exhibit an immense variety of biological activity from anti-inflammatory, analgesic <sup>104</sup>, antimalarial <sup>105</sup>, wound healing <sup>106</sup>, antibacterial <sup>106a, 107</sup> and many others <sup>104b, 104d, 105, 108</sup>. Pseudopterosin A methyl ether a semisynthetic derivative of pseudopterosin presented anti-inflammatory, In double blind phase II clinical trials pseudopterosins increased reepithelization accelerated the wound healing process <sup>109</sup>. Pseudopterosins have even made their way into commercial use, where partially purified extracts containing pseudopterosins are incorporated in cosmetic skin care products <sup>104a, 110</sup>. Recent evidence in our own laboratory, through the use of the FRAP assay, shows that pseudopterosins can serve as antioxidants, making these compounds a promising



area of study in the treatment of neurological disorders which result from oxidative stress<sup>102</sup>.

Pseudopterosin diterpene Pseudopterosins A-D (**41-44**) were first isolated from samples collected in the Bahamas by Fenical and collaborators from *P.elisabethae* (see figure 34)<sup>104a, 111</sup>. Since then *P. elisabethae* has yielded 26 pseudopterosins (PsA–PsZ) isolated from specimens collected in the Bahamas<sup>111</sup>, Bermuda<sup>104d</sup>, the Florida Keys<sup>112</sup>, and the Columbian Caribbean<sup>104d, 113</sup>.

In light of the strong precedence for promising biological activity exhibited by this class of compounds, sufficient quantities of pseudopterosins, were isolated and were then subjected to various biological assays for assessment. The previously mentioned ability of these compounds to serve as antioxidants prompted us to undertake further screening in *in-vivo* studies on *Drosophila Melanogaster* where they were assessed for their ability to protect against neurodegradation under oxidative stress and, more specifically, mitochondrial dysfunction resulting in ROS.

#### **Marine Organism Collection for Activity Guided Isolation:**

The isolation of marine extracts began with collection of samples from off the coast of Islamorada, Florida (see Figure 23). Various fragments of representative species were collected by hand at mangrove channels from Islamorada, Florida Keys (Figure 24). Sample collection did not involve the removal of whole colonies; but only portions of individual organisms. The organisms were cut from the main axis with sharp scissors. Organisms were immediately labeled and stored in a freezer. Prior to extractions, samples were subjected to freeze drying in order to remove all residual water contained within the organism.



**Figure 23.** Map of the hydrography of the collections region in Islamorada, Florida.

**Source:** “Islamorada, Florida” 24.9358° N, 80.6136° W. Google Earth September 20, 2015

### **Isolation and screening of marine extract for antioxidant activity**

In order to streamline the analysis of our collection of marine organisms, a small-scale standardized solid phase extraction (SPE) was used to enable rapid fractionation of multiple samples. These were then screened and prioritized for scale-up isolation after initial evaluation of antioxidant activity of the extracts. The crude fractionation of the 50+ organisms collected and extracted using a solid phase extraction (SPE) 12-port vacuum manifold allowed fractionation of multiple samples. The extracts were fractionated into three fractions - polar, medium-polar and non-polar. These “enriched” fractions were then examined using nuclear magnetic resonance (NMR) for the presence of novel compounds and screened for antioxidant activity. Samples of each fraction were loaded onto 96-well plates with FRAP reagent. (Figure 24) Activity was compared

to the linear calibration curve from Trolox standards of known concentrations to compare relative antioxidant ability and aid in the selection and prioritization of our compounds.



**Figure 24.** Small scale extraction and extract enrichment procedure.

Source: Andrew Hall 2013

### **FRAP protocol verification**

The FRAP method has the ability to quantify the amounts of total antioxidants or reductants in extracts. The FRAP assay is also the only assay which directly measures antioxidants or reductants in a single sample. The first step, to verify the assay, was performed correctly. In order to do this we compared the standard assay to that of a serial dilution of the stoichiometric antioxidant Trolox to verify a linear relationship between antioxidant capabilities compared to concentration (Figure 25). A direct linear relationship confirming the reliability and that the experimental protocol was accurate, thereby indicating that this assay would properly assess the antioxidant activity of our extracts and lead us to the isolation and screening of our Islamorada collection.

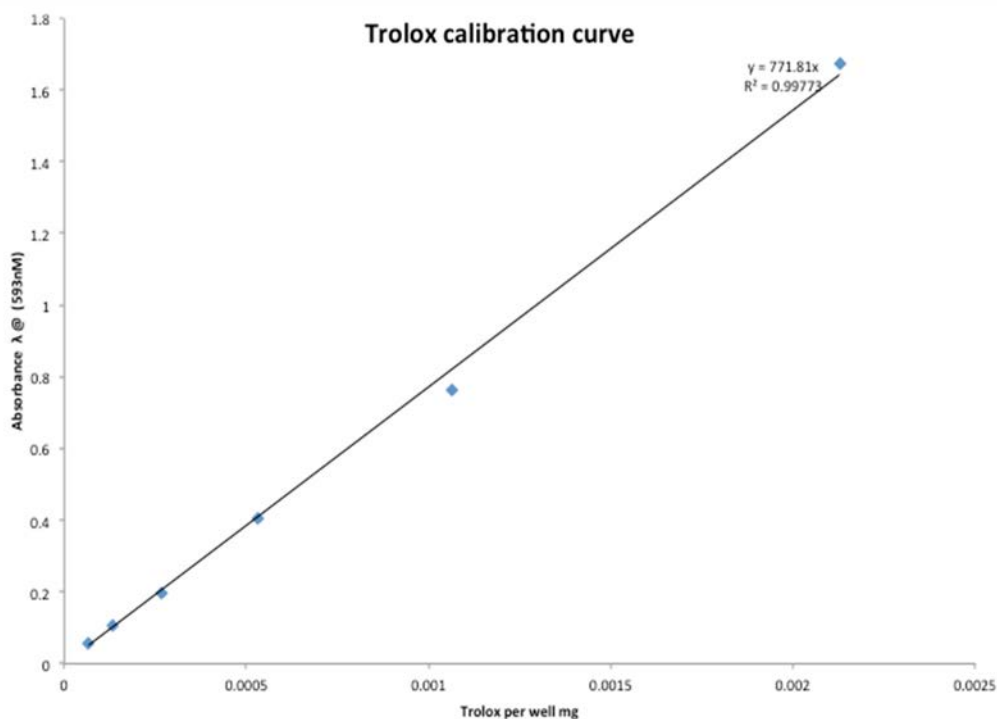
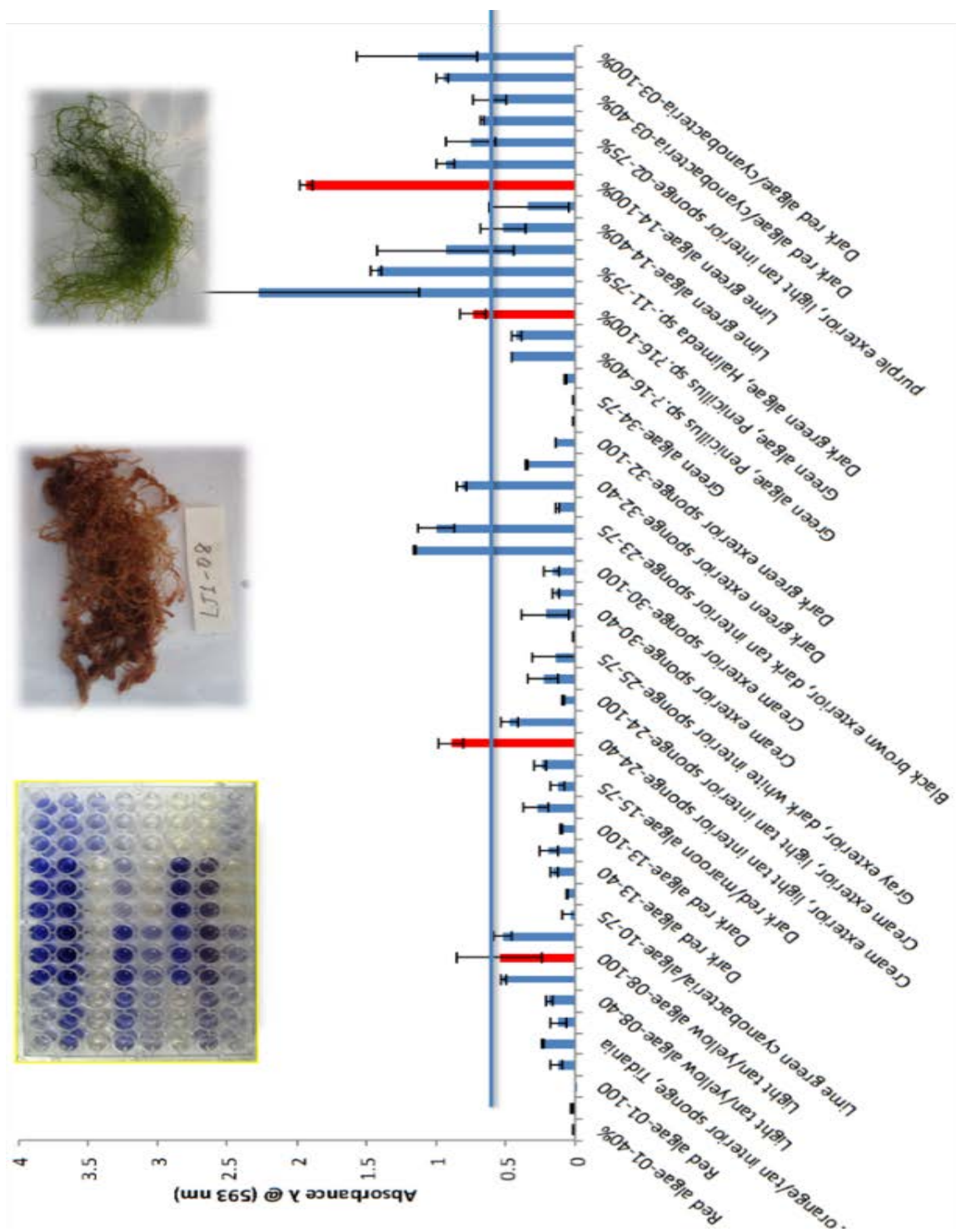


**Figure 25.** An example of a standard curve generated using concentrations of Trolox.

### Activity guided isolation from marine extracts

As previously indicated these “enriched” fractions were then examined for the presence of novel compounds that show antioxidant activity. The results from the samples fraction assayed with FRAP reagent, was assessed by comparing the relative absorbance value of the extract with that of the trolox values. The results indicated only two potential organism extract with sufficient enough activity relative to antioxidant activity that warranted further study and isolation. The two organisms were *Halimeda* (which has already been extensively studied) and green algae (phylum: chlorophyta and subphylum chlorophytina). It was these algae which were ultimately selected for workup. Active fractions were subject to 1D and 2D NMR along with HPLC analysis. Preparative HPLC separation was performed using an evaporative light scattering detector (ELSD).



### Isolation of 1-O-palmitoyl-2-O-myristoyl-3-O-(6-sulfo- $\alpha$ -D-quinovopyranosyl)-glycerol

Specimen LJ-14 showed the strongest antioxidant activity that leads us to the selection of this sample for the identification of the bioactive components. Through taxonomic identification we were able to identify this species, (seen in Figure 27) as belonging to the Phylum: Chlorophyta and Subphylum *Chlorophytina pithophoraceae*.



**Figure 27.** Marine algae (LJ-14) collected from Islamorada, Florida Keys.

The specimen LJ-14 (26 g dry wt.) was extracted with MeOH and fractionated on polymeric HP-20 chromatographic support into three fractions (40, 75, and 100%  $(\text{CH}_3)_2\text{CO}$  in  $\text{H}_2\text{O}$ ). The fractions were then subjected to  $^1\text{H}$  NMR to identify the presence of unusual metabolites. The 75%  $(\text{CH}_3)_2\text{CO}$  in  $\text{H}_2\text{O}$  fraction found to contain the presence of proton signals indicating the presence of a glycoside were subjected to repeated preparative  $\text{C}_{18}$  HPLC using a gradient elution from 20-100%  $\text{CH}_3\text{CN}$  in  $\text{H}_2\text{O}$  to yield compound **(40)** (LJ-14-75-F9; 9.6 mg).

#### **Structural elucidation of sulfo- $\alpha$ -quinovopyranosyl glycolipid (40)**

Compound (**40**) was isolated as a colorless oil with a HRMS  $[M + H]^+$  765.4882 (calculated for  $C_{39}H_{73}O_{12}S$ ). Careful analysis of the  $^1H$ - and  $^{13}C$ -NMR data including  $^1H$ - $^1H$  COSY, TOCSY, DEPT, and HSQC spectra, allowed the assignment of all  $^{13}C$ - and  $^1H$ -NMR signals (Table 2). Three spin systems were recognized, the first one was assigned to a glycerol moiety  $\delta_H$  4.34 and 4.14 ( $\delta_C$  63.5);  $\delta_H$  5.13 ( $\delta_C$  70.2);  $\delta_H$  3.89 and 3.34 ( $\delta_C$  65.8). The second spin system signals were attributable to two fatty acyl groups whose terminal methyl signals appeared overlapped at  $\delta_H$  0.84. The third spin system indicated the presence of a glycosyl moiety. The methylene protons at  $\delta_H$  2.90 and 2.54 showed attachment to the same carbon in agreement with the signal at  $\delta_H$  3.77, indicating that all these signals belongs to an hexapyranose. The relative small coupling constant value of the anomeric proton (H-1''),  $J = 3.5$  Hz, indicated  $\alpha$  orientation of the glycosidic union, while the large vicinal coupling seen indicated the glucopyranosyl nature of the sugar moiety. The presence of a 6'''-sulfo- $\alpha$ -quinovopyranosyl was determined on the basis of HRMS and non-decoupled HSQC in which both 6H protons showed a  $J_{CH} = 148$  Hz which is consistent with sulfo-quinovopyranosyl (Figure 28 and 29) <sup>114</sup>.

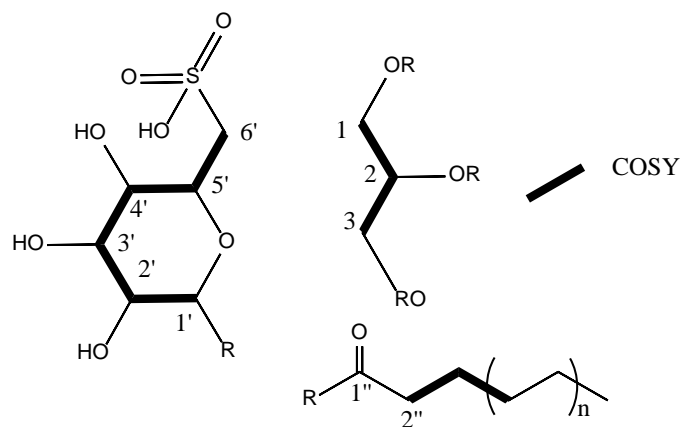


**Figure 28.** Key COSY correlation compounds (40)

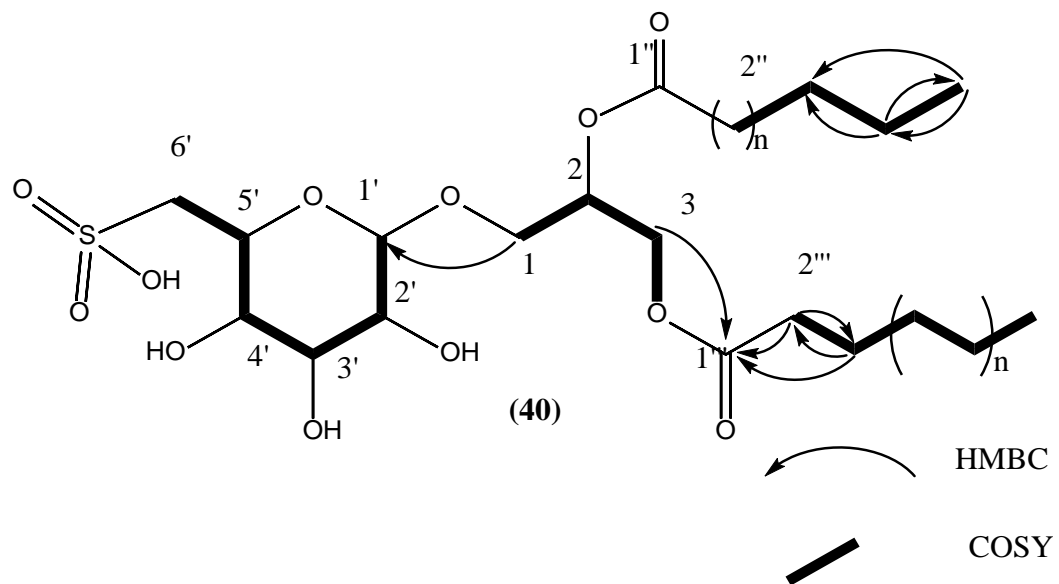


**Figure 29.** Key HMBC correlations



**Table 2:** NMR table for 1-O-palmitoyl-2-O-myristoyl-3-O-(6-sulfo- $\alpha$ -D-quinovopyranosyl)-glycerol(**40**), Recorded in CD<sub>3</sub>OD, 400 MHz, chemical shifts, multiplicity and coupling constants (*J*, Hz) were assigned by means of <sup>1</sup>H, <sup>13</sup>C NMR and 2D NMR data.

Pos.	Synthetic Product (33)		COSY	HMBC
	$\delta_H$ (mult., <i>J</i> in Hz)	$\delta_C$		
Glycerol	-		-	-
1 $\alpha$	4.34 d	63.5	1b',2	2,3,1'''
1 $\beta$	4.14 dd (11.93,7.63)	-	1a,2	2,3,1'''
2	5.13 (d 5.09)	70.2	1b,3a,b	1,3,1''
3 $\alpha$	3.89dd (10.37,6.06)	65.8	3b	1',1,2
3 $\beta$	3.34 (m)	-	2,3a	1'1'2
Sugar				
1'	4.57 (d 11.3)	98.8	2'	3,5',3'
2'	3.18 (m)	72.1	1',3'	4'
3'	3.33-3.41 (m)	73.6	2',4',5	1',5'
4'	2.9 (m)	74.8	3',5'	6',2'
5'	3.77(m)	69.3	6'a,b, 4'	1',3'
6 $\alpha$ '	2.54 (dd,14.1, 7.0)	54.4	5', 6'b	4',5'
6 $\beta$ '	2.92dd (11.9, 7.6)	-	5',6'a	4',5'
Fatty acid				
1''		173.2		
2''	2.25d (m)	39.3	3''	1''
3''	1.48 (brs)	33.2	2''	1''
4''-15''	1.23 (brs)	20.7-3		
16''	0.84 (t, 6.5)	14.3		
Fatty acid				
1''		173.2		
2''	2.25 (d)	39.3	3'''	1'''
3''	1.48 (brs)	33.3	2'''	1'''
4''-13''	1.23 (brs)	20.7-9.0	-	2,3,1'''
14''	0.84 (t, 6.5)	14.3		2,3,1'''
3''	1.68 (m)	18.5	-	2'', 4''
4''	0.95 (t, 7.0)	13.5	-	3''
C14- ester	-		-	-
1'	-	170.6	-	-
2'	2.05 (m)	21.6	-	1'

With the planar structure established, confirmation of the fatty acid chain was required. To do this we employed the use of fatty acid methyl esters (FAMES) analysis<sup>115</sup>. This is a common technique used for determination of fat content and fatty acid profiles in foods. The triglycerides, which cannot be analyzed directly by gas chromatography (GC), were first hydrolyzed and derivatized into their corresponding methylesters. In this process KOH is the presence of methanol to hydrolyze the ester bonds and the free fatty acid and in the process they converted to the corresponding FAMES<sup>115-116</sup>. FAMES are moderately polar and sufficiently volatile to be determined by GC analysis. Confirmation was achieved by GC analysis and standards, and the presences of both mystric acid and palimitic acids were noted. (Figure 3.8)<sup>115-116</sup>.

## GC-FID Analysis

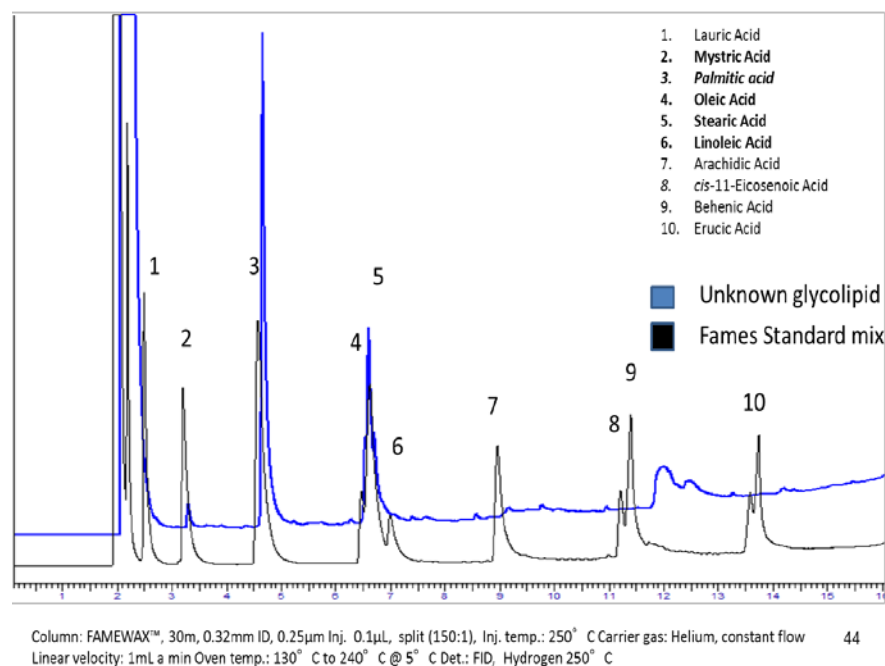
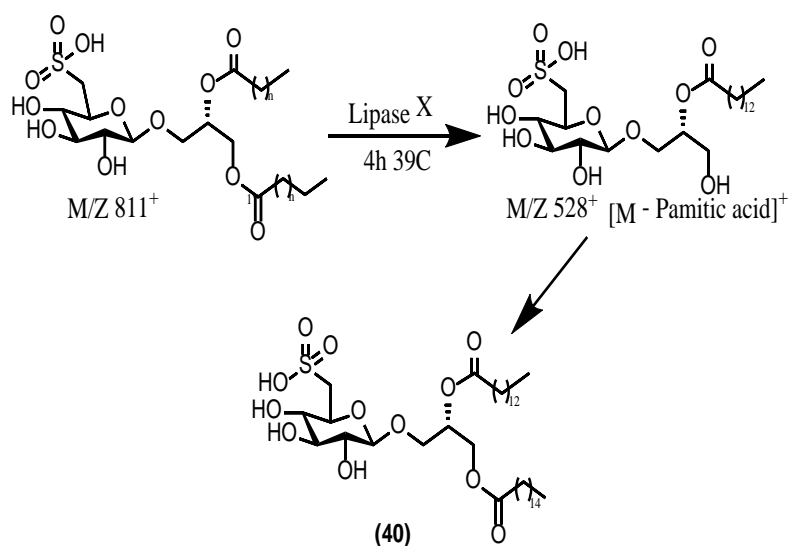


**Figure 30.** Sample GC FAMES coromatagram comparing unkown to standards.

Confirmation of the position of these of the fatty acid side chains, was achieved through the use of selective enzymatic cleavage of the fatty acids with lipase X<sup>115, 117</sup>. This is a process by which the primary position on the C3 position of the triglyceride is more readily accessible and will therefore cleave faster than at the C2 position (Figure 31)<sup>117</sup>. The reaction mixture was extracted, concentrated and analyzed by LC-MS. This resulted in a parent ion at  $m/z$  811  $[M + 2Na]^+$  and a fragment corresponding to a  $[M - \text{Pamitic acid}]^+$ ; ion at 528  $m/z$  thereby confirming the structure as that of 1-*O*-palmitoyl-2-*O*-myristoyl-3-*O*-(6'''-sulfo- $\alpha$ -D-quinovopyranosyl)-glycerol<sup>117b, 118</sup>.



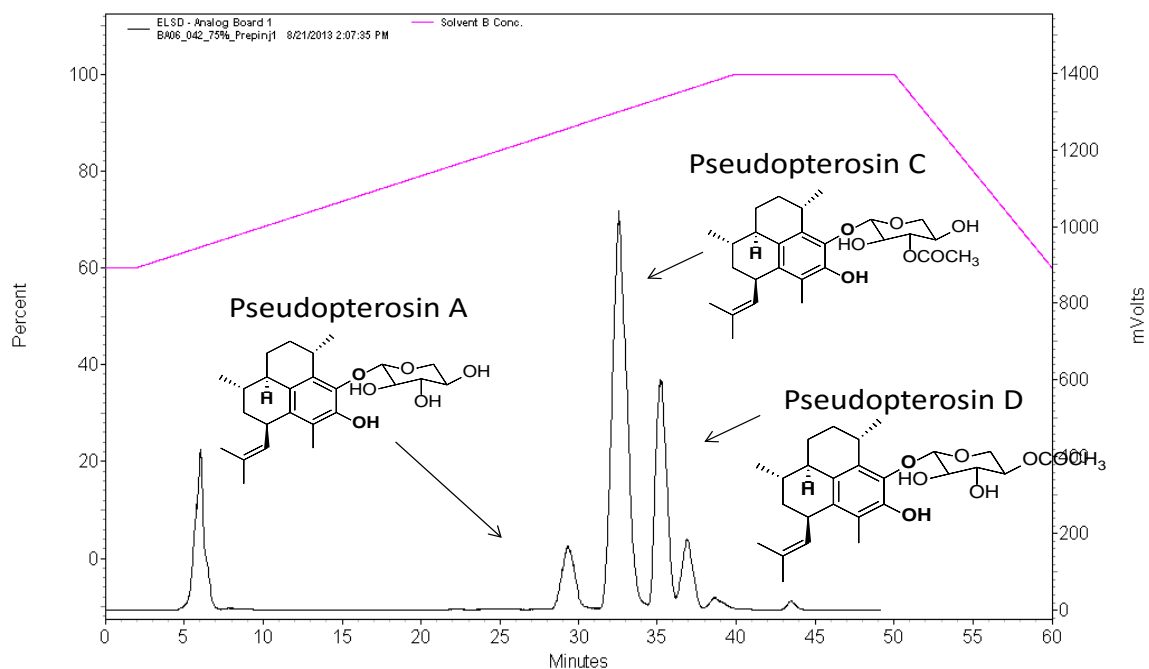
1-*O*-palmitoyl-2-*O*-myristoyl-3-*O*-(6-sulfo- $\alpha$ -D-quinovopyranosyl)-glycerol  
**Figure 31.** Enzymatic cleavage of the fatty acids using Lipase X

## **Isolation and Pharmacological evaluation of Pseudopterosins Terpenes from Gorgonian Octocoral Pseudopterogorgia**

### **Collection of Pseudoterogorgia**

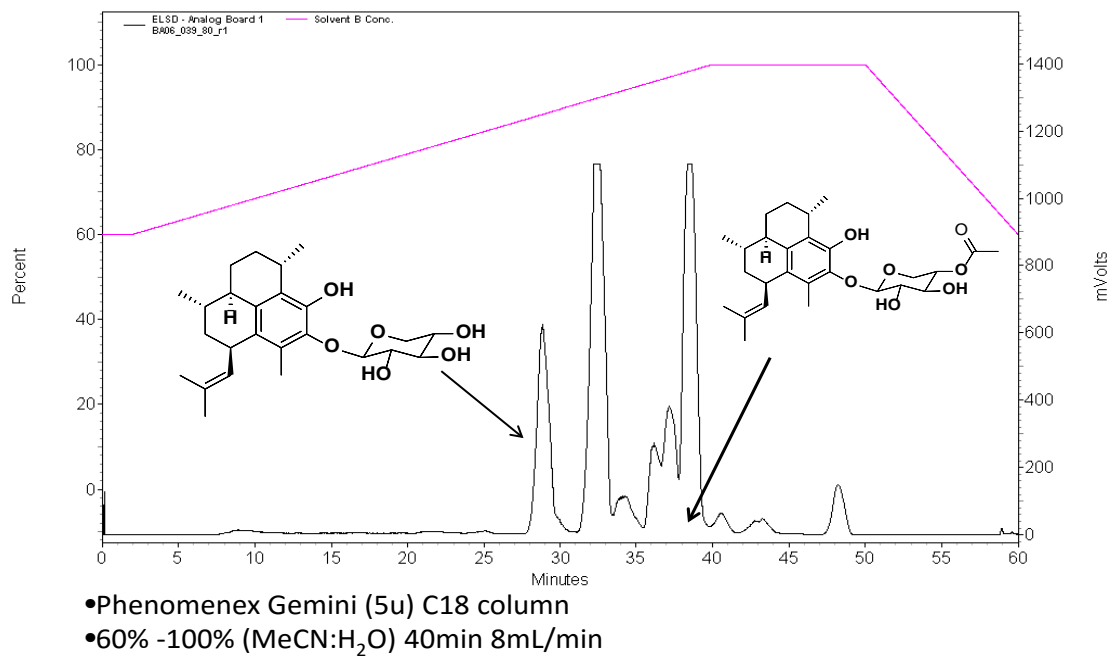
*Pseudopterogorgia spp.* colonies were collected using self-contained underwater breathing apparatus (SCUBA) at a depth of 5-30 m from the Bahamas. Two particular collections were chosen- one from Sandy Point, Eleuthera and the other from off the coast of San Salvador- both of which showed the greatest likelihood of possessing the targeted chemistry. These organisms were cut from the main axis with sharp scissors, immediately labeled, air dried and stored in the freezer until time of use. Prior to extraction samples were subjected to freeze drying in order to remove all residual water contained within the organism.

Samples were then extracted using methanol for repeated extraction cycles. Methanolic extracts were then partitioned into three discrete fractions of decreasing polarity using a large, reverse-phase HP-20 chromatograph. Approximately 35 mg of each 75% fraction was subjected to repeated, preparative HPLC separation on a C-18 column 60-90% ACN/H<sub>2</sub>O for 40min followed by 10 min 90% ACN/ H<sub>2</sub>O for 10 min (see Figures 32 & 33). The fractions were collected by hand and subjected to repetitive HPLC injection until a total of 11 pseudoterosin were isolated in <20mg quantities for biological evaluation (see Figure 34). Full structural elucidations were performed by Dr. Prasoon Gupta and this work focuses on the re-isolation and subsequent confirmation of structure and biological activity and screening of these compounds.



- Phenomenex Gemini (5u) C18 column
- 65% -100% (MeCN:H<sub>2</sub>O) 40min 3mL/min

**Figure 32.** Sample chromatogram from the isolation of pseudoterosin (A-D) (41-44).



- Phenomenex Gemini (5u) C18 column
- 60% -100% (MeCN:H<sub>2</sub>O) 40min 8mL/min

**Figure 33.** Sample chromatogram from the isolation of pseudoterosin iso A, C,D (45-47)

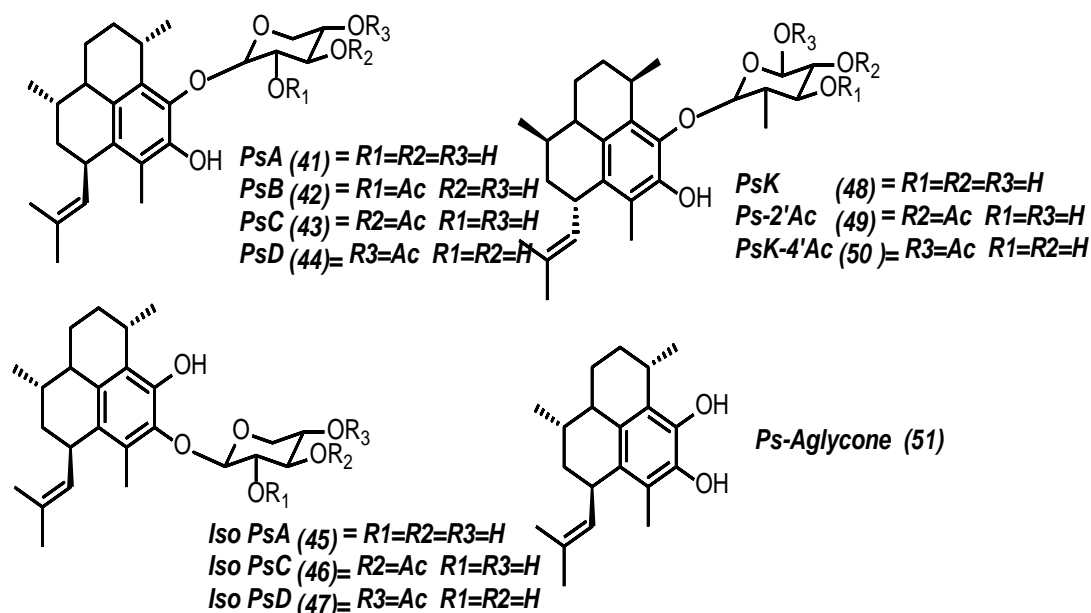


**Figure 34.** Structure of isolated pseudopterosins: pseudopterosin's (A-D)(41-44), Iso-pseudopterosins (A, C, D) (45-47), pseudopterosin-aglycone(51), and pseudopterosin (K, 2' AC, 4' AC) (48-50).

### Spectroscopic confirmation of iso-Pseudopterosins

As a continuation of our study of marine natural products, we describe the structural elucidation of the aforementioned series of iso-pseudopterosins. The structures of the new compounds were established using spectroscopic comparison of previously assigned method by Dr. Prasoon Gupta identified by comparison of their spectroscopic published data (Mass and NMR) <sup>104b</sup>.

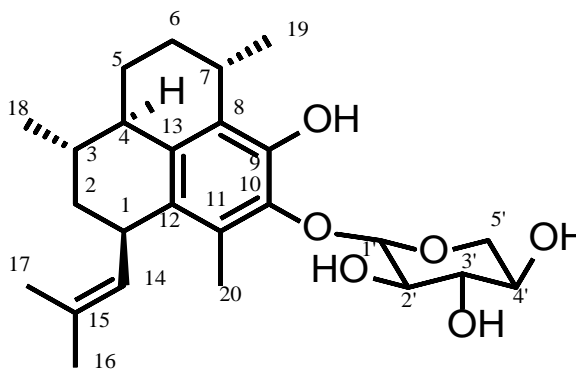


**Figure 35.** Structure of iso-pseudopterosins A (45)

Data from high-resolution mass and  $^{13}\text{C}$  NMR spectrometry established a molecular formula for these metabolites Pseudopterosin iso-PsA (**45**) had a HRESIMS (positive-ion)  $m/z$   $[\text{M} + \text{Na}]^+$  455.2415 (calculated for  $\text{C}_{25}\text{H}_{36}\text{O}_6\text{Na}$ , 455.2409) Both pseudopterosin iso-PsC (**46**) and PsD (**47**) had a HRESIMS (positive-ion)  $m/z$   $[\text{M} + \text{H}]^+$  475.2693 (calculated for  $\text{C}_{27}\text{H}_{39}\text{O}_7$ , 475.2695) matching that of matching that of pseudopterosins (B-D) (**42-44**) and showing evidences of similar acetylation pattern. The  $^1\text{H}$  NMR spectrum contained in the diagnostic H8 methyl singlet ( $\delta$   $^1\text{H}$  2.13, 2.11) together with a infrared absorption band at 1732, and 1732  $\text{cm}^{-1}$  <sup>1104b</sup>.

Acid hydrolysis of pseudopterosin iso A-C and D (**45-47**), each yielded the same pseudopterosin A-F aglycone (**51**) skeletal profile whose structure was determined through X-ray crystallography of Pseudopterosin C (**43**), which matched all previously assigned spectroscopic assignments confirming this same backbone <sup>104b, 119</sup>.

With all iso-pseudopterosins A, C, D (**45-47**), possessing the same planar structure, key spectroscopic correlations were the same, but with variations in the acetylation of  $\beta$ - Xylose as previously mentioned. The aforementioned  $^1\text{H}$  NMR spectrum diagnostic methyl singlet ( $\delta$   $^1\text{H}$  2.13, 2.11) was the most significant difference between these isomeric variants. Acetylation of iso-pseudopterosins A, C, and D (**45-47**), in excess acetic anhydride in pyridine, all produced the same tetra acetylated product offering further evidence of the similarity of this new backbone and which differs only in the position of acetylation. Base hydrolysis of the iso series all yielded the same un-acetylated iso-PsA further confirming acetylation variances in the structure. Structural assignment was based on key COSY and HMBC correlations which compared the chemical shifts of the acetylated positions of that of C-3' ( $\delta_{\text{C}}$  79.5-  $\delta_{\text{H}}$  4.75) and C-4' ( $\delta_{\text{C}}$  81.6-  $\delta_{\text{H}}$  4.90) and leading to their corresponding  $^1\text{H}$  downfield shift. This is consistent

with the findings from previously isolated iso- pseudopterosins (A,C, and D) (**45-47**) (Figure 36)<sup>104b, 120</sup>. This data, in conjunction with HMBC correlations, gave credence to support the position of acetylation and the planar structure of iso-Pseudopterosins C and D (**45-47**) (Figure 36).

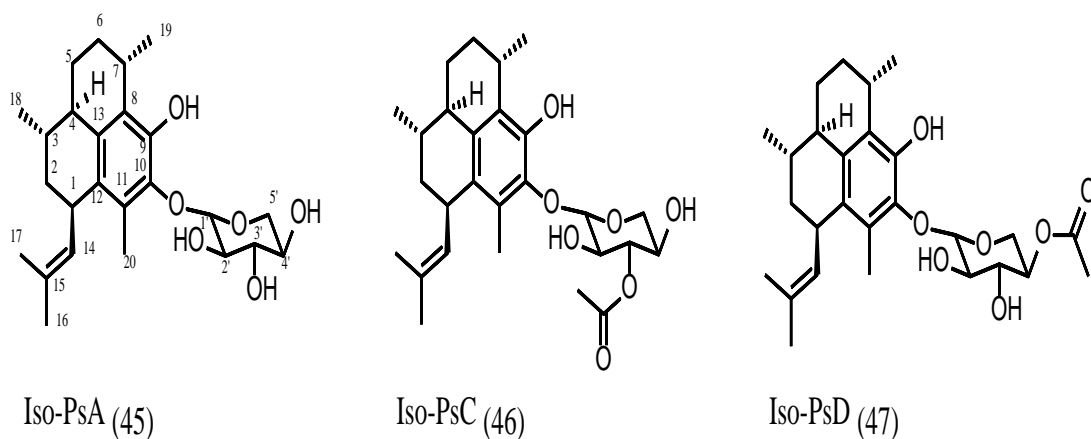


**Figure 36** Structures of Iso-pseudopterosins A,C,D (**45-47**)

### Cell cytotoxicity data

In order to evaluate the variation in cytotoxicity of the pseudopterosins, cell viability and cytotoxicity assays were used to better assess the ability of these compounds and their toxicity. The course of this work involved the use of a chemical enzyme-based method using an MTS cell proliferation assay<sup>121</sup>. This assay relies on a reductive coloring reagent and dehydrogenase in a viable cell to determine cell viability for squamous cell carcinoma cells (SCC-25)<sup>121</sup>. It is best suited for measuring the percentage of living cells using a colorimetric index to assess cellular metabolic activity. This Tetrazolium Dye Assay was used to measure cytotoxicity by plotting an index of controls compared to cultures co-incubated with the subject compounds in triplicate. Initial studies and follow up studies of the compounds isolated during the course of our study of pseudopterosins showed cytotoxic values (12–25  $\mu$ M) that are consistent with



previous reports<sup>104a, 107, 122</sup> (Figure 37 and 38) A full cytotoxicity dose response curve was obtained with a IC<sub>50</sub> for iso-PsA(45) and shown to be 18  $\mu$ M with no cytotoxic effect below 12  $\mu$ m. This implies that pseudopterosins could possibly serve as an effective therapeutic probe below 12  $\mu$ M (Figure 39).

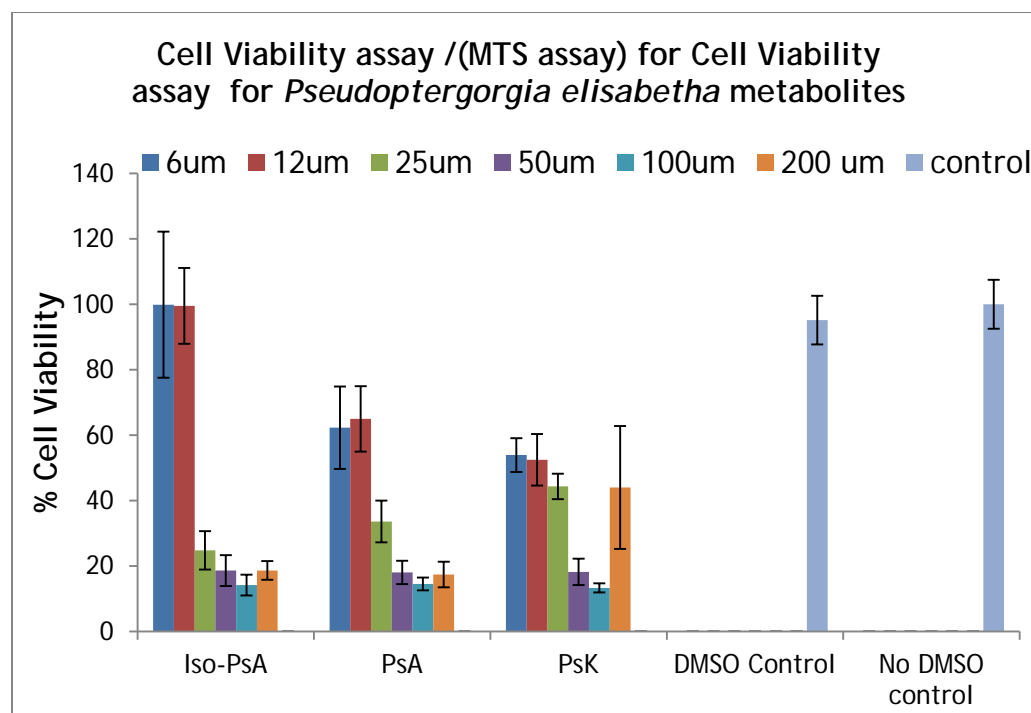


**Figure 37.** Cell cytotoxicity data for pseudopterosins Iso-PsA(45), PsA(41), and PsK (48) N=3.

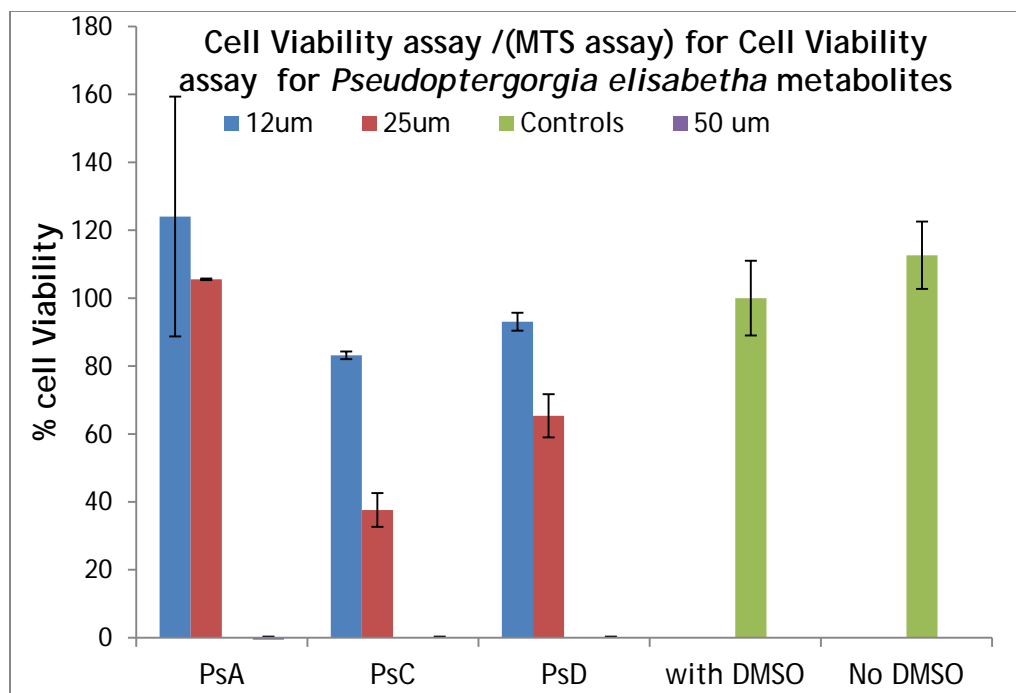


**Figure 38.** Cell cytotoxicity data for pseudopterosins Iso-PsA (45), PsA (41), and PsK (48) N=3 .

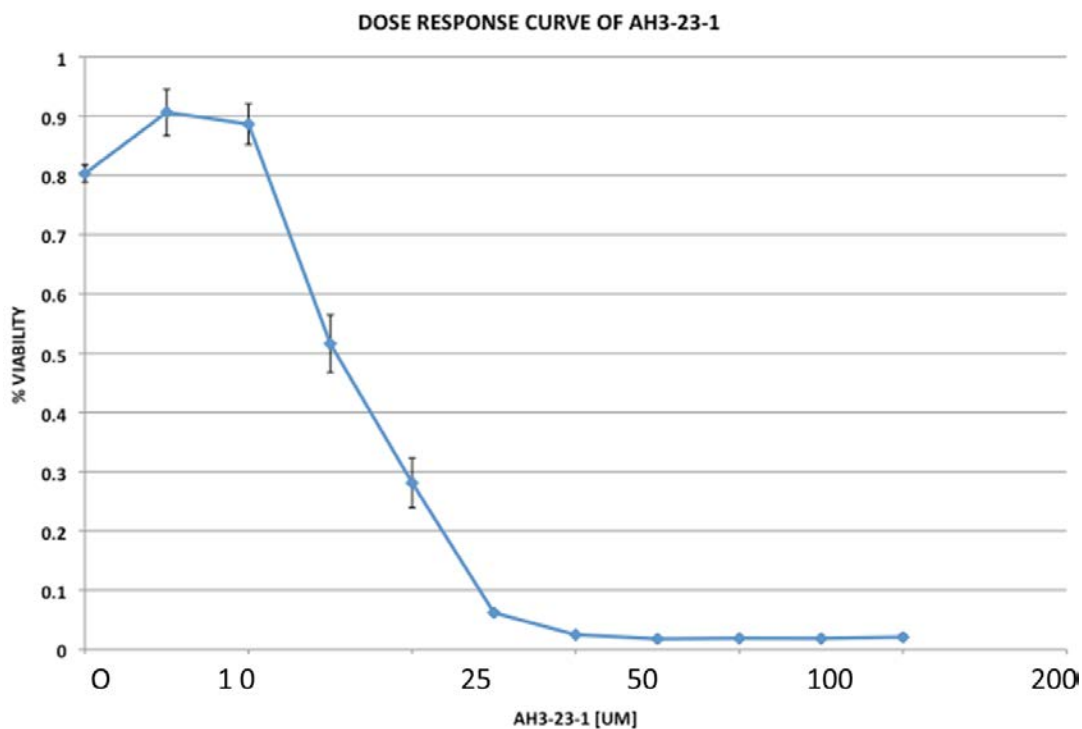


**Figure 39.** Dose response cell cytotoxicity data for iso-PsA (45)

**AFM imaging Assay for measuring A $\beta$ <sub>40</sub> plaque formation**

Given pseudopterosin's ability to protect neuronal function under oxidative stress, we further examined other potential roles these compounds may play in combatting neurological disorders. There is strong evidence that phenolic antioxidants have the ability to serve in dual roles. Many terrestrial-based phenolic antioxidants have exhibited an ability to both inhibit plaque formation and combat the resulting mitochondrial dysfunction and oxidative stress which leads to neuronal cell death. We chose to screen pseudopterosin compounds further using a commonly applied technique called Atomic Force Microscopy (AFM) in collaboration with Dr. Du and Mr Clifford Morris. We utilized this physical conformation to examine the roles that pseudopterosins may play in the aggregation of A $\beta$ <sub>40</sub> plaque formation on freshly prepared mica. This is a common technique used for the evaluation of amyloid plaques where adsorption of reaction solutions containing A $\beta$ <sub>40</sub> oligomers at set time intervals is used to track plaque formation. Subsequent imaging using AFM is used to generate a physical image of these plaques. As it is a physical representation, confirming the effect of adsorption on plaque aggregation is an absolute way of determining its effects. Testing is accomplished by co-incubation of the compound with freshly prepared amyloid beta oligomers which then allows the effect of plaque formation to be assessed. Stock solutions of the pseudopterosins were prepared in DMSO and diluted to a final concentration with A $\beta$ <sub>40</sub>, allowed to incubate and then aliquoted on the AFM media. Samples are adsorbed onto fresh mica on which subsequent imaging takes place. Samples were dried for subsequent AFM imaging using the

tapping mode on an Asylum Research MFP 3D AFM system with MikroMasch NSC15/AI BS cantilevers.

The results presented show that PsA, and its isomeric variant, iso-PsA, both exhibit similar reactivity and a strong ability to suppress and modulate A $\beta$ <sub>40</sub> aggregation. Controls of A $\beta$ <sub>40</sub> aggregation were established during the course of the study and showed consistent amorphous fibril amyloid plaques with increasing coverage over the 6 day study. (Figure 40) After 3 days PsA(**41**) showed an ability to suppress, though not completely inhibit, A $\beta$ <sub>40</sub> fibril formation (Figure 41). After 6 days, more fibers were observed but were atypical, forming disordered aggregates compared to controls. Small fibrils still formed in the presence of PsA(**45**) but significantly less compared to the controls. Iso-PsA(**45**) showed an ability to suppress fibril formation after 3 days, but after 6 days the formation of spherical agglomerates could be observed (Figure 41). Ps-aglycone (**51**) permitted fibril formation, however, these were off-pathway amorphous agglomerates which are very dense across the entire surface. This is consistent with previous reports regarding exposed catechol flavonoid ECGC<sup>85c</sup>(Figure 42) This work provides preliminary evidence of pseudoterosin ability to serve as an anti-amyloidogenic inhibitor and the need to further evaluate these compounds in biologically relevant assays which better model this disease in a proper physiological setting are indicated.

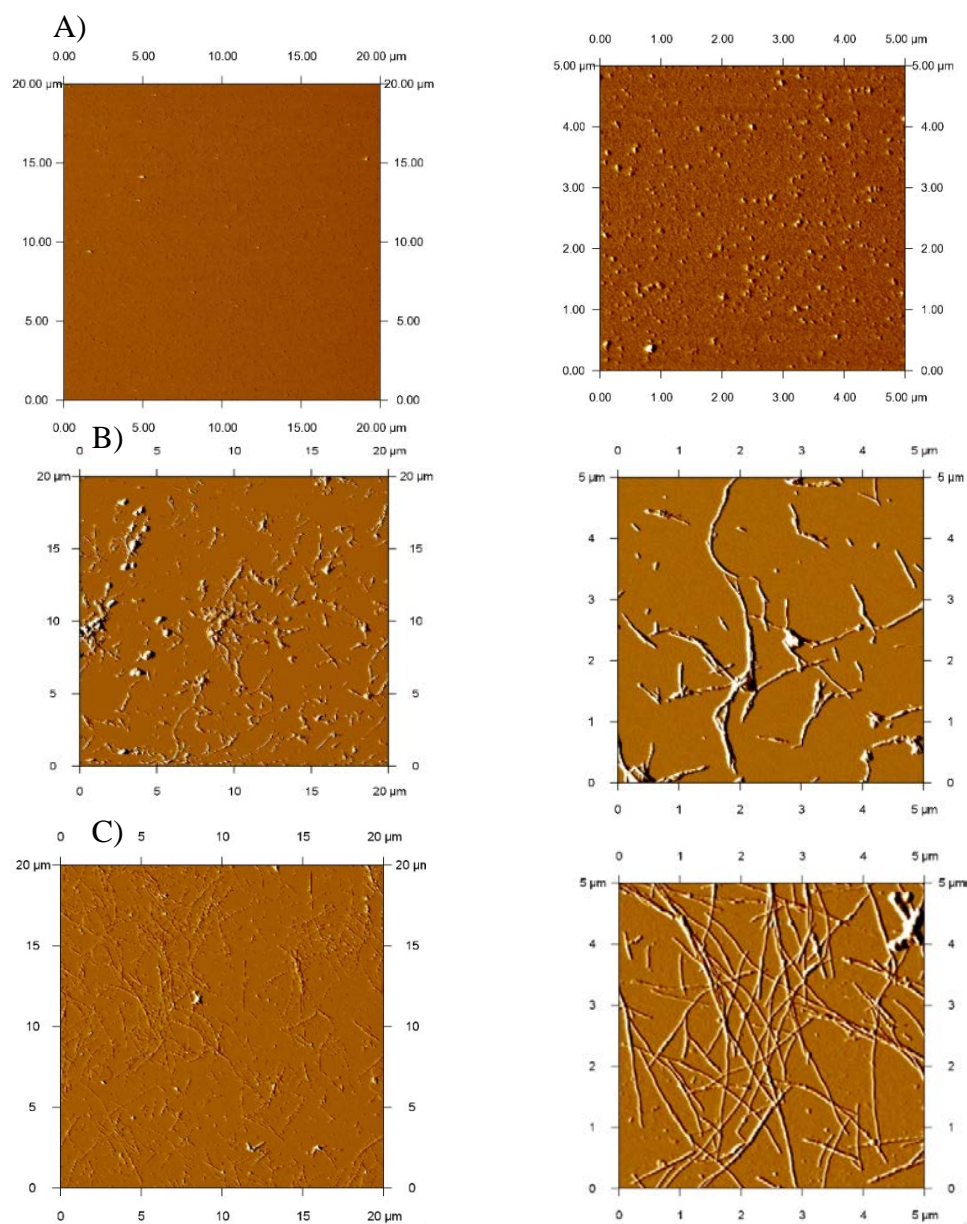


**Figure 40.** Tapping mode AFM images of  $A\beta_{40}$  amyloidogenesis.  $A\beta_{40}$  (30  $\mu\text{M}$ ) in pH 7.4 phosphate buffer (50 mM Na-phosphate, 150 mM NaCl) incubated at 37  $^{\circ}\text{C}$  for (A) 0 days, (B) 3 days, and (C) 6 days.

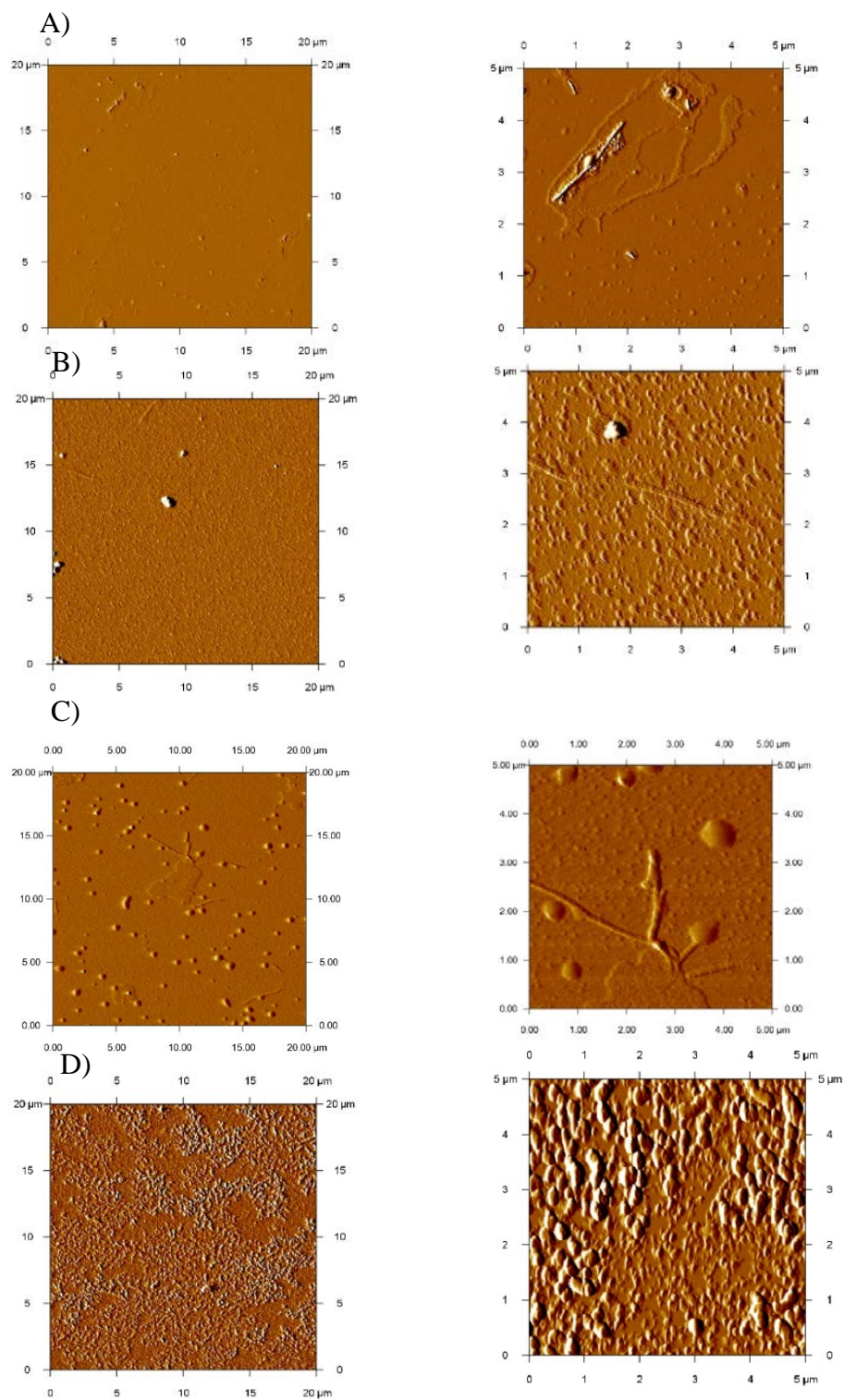


**Figure 41.** Tapping mode AFM images of A $\beta$ <sub>40</sub> in the presence of PsA(41) and iso-PsA (45) (200 μM). A $\beta$ <sub>40</sub> (30 μM) in pH 7.4 phosphate buffer (50 mM Na-phosphate, 150 mM NaCl) incubated at 37 °C for (A) PsA (41) 3 days, (B)PsA 6 days (40), (C)iso-PsA (45) 3 days, (D)iso-PsA (45) 6 days.



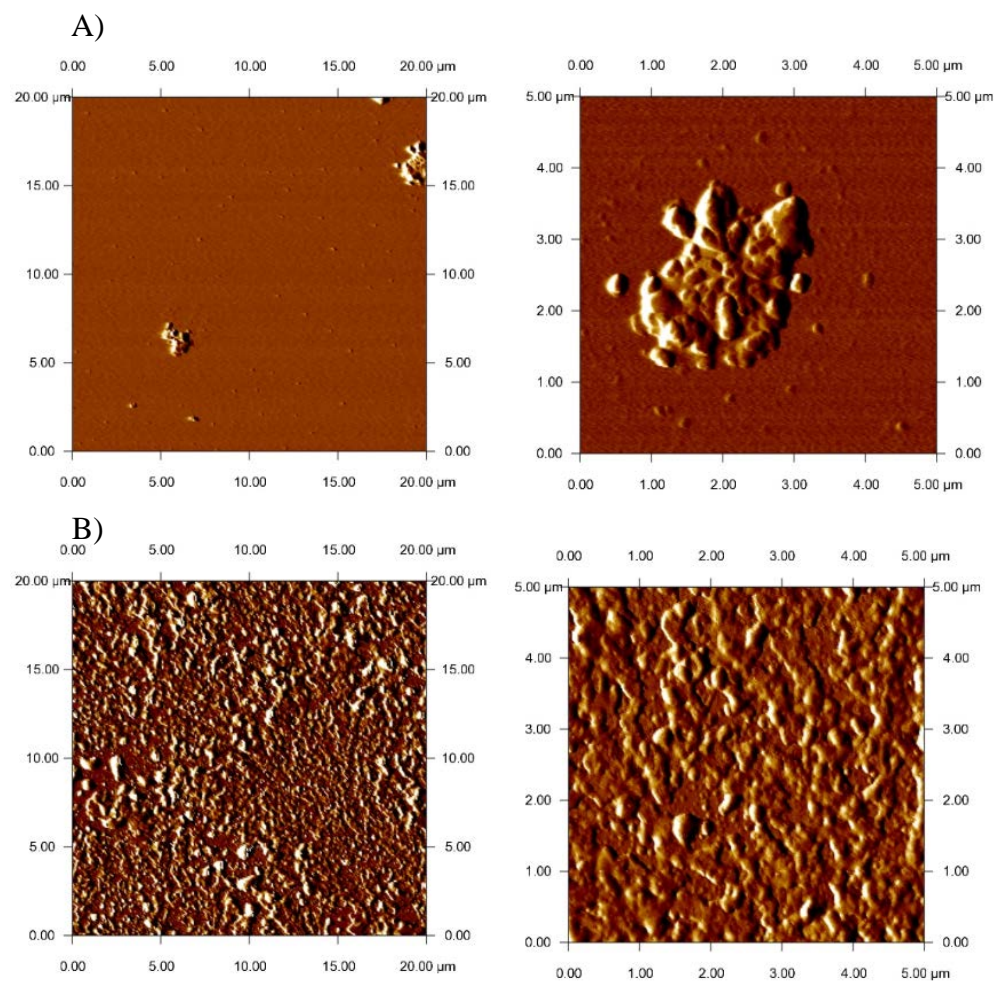


**Figure 42.** Tapping mode AFM images of A $\beta$ <sub>40</sub> in the presence of Ps-aglycone (**51**)(200  $\mu$ M). A $\beta$ <sub>40</sub> (30  $\mu$ M) in pH 7.4 phosphate buffer (50 mM Na-phosphate, 150 mM NaCl) was incubated on a speci-mix aliquot mixer at 37 °C for (A) 3 days, (B) 6 days.

## Conclusion

Through this work we demonstrated the successful isolation and characterization of marine natural products that show antioxidant activity as well as their pharmacological evaluation.

Sulphanoglycolipids or glycolipids type compound provide energy are commonly found on the outer cell membranes where they serve as both a recognition site for specific chemicals and, through cellular attachment to tissues, as an aid in maintaining membrane stability<sup>123</sup>. Sulfoglycolipids with myristoyl and palmitoyl were initially isolated from chondria *crassicaulis*<sup>118a</sup>. These types of compounds have been shown to be DNA polymerase inhibitive, they exhibit immunosuppressive effects, offer HIV reverse transcriptase inhibition, are antimicrobial, show anti-tumor activity and combat cytotoxicity<sup>124</sup>. They have even shown antiprotozoal activity in *E. histolytica*, *lobophora variegata*, and *T. vaginalis*<sup>117, 125</sup>. The results show that proper dereplication strategies are useful to expedite time spent on chemistry. These results do show the successful application of an assay-guided isolation protocol using the FRAP. These results also show the need for secondary assay screening in order to further evaluate these compounds using secondary assays of greater complexity assess the true therapeutic potential of a natural product in a biological setting.

Through this work and previous work with the isolation and pharmacological evaluation of pseudopterosins from *Pseudopterogorgia* spp shows strong implications into the pharmacological potential of these compounds for neurodegenerative diseases. pseudopterosins: (A-D) (**41-44**), Iso-pseudopterosins (A,C,D) (**45-47**), pseudopterosins-aglycone (**51**), and pseudopterosins (K, 2'AC, 4'AC) (**48-50**) were all isolated and successfully characterized. These compounds were further assessed for cytotoxicity, where



a relative  $IC_{50}$  value of 18 $\mu$ m to 21 $\mu$ M well within previously established cytotoxic ranges. The results of both the AFM Pseudopterosins may serve as novel therapeutic probes to combat neurodegenerative diseases. Indeed, this work provides preliminary evidence that pseudopterosins are potentially valuable therapeutic probes for the treatment of neurodegenerative disease however with further study and pharmacological scrutiny these compounds can and should be assessed properly for their true therapeutic value.

## Material and Methods

### Collection and Identification of Marine Material

#### *Pseudopterogorgia spp*

Colonies were collected by Self-Contained Underwater Breathing Apparatus (scuba) at a depth of 5-30 m at various sites around the Bahamas and Key Largo, Florida. Sample collection never involved removal of whole colonies and only a terminal fragment of each individual colony was cut from the main gorgonian axis with sharp scissors. Gorgonian fragments were air-dried and stored in the freezer. Samples remained frozen until extraction. Taxonomic identification of each colony was made by comparison of the gross colony architecture and by the morphology and dimensions of the three most common sclerite types (i.e., spindles, anthocodial rods, and scaphoids).

#### *Briareum asbesinum*

The gorgonian *Briareum asbesinum* was collected by hand using SCUBA at a depth of 13.70-15.20 m from Hillsboro Ledge, Boca Raton Florida. The specimens were immediately frozen and kept at -20 °C until extraction. A voucher specimen has been deposited in the Department of Chemistry and Biochemistry, Florida Atlantic University, Boca Raton Florida (FAU02-010).

### Small Scale Solid-Phase Extraction

The organic extracts were fractionated using a Solid Phase Extraction (SPE) 12-port vacuum manifold. The organic extract (5-15 mL) was concentrated onto polymeric HP-20 (3 g) using a savant vacuum centrifuge system. The HP-20 was transferred into a

40-mL syringe-barrel SPE column. After washing of the column with 20 mL of water, the column was eluted, drop-wise, with 15 mL fractions of: (a) H<sub>2</sub>O, (b) 40% (CH<sub>3</sub>)<sub>2</sub>CO, (c) 75% (CH<sub>3</sub>)<sub>2</sub>CO: H<sub>2</sub>O and (d) (CH<sub>3</sub>)<sub>2</sub>CO. The eluent was collected in scintillation vials (20 mL) and dried in a vacuum centrifuge.

### **Large Scale Extraction**

The specimen samples (up to 2kg wet wt.) were extracted with methanol (3 × 800 mL) for 24 hours. The third, second, and then the first extracts were passed through a column of HP-20 resin (2.5 × 25 cm) equilibrated with methanol. The combined eluents were diluted with 3 L of water and passed again through the column. The column was eluted with 800 mL fractions of: a) H<sub>2</sub>O, (b) 40% (CH<sub>3</sub>)<sub>2</sub>CO, (c) 75% (CH<sub>3</sub>)<sub>2</sub>CO: H<sub>2</sub>O and (d) (CH<sub>3</sub>)<sub>2</sub>CO. Fraction C was concentrated to dryness and subjected to column chromatography.

### **Semi-Preparative HPLC Separation**

#### **Pseudopterosin**

Isolation of Pseudopterosin was accomplished through the use of the 75% acetone/water fraction (30 mg) and subjected to semi-preparative HPLC separation on reversed phase. A post-column, fixed flow splitter was used to split the flow in a ratio of 1:20 to the ELSD and the fraction collector respectively. Samples were purified on C18 reversed-phase HPLC (Gemini 10 × m; 21.2 × 250 mm; 8 mL/min; 20-100% acetonitrile/water over 60 min) respectively.

#### **Briareum asbestinum**

The sample of *Briareum asbestinum* (500 g wet wt.) was extracted with MeOH (3 × 800 mL) for 24 h. The third, second, and then the first extracts were passed through a

column of HP-20 resin ( $2.5 \times 25$  cm) equilibrated with MeOH. The combined eluents were diluted with water (2.5 L) and passed again through the column. The column was eluted with 800 mL fractions of: a)  $\text{H}_2\text{O}$ , (b) 40%  $(\text{CH}_3)_2\text{CO}$ , (c) 75%  $(\text{CH}_3)_2\text{CO}$ :  $\text{H}_2\text{O}$  and (d)  $(\text{CH}_3)_2\text{CO}$ . Fraction c was concentrated to dryness and was subjected to column chromatography on HP-20SS resin eluting with increasing concentrations of acetonitrile in water (40%-100%).

### **Instrumentation**

Solid phase extractions (SPE) were performed on HP-20 resin (3.0 g) in a 40-mL syringe-barrel column using a 12-port manifold (Altech Associates, Inc). Semi-preparative HPLC separation were performed on a PRP-1 column (10 x 250 mm, 10  $\mu\text{m}$ , Hamilton) using a Shimadzu HPLC system consisting of a Shimadzu DGU-20A online degasser, Shimadzu LC-20AT quaternary solvent delivery system, SPD-M20A Photodiode array detector, a Shimadzu LTII evaporative light scattering detector (ELSD), and a FRC-10A fraction collector (a *QuickSplit*<sup>TM</sup> Flow Splitter (ASI, El Sobrante, CA) was used to split the flow in 1:20 to the ELSD and fraction collector). The system was controlled with an SCL-10AVP system controller using EZ Start chromatography software. Emission spectra of the photo reactors used in this study were recorded using an Ocean Optics USB 2.0 Fiber Optic Spectrometer with attached fiber optic cable. UV spectra were determined with a PerkinElmer LAMBDA 365 spectrophotometer. Photochemistry experiments were carried out using a RAYONET Model RMR-600 photochemical reaction chamber. Reactions using UV-C light utilized the 2537Å bulb, and UV-A light experiments were conducted with the 3500 Å series bulb.

## Structural elucidation

These purified compounds were characterized using many advanced, non-destructive spectroscopic techniques. Optical rotations were measured on a Jasco P-2000 Polarimeter. IR spectra were recorded on a Thermo Electronic Corporation Nicolet IR-100 Spectrophotometer. All NMR Spectra were acquired with a Varian Mercury plus 400 spectrometer. Unless otherwise specified, proton ( $^1\text{H}$ ) and carbon ( $^{13}\text{C}$ ) spectra were recorded at 25 °C in  $\text{CDCl}_3$ ,  $\text{CD}_3\text{OD}$  and Toluene- $d_6$  using referenced internally to the residual solvent peak ( $\text{CD}_3\text{OD}$ :  $^1\text{H}$ ,  $\delta$  3.30 ppm;  $^{13}\text{C}$ ,  $\delta$  49.0 ppm;  $\text{CDCl}_3$ :  $^1\text{H}$  7.26 ppm;  $^{13}\text{C}$  77.0 ppm). Short- and long-range  $^1\text{H}$   $^{13}\text{C}$  correlations were determined with gradient-enhanced inverse-detected HSQC and HMBC experiments, respectively. NOE correlations were detected with ROESY experiments with a 0.5 s mixing time.

**Chapter 2 Materials and Methods:** Hemisynthesis of Briarane Diterpenoids: Transannular Forward and Retro  $6\pi$  electrocyclizations Induced by a UVA/UVB Photochromic Switch.

## Thermal transformations

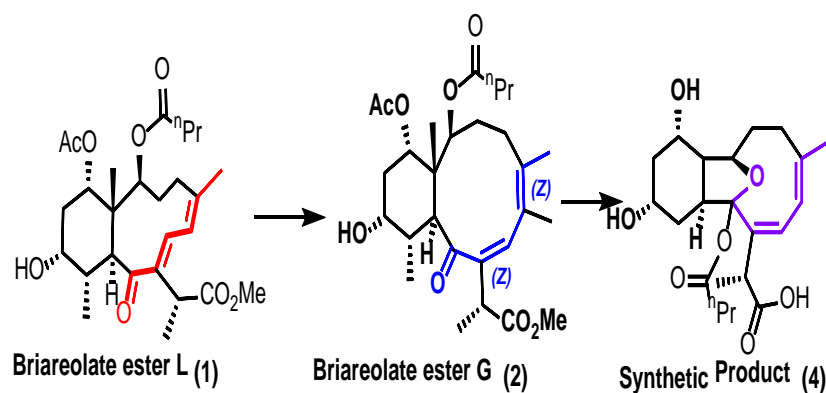
For thermal procedures, (entry 1-4), 600  $\mu\text{l}$  aliquots of solutions containing 10mg/ml of Briareolate ester L, Briareolate ester G were prepared in  $\text{C}_6\text{D}_5\text{CD}_3$ , in an NMR tube. Each solution was heated at 90 °C for up to 3 days with the NMR spectrum recorded daily. After 3 days no transformation was recorded or observed. The same sample solutions were transferred to a glass pressure reaction vessel chamber and sealed. Solutions were then heated to 160°C overnight. Sample solutions were then removed, allowed to cool and transferred to NMR tube for NMR spectra recording. Both solutions containing both Briareolate ester L, and Briareolate ester G exhibited decomposition.

Please note that all solutions and reactions were covered with aluminum foil to exclude ambient light.

### **Acid Catalyzed transformations**

For acid-catalyzed transformation procedures preparation of 600  $\mu$ l aliquots of solutions containing (10mg/ml, 20mM) of Briareolate ester L in  $\text{CD}_3\text{OD}$ ,  $\text{CDCl}_3$  and toluene- $\text{d}_6$  were prepared and covered with aluminum foil to exclude ambient light. These were maintained at ambient temperature for 1 week in order to show the stability of the compounds in solution (entry 5 and 6). After one week there was no observed transformation or decomposition in solvents. After one week 1  $\mu$ l of Tri fluoro-acetic acid (TFA) was transferred via syringe into the solution of Briareolate ester L in  $\text{CDCl}_3$  (entry 7 & 8). NMR spectra was recorded daily and on day 2 of the reaction Briareolate ester L was found to have transformed completely into a 17:83 mixture of Briareolate ester G and a new synthetic product (entry 7). On day 3 of the reaction, Briareolate ester 6 was also completely transformed into <99% solution of new semisynthetic product. After one week the 0.3 mg of *p*-toluenesulfonic acid (PTSA) was transferred into the solution of Briareolate ester L in  $\text{C}_6\text{D}_5\text{CD}_3$  solution containing (10 mg/mL, 20 mM) of Briareolate ester L in  $\text{C}_6\text{D}_5\text{CD}_3$ . This solution was heated to 90  $^\circ\text{C}$  and monitored via NMR. No observed transformation or decomposition was observed after 3 days (entry 9). After three days an additional 4 mg of *p*-toluenesulfonic acid (PTSA) was transferred into the solution. The NMR tube was then sealed and stored in the complete absence of light. NMR data were recorded after 1 week and the new synthetic compound (**33**) was observed (entry 10). The solution was then subjected to liquid/liquid  $\text{CHCl}_3$ :  $\text{H}_2\text{O}$

extraction to remove trace acid. The sample was then dried to completion and reconstituted in  $\text{CDCl}_3$  for comparative NMR analysis.



Entry	Starting material	Solvent	Acid	T °C	time (days)	Observed product
1	L	Toluene- $\text{d}_6$	-	90	3	NR
2	L	Toluene- $\text{d}_6$	-	160	1	Decomp
3	G	Toluene- $\text{d}_6$	-	90	3	NR
4	G	Toluene- $\text{d}_6$	-	160	1	Decomp
5	L	$\text{CDCl}_3$	-	25	3	NR
6	L	$\text{CD}_3\text{OD}$	-	25	3	NR
7	L	$\text{CDCl}_3$	TFA(1eq.)	25	2	17:83 <sup>(*)</sup>
8	L	$\text{CDCl}_3$	TFA (1eq.)	25	3	New product (4)
9	L	Toluene- $\text{d}_6$	PTSA <sup>(*)</sup>	90	3	NR
10	L	Toluene- $\text{d}_6$	PTSA <sup>(*)</sup>	25	5	New product (4)

(\*)= PTSA used in catalytic amounts (10 mol%)(\*)= PTSA used in (5eq.)<sup>(\*)</sup>= Ratio of Briareolated ester G to new Acid product

**Table 3.** Summary of Results from Thermal and Acid Methods

### Nucleophilic assisted isomerization for Briareolate esters:

In-order to test for nucleophilic assisted isomerization, 5mg of Briareolate ester L was reacted with 1eq of  $\text{C}_6\text{H}_6\text{S}$  at  $25^\circ\text{C}$  in 750 $\mu\text{L}$  of  $\text{C}_6\text{D}_5\text{CD}_3$  (13.5mM) in an NMR tube. This yielded the 1,4 addition enol product which was observed after 10min, with no formation of Briareolate ester B during the course of beta elimination. Additional

attempts for the nucleophilic assisted, acid catalyzed isomerization were performed by adding stoichiometric amounts of either TFA, PTSA or scandium triflate directly to the NMR tube. Again, there was no observed conversion to Briareolate ester G, nor reversal back to Briareolate ester L. This data indicates that standard  $\beta$ -elimination of the nucleophilic leads to complete reversal to Briareolate ester L.

**CHAPTER 3 Materials and methods:** Isolation of Marine Natural Products Protective against Oxidative Stress.

#### **FRAP Assay**

FRAP reagent was prepared immediately before each assay with 300 mM acetate buffer, 10 mM 2,4,6-tripyridyl-s-triazine (TPTZ) solution, and 20 mM  $\text{FeCl}_3$  in a 10:1:1 ratio. Reagent was heated to 37° prior to use. Assays were prepared in 96-well microtiter plates using 150  $\mu\text{L}$  of warm FRAP reagent with 20  $\mu\text{L}$  of sample. A blank reading of the plate was taken before addition of samples. Following addition of the sample compounds, absorbance readings at 593 nm were recorded at 30, 90, and 120 minutes (SpectraMax M2 microplate reader; Molecular Devices). The 90 min reading was selected for calculation of FRAP equivalence values. Standard curves were produced using 50, 125, 250, 500, and 1000  $\mu\text{M}$

**CHAPTER 4 Materials and methods:** Isolation and pharmacological evaluation of pseudopterosins terpenes from gorgonian octocoral pseudoterogorgia.



### **Acid hydrolysis of pseudopterosins (41-48) to pseudopterosins aglycone (51)**

To a mixture of pseudopterosins 1N HCl methanolic solution (2 mL). The reaction vessel was agitated at 50°C for 3 hours and then the solution was cooled to 25°C, and water added (10 mL). The solution was extracted with methylene chloride (3 x 2 mL), the organic extracts combined and dried. Subsequent semi-preparative RP-C18 HPLC using a linear gradient of C<sub>2</sub>H<sub>3</sub>N:H<sub>2</sub>O (50:50 C<sub>2</sub>H<sub>3</sub>N:H<sub>2</sub>O to 100% C<sub>2</sub>H<sub>3</sub>N over 30 minutes, hold for 10 minutes) as mobile phase. FRAP assays.

### **Base hydrolysis of pseudopterosins (41-48) to pseudopterosins**

To a mixture of pseudopterosins 2N NaOH MeOH solution (2 mL). The reaction vessel was agitated at 50°C for 8 hours and then the solution was cooled to 25°C, and H<sub>2</sub>O added (10 mL). The solution was extracted with methylene chloride (3 x 2 mL), the organic extracts combined and dried. Subsequent semi-preparative RP-C18 HPLC using a linear gradient of acetonitrile:water (50:50 C<sub>2</sub>H<sub>3</sub>N:H<sub>2</sub>O to 100% C<sub>2</sub>H<sub>3</sub>N over 30 minutes, hold for 10 minutes) as mobile phase.

### **Acetylation pseudopterosins (41-48) to pseudopterosins**

To a mixture of pseudopterosins (2 mL) in pyridine excess acetic anhydride was added and allowed to react overnight. Water was subsequently added (10 mL) to quench the reaction. The solution was extracted with methylene chloride (3 x 2 mL), the organic extracts combined, dried. Subsequent semi-preparative RP-C18 HPLC using a linear gradient of C<sub>2</sub>H<sub>3</sub>N:H<sub>2</sub>O (50:50 C<sub>2</sub>H<sub>3</sub>N:H<sub>2</sub>O to 100% C<sub>2</sub>H<sub>3</sub>N over 30 minutes, hold for 10 minutes) as mobile phase.

### **MTS cell cytotoxicity**

Cell suspensions (100,000 cells) containing the indicated supplement were plated in 96 well microtiter plates using 100 µl of the indicated cell suspension. The plates were incubated for 48 hr at 37°C in a 5% CO<sub>2</sub> incubator. The culture medium was then removed and the cells washed once with fresh culture medium with serum. After removal of the wash solution, fresh culture medium with serum that contained the indicated analyte was added to the cells, and the cells were incubated for 24 hours. Cell viability was determined by the CellTiter 96 Aqueous One Cell Proliferation Assay (Promega; Madison, WI) according to the manufacturer's instructions. This assay utilizes a novel tetrazolium compound that metabolically active cells convert to a water soluble formazan by the action of cellular dehydrogenases. This is measured by absorbance at 490 nm using a colorimetric microtiter plate reader (SpectraMax Plus384; Molecular Devices).

## Appendix

Appendix A: Biosynthetic Production of Marine Secondary Metabolites from	
<i>Briareum asbestinum</i> .....	86
Appendix B: Spectroscopic data of 1-O-palmitoyl-2-O-myristoyl-3-O-(6-sulfo- $\alpha$ -	
D-quinovopyranosyl )-glycerol.....	110
Appendix C: Spectroscopic data of Pseudopterosins.....	115

## Appendix A: Photochemical Kinetic equations

### Kinetic equations for UVA Photochemical Reactions with Briareolate ester L:

**Briareolate ester L Model:** ExpDec1

$$Y = 44.233 \times e^{\frac{-x}{61.88}} + 37.04 \times e^{\frac{-x}{0.89}} + 18.72$$

**Briareolate ester G Model:** intermediate

$$Y = 33.0 \times e^{\frac{-x}{0.88}} + 34.97 \times e^{\frac{-x}{0.63.03}} + 23.17$$

**Briareolate ester B Model:** ExpDec1

$$Y = 66.2 \times e^{\frac{-x}{56.27}} + 68.7$$

### Kinetic equations for UVC Photochemical Reactions with Briareolate ester L:

**Briareolate ester L Model:** ExpAssoc

$$Y = 100 - 16.3 \times \left(1 - e^{\frac{-x}{0.22}}\right) - 47.7 \times \left(1 - e^{\frac{-x}{6.764}}\right)$$

**Briareolate ester G Model:** Asymptotic1

$$Y = 18.4 \times 0.89^x$$

**Briareolate ester B Model:** N/A- no change observed

### Kinetic equations for UVC Photochemical Reactions with Briareolate ester B:

**Briareolate ester L Model:** ExpAssoc

$$Y = 11.7 + 13.1 \times \left(1 - e^{\frac{-x}{10.9}}\right) + 13.1 \times \left(1 - e^{\frac{-x}{10.9}}\right)$$

**Briareolate ester G Model:** Exp3P2

$$Y = e^{(4.1 \times x - (1.73e^{-4}) \times x^2)}$$

**Briareolate ester B Model:** Asymptotic1

$$Y = 68.8 - 44.5 \times 0.943^x$$

**Kinetic equations for isomerization photostationary state under UVA:**

**Briareolate ester L Model:** ExpDec1

$$Y = 108.95 \times \left( e^{\frac{-x}{1.739}} \right) + 65.52$$

**Briareolate ester G Model:** ExpDec1

$$Y = -108.95 \times \left( e^{\frac{-x}{1.739}} \right) + 34.47$$

**NMR from Isolated Briareolated esters**

Briareolate ester L (19) (200mg), Briareolate ester G (20) (20mg): and Briareolate ester B (22) (10mg) were all isolated as a colorless oil and all spectroscopic data matched that of previously reported data.

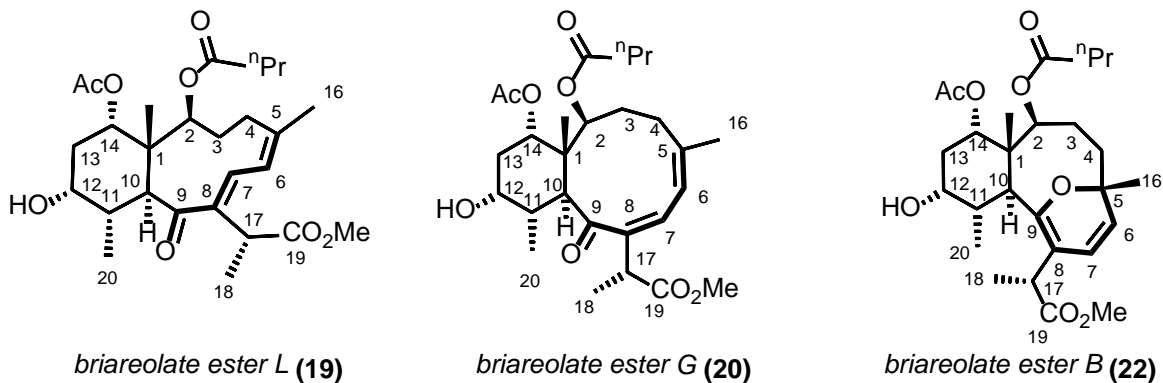


**Figure 43.** Labeled structures of Briarolate ester L (19), ester G (20), and ester B (22)

**Table 4.** NMR table for Briareolate esters L (**19**) Briareolate esters G (**20**) Briareolate esters B (**22**), Recorded (CD3OD at 400MHz).

Pos.	Ester L (19)	Ester G (20)	Ester B (22)
	$\delta_H$ (mult., $J$ in Hz)	$\delta_H$ (mult., $J$ in Hz)	$\delta_H$ (mult., $J$ in Hz)
1			
2	5.52 ( d 8.0)	5.13 (br d, 8.0)	4.98 (br d, 8.0)
3 $\alpha$	2.50 (dd, 16.5/11.0)	2.18 (m)	2.06 (m)
3 $\beta$	1.24 (m)	1.34 (m)	1.39 (m)
4 $\alpha$	2.29 (m)	2.20 (m)	2.16 (m)
4 $\beta$	2.17(m)	1.32(m)	1.32(m)
5			
6	6.22 (br s)	6.14 (br s)	5.63 (d)
7	7.71 (br s)	6.71 (br s)	5.93 (d)
8	-	-	-
9	-	-	-
10	3.81 (d, 11.5)	3.67, (d)	3.63, (d, 11.5)
11	2.28 (m)	2.21 (m)	2.22 (m)
12	3.78 (br q, 3.0)	4.72(m)	4.90(m)
13 $\alpha$	2.07 (dt, 16.0/3.0)	1.95 (m)	2.16 (m)
13 $\beta$	1.93 (dt, 16.0/3.0)	1.95 (m)	2.16 (m)
14	4.81 (br s)	4.60 (m)	4.89 (m)
15	0.89 (s)	1.37 (s)	1.37 (s)
16	1.74 (s)	2.17 (s)	1.33 (s)
17	3.53 (q, 6.0)	3.45 (q, 6.0)	3.57 (q, 6.0)
18	1.27 (d, 7.0)	1.32 (d, 7.0)	1.32 (d, 7.0)
19			
20	0.89 (d, 7.0)	0.88 (d, 7.0)	0.83 (d, 7.0)
OCH	3.62 (s)	3.63 (s)	3.73 (s)
C-2			
-	2.20 (m)	2.30 (m)	2.37 (m)
-	1.60 (m)	1.60 (m)	1.66 (m)
-	0.93(t, 7.0)	0.95(t, 7.0)	0.95(t, 7.0)
C-14 ester			
	2.07 (S)	1.92 (s)	1.90 (s)

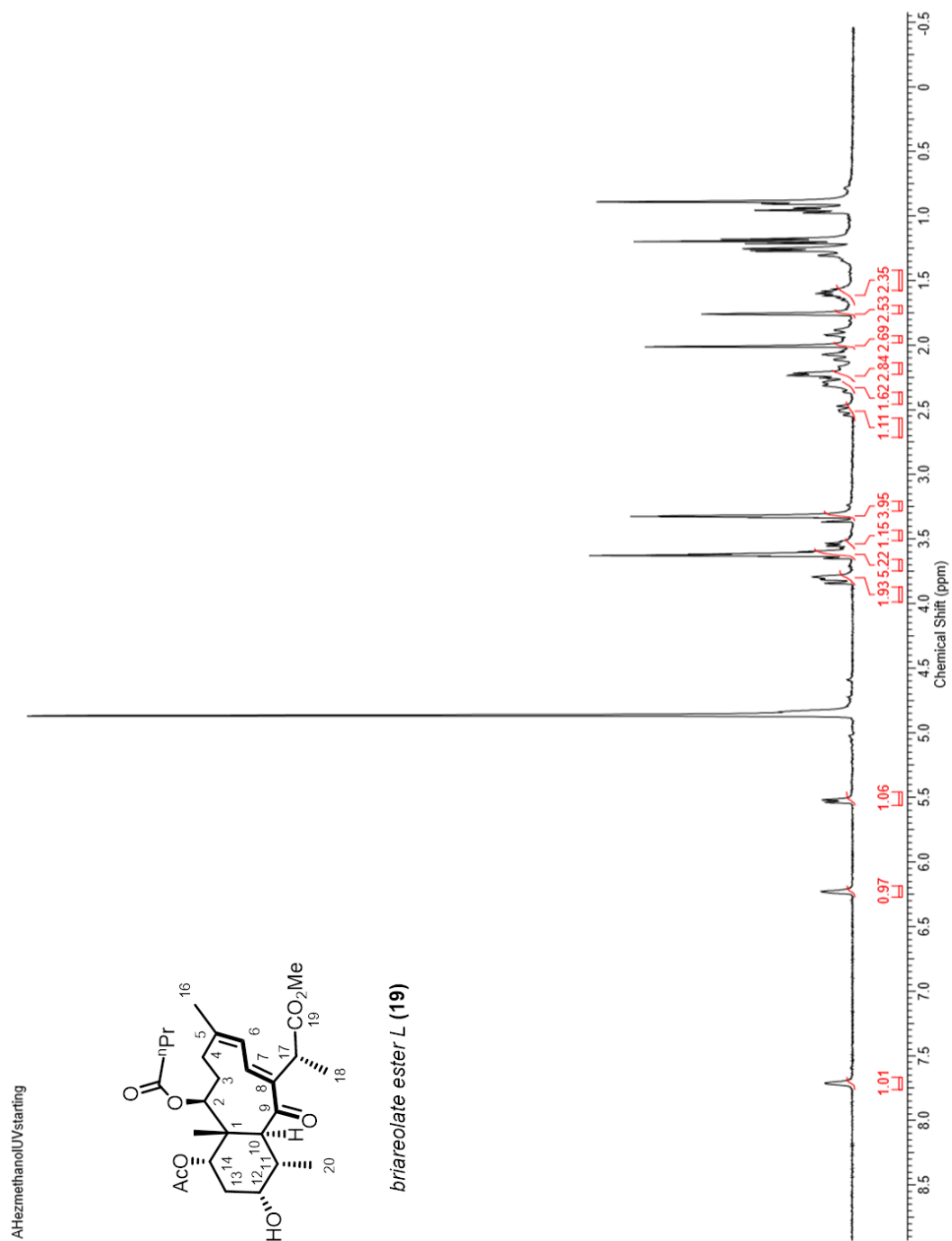


**Figure 44.** <sup>1</sup>H NMR spectrum of Briareolate ester L (**1**) (CD<sub>3</sub>OD, 400 MHz).

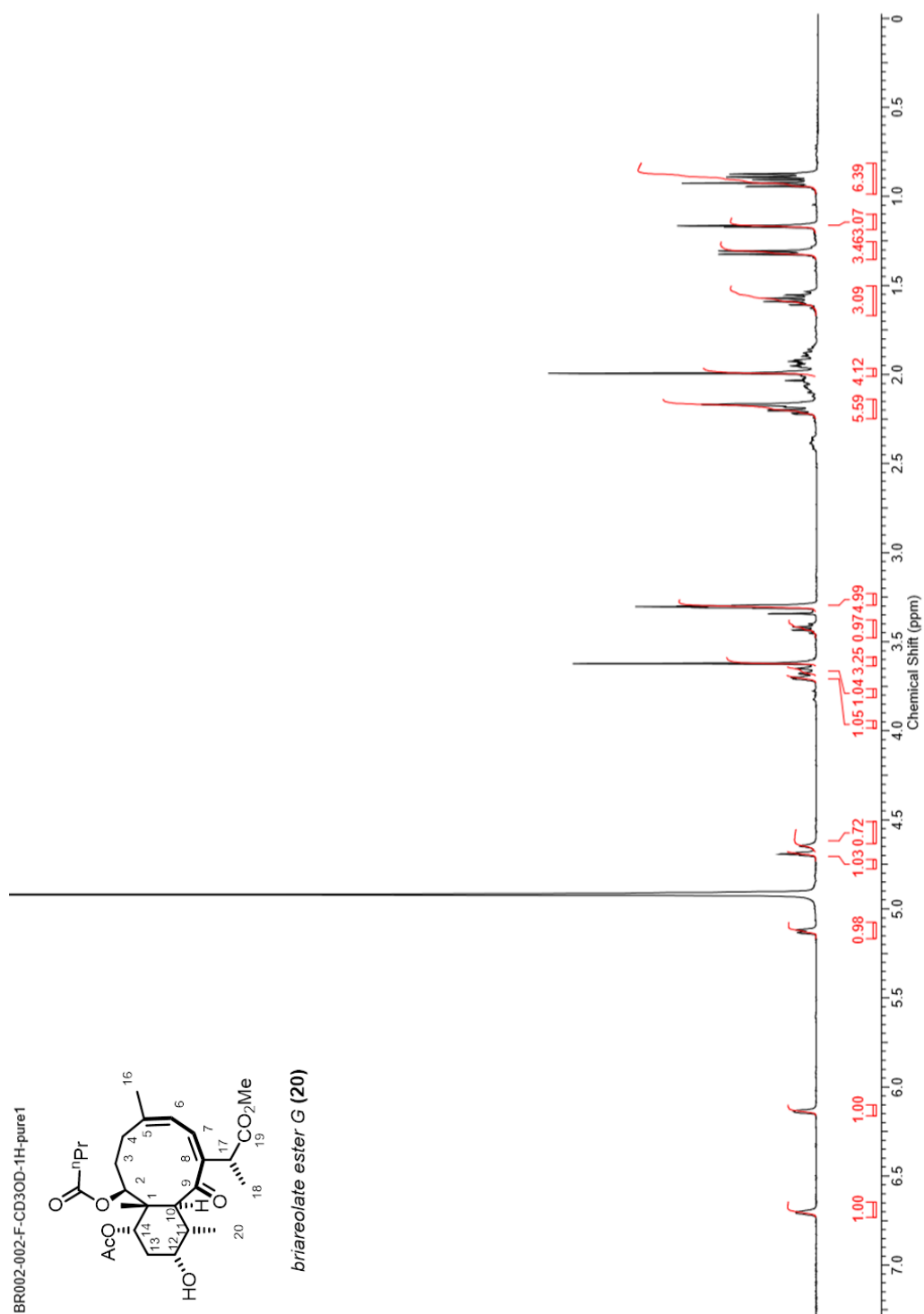


**Figure 45.**  $^1\text{H}$  NMR spectrum of Briareolate ester G (2) ( $\text{CD}_3\text{OD}$ , 400 MHz)



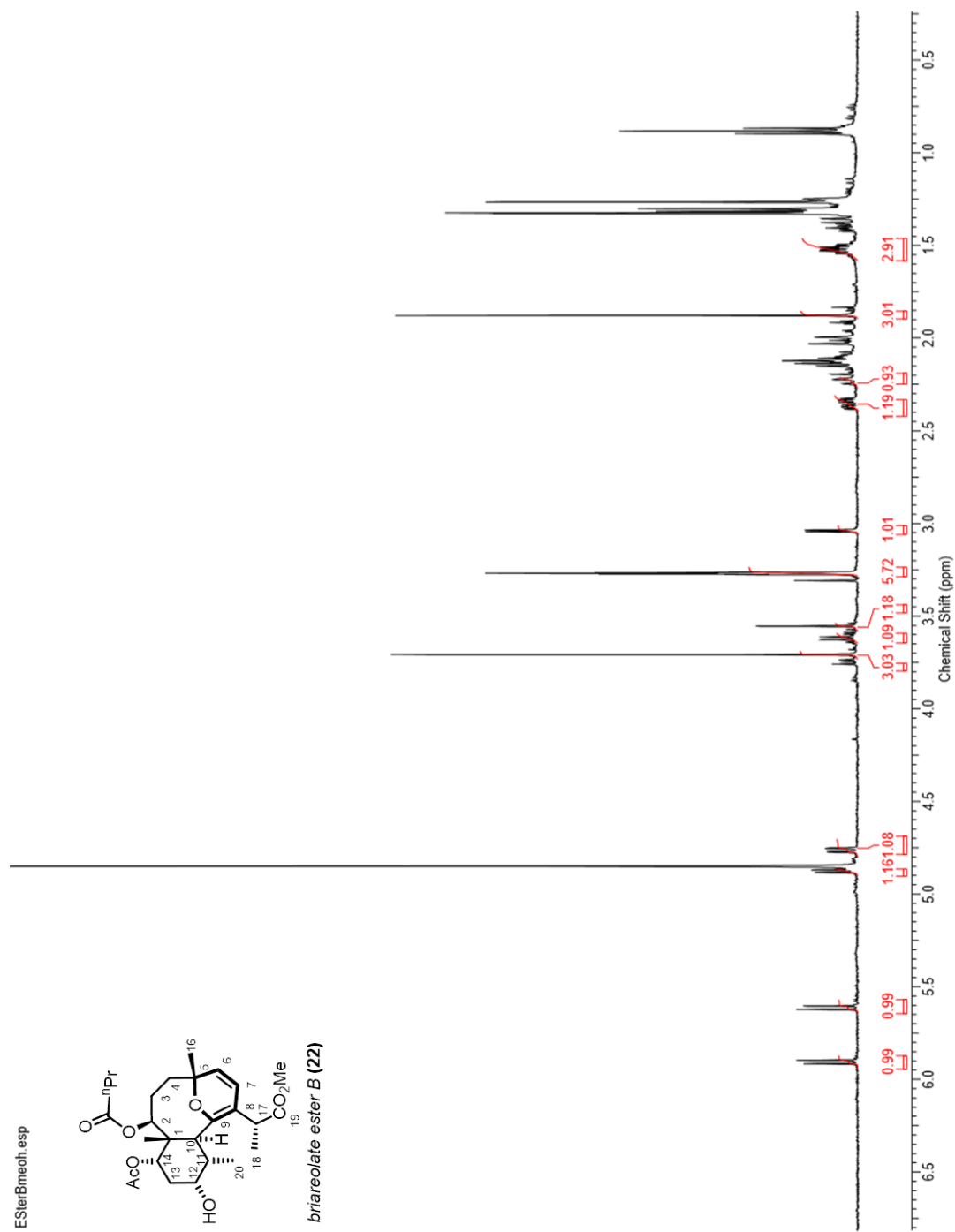


**Figure 46.**  $^1\text{H}$  NMR spectrum of Briareolate ester B (**3**) ( $\text{CD}_3\text{OD}$ , 400 MHz).

**Table 5.** NMR tables for Briareolate esters L(1) Briareolate esters G(2) Briareolate esters B(3), Recorded (CDCl<sub>3</sub>, 400MHz).

Pos.	Ester L (1)		Ester G (2)		Ester B (3)	
	$\delta_H$ (mult., <i>J</i> in Hz)	$\delta_C$	$\delta_H$ (mult., <i>J</i> in Hz)	$\delta_C$	$\delta_H$ (mult., <i>J</i> in Hz)	$\delta_C$
1		46.8		44.8		45.7
2	5.50 ( d 8.0)	79.9	4.98 (m)	73.6	4.95 (br d, 8.0)	77.9
3 $\alpha$	2.48 (dd, 16.5/11.0)	31.9	1.87 (m)	30.8	2.06 (m)	28.6
3 $\beta$	1.26 (m)		1.87 (m)		1.39 (m)	
4 $\alpha$	2.29 (m)	34.8	2.37 (m)	28.7	2.20 (m)	34.8
4 $\beta$	2.17(m)		2.10(m)		1.39(m)	
5		141.7		144.8		75.1
6	6.21 (br s)	118.5	6.07 (br s)	123.5	5.60 (d)	129.8
7	7.68 (br s)	147.0	6.63 (br s)	138.1	5.96 (d)	120.1
8	-	148.1	-	144.3	-	117.3
9	-	201.4	-	205.7	-	150.9
10	3.80 (d, 11.5)	48.4	3.54, (d, 11.0)	45.8	3.65, (d, 11.5)	37.4
11	2.28 (m)	35.9	2.01 (m)	38.9	2.21 (m)	31.8
12	3.77 (br q, 3.0)	70.5	3.65(br q, 3.0)	71.0	5.11(br q, 3.0)	72.0
13 $\alpha$	2.07 (dt, 16.0/3.0)	32.7	2.08 (m)	31.5	2.08 (m)	31.2
13 $\beta$	1.89 (dt, 16.0/3.0)		1.93 (m)		2.08 (m)	
14	4.81 (br s)	76.0	4.95 (m)	75.6	4.89 (m)	74.0
15	0.87 (s)	12.6	1.21 (s)	14.4	1.37 (s)	15.0
16	1.73 (s)	27.1	2.17 (s)	27.1	1.36 (s)	23.8
17	3.52 (q, 6.0)	40.2	3.47 (q, 6.0)	44.22	3.71 (q, 6.0)	37.8
18	1.24 (d, 7.0)	16.8	1.37 (d, 6.8)	18.9	1.32 (d, 7.0)	14.5
19		176.5		174.6		174.3
20	0.89 (d, 7.0)	17.6	0.92 (d, 7.0)	17.7	0.83 (d, 7.0)	15.3
OCH <sub>3</sub>	3.60 (s)	52.5	3.65 (s)		3.83 (s)	51.9
C-2		175.5		173.4		172.2
-	2.20 (m)	37.7	2.21 (m)	36.4	2.26 (m)	36.46
-	1.60 (m)	19.7	1.61 (m)	18.1	1.66 (m)	18.36
-	0.93(t, 7.0)	14.5	0.91(t, 7.0)	13.7	0.95(t, 7.0)	13.95
C-14 ester		173.2		169.1		169.7
	2.07 (S)	22.3	1.92 (s)	21.3	1.92 (s)	21.0

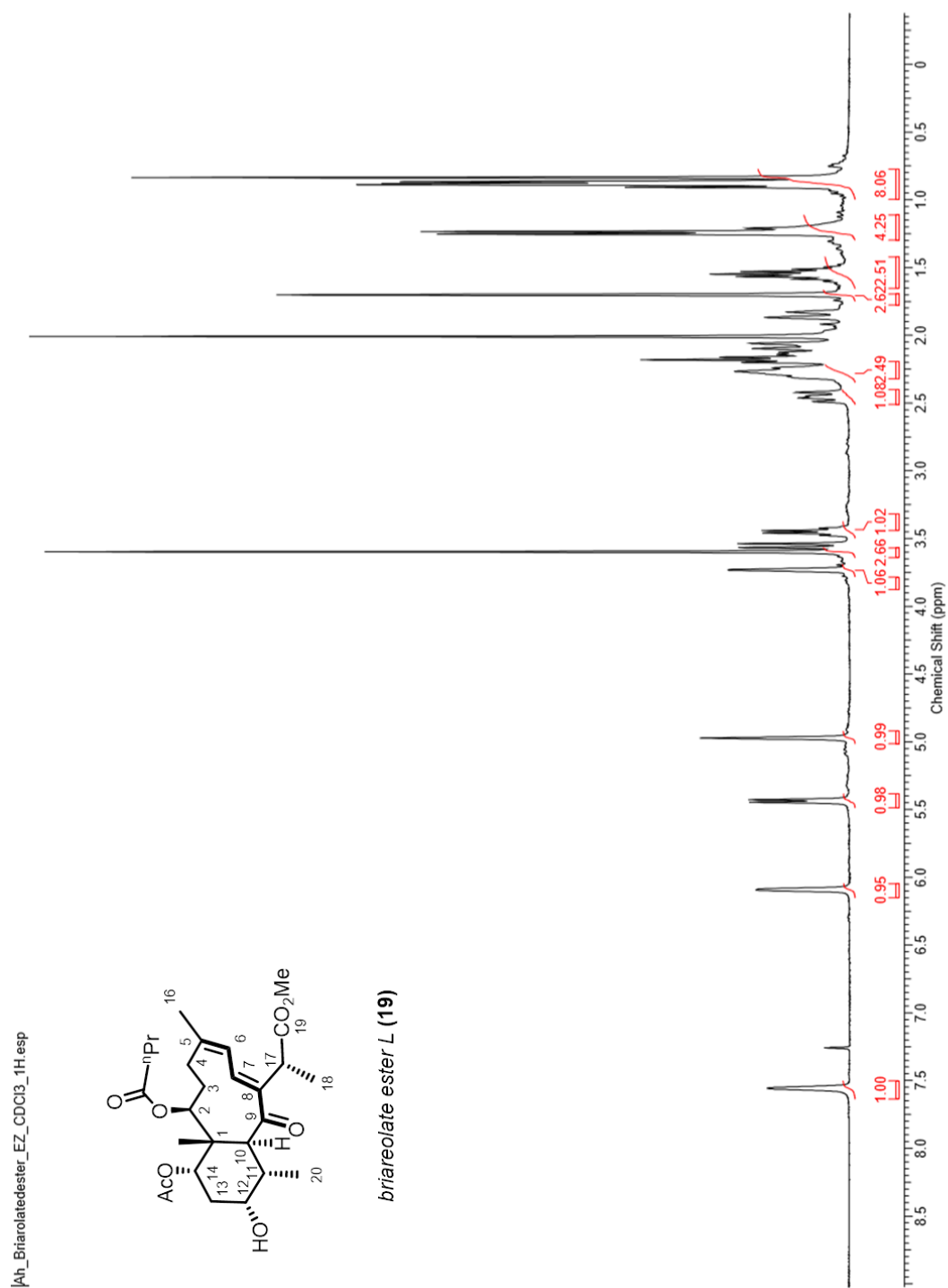


**Figure 47.**  $^1\text{H}$  NMR spectrum of Briareolate ester L (1)( $\text{CDCl}_3$ , 400 MHz).



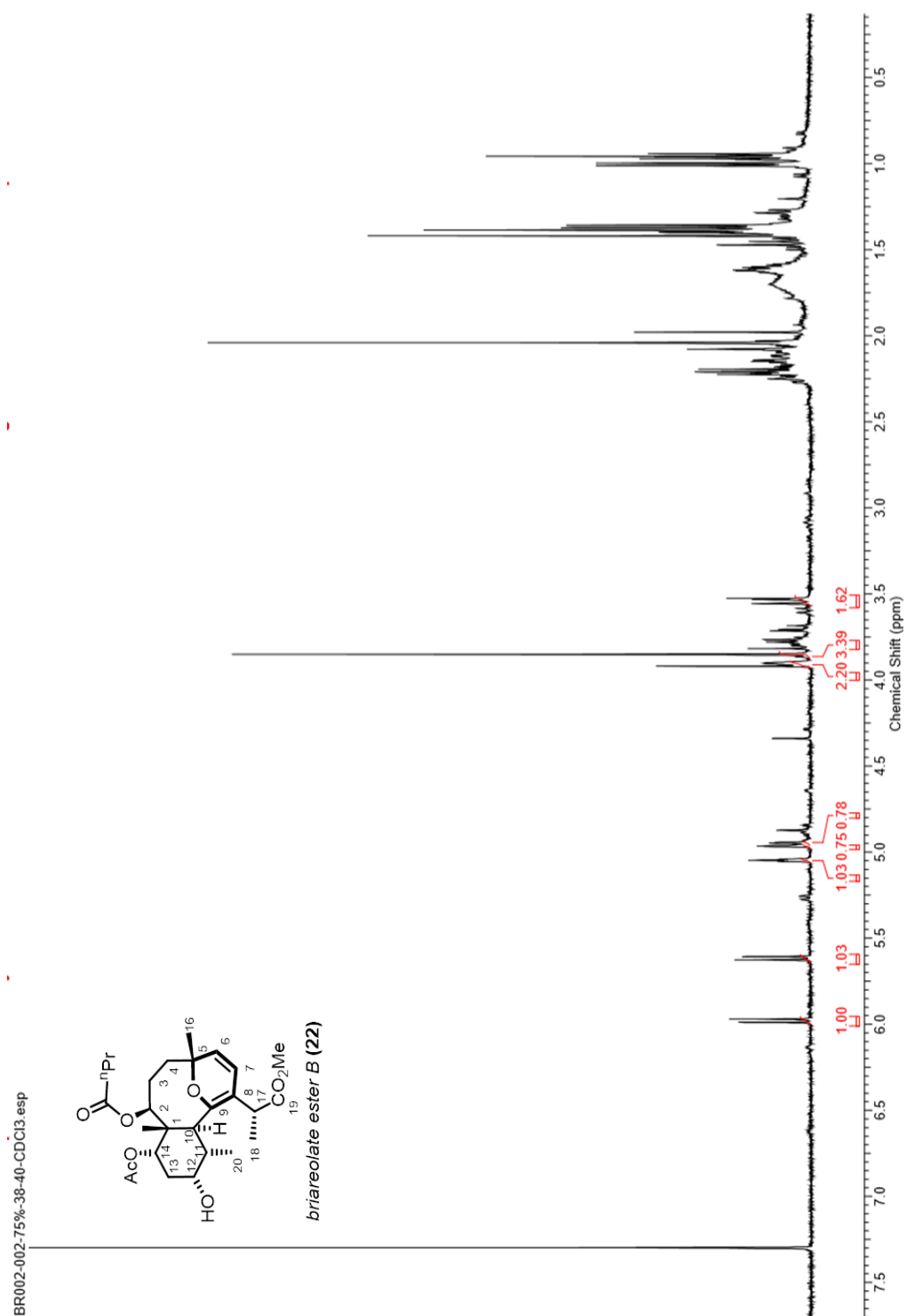


**Figure 49.** <sup>1</sup>H NMR spectrum of Briareolate ester B (**3**) (CDCl<sub>3</sub>, 400 MHz).



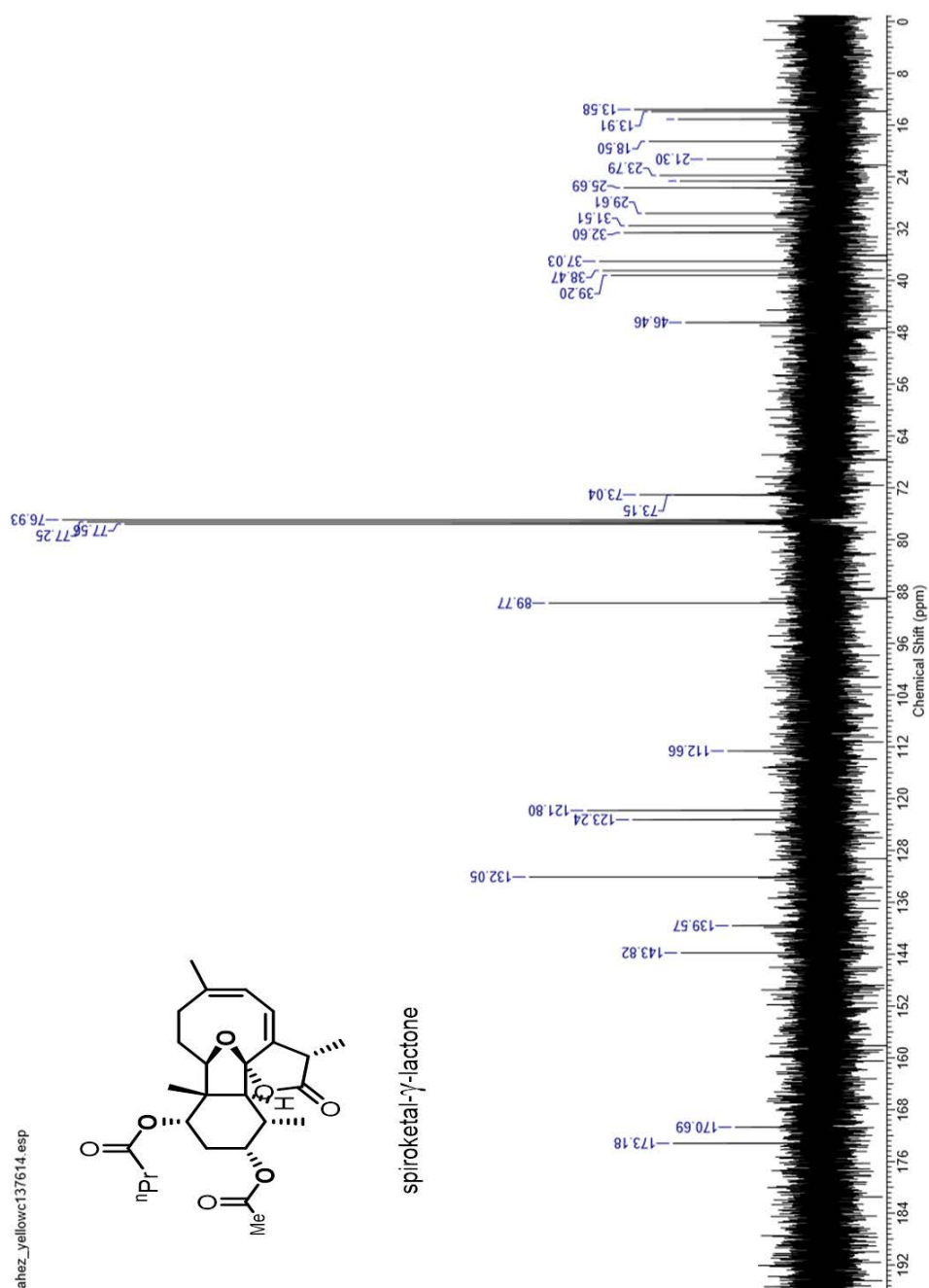


**Figure 51.** <sup>13</sup>C NMR spectrum of spiroketal  $\gamma$  lactone (**33**)(CDCl<sub>3</sub>, 400 MHz).

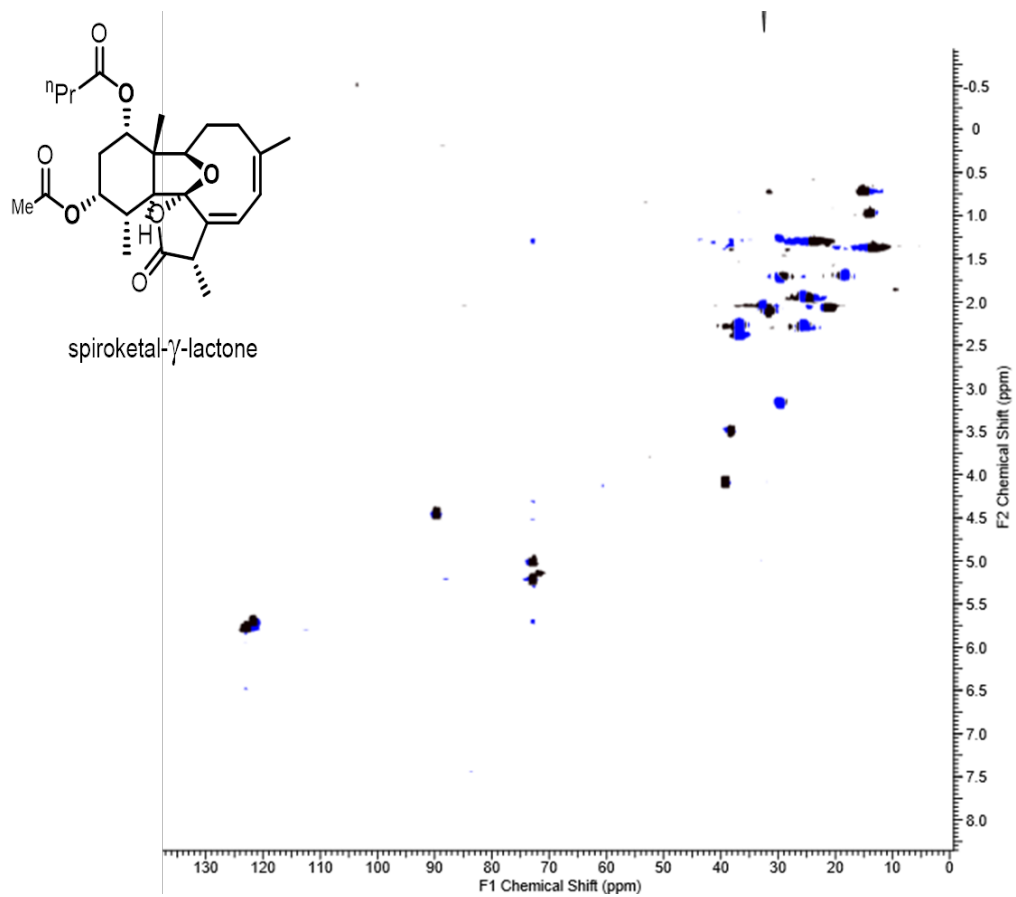


**Figure 52.** gHSQC NMR spectrum of spiroketal  $\gamma$  lactone (**33**)(CDCl<sub>3</sub>, 400 MHz).



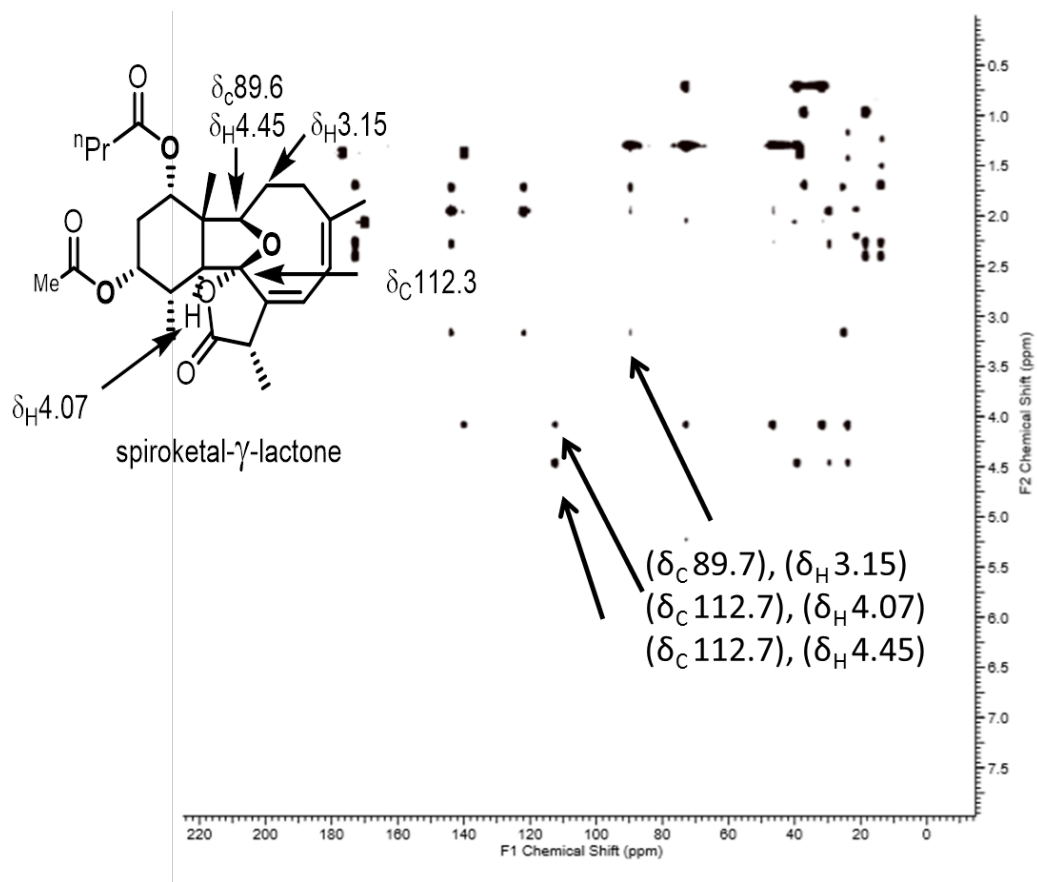


**Figure 53.** gHMBC NMR spectrum of spiroketal  $\gamma$  lactone (**33**)(CDCl<sub>3</sub>, 400 MHz).

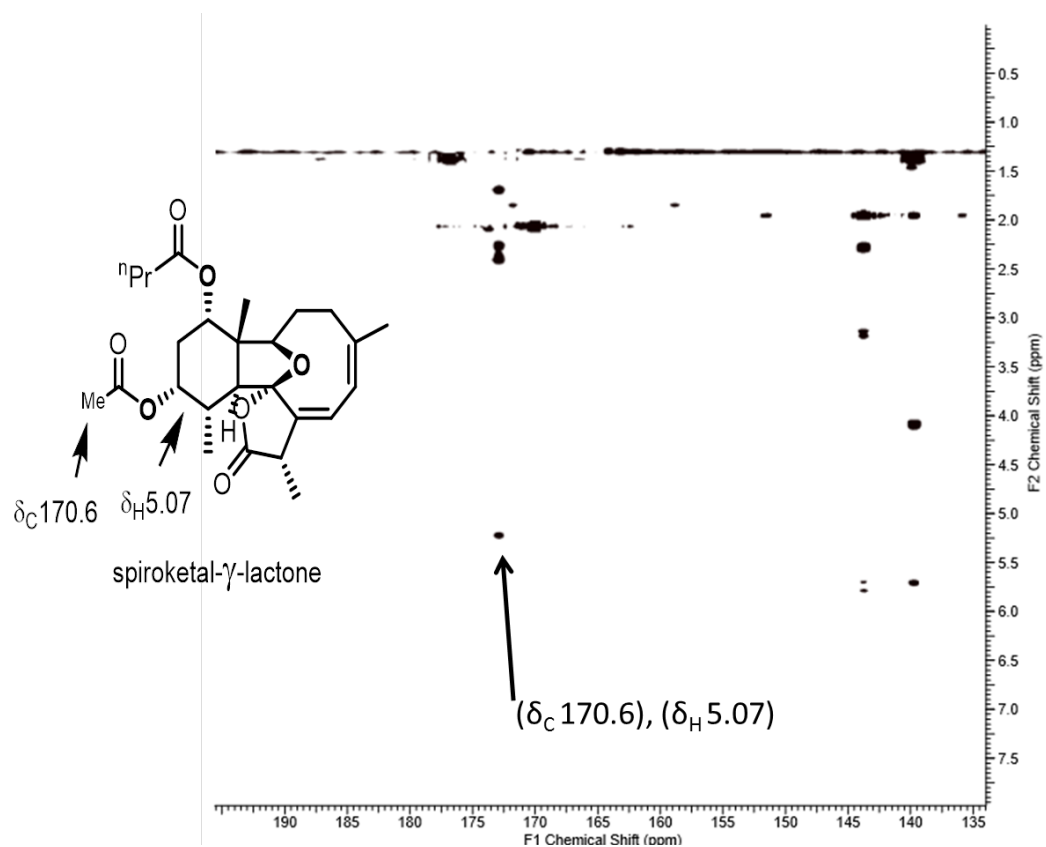


**Figure 54.** gHMBC  $J_{CH3}$  NMR spectrum of spiroketal  $\gamma$  lactone (**33**)( $CDCl_3$ , 400 MHz).

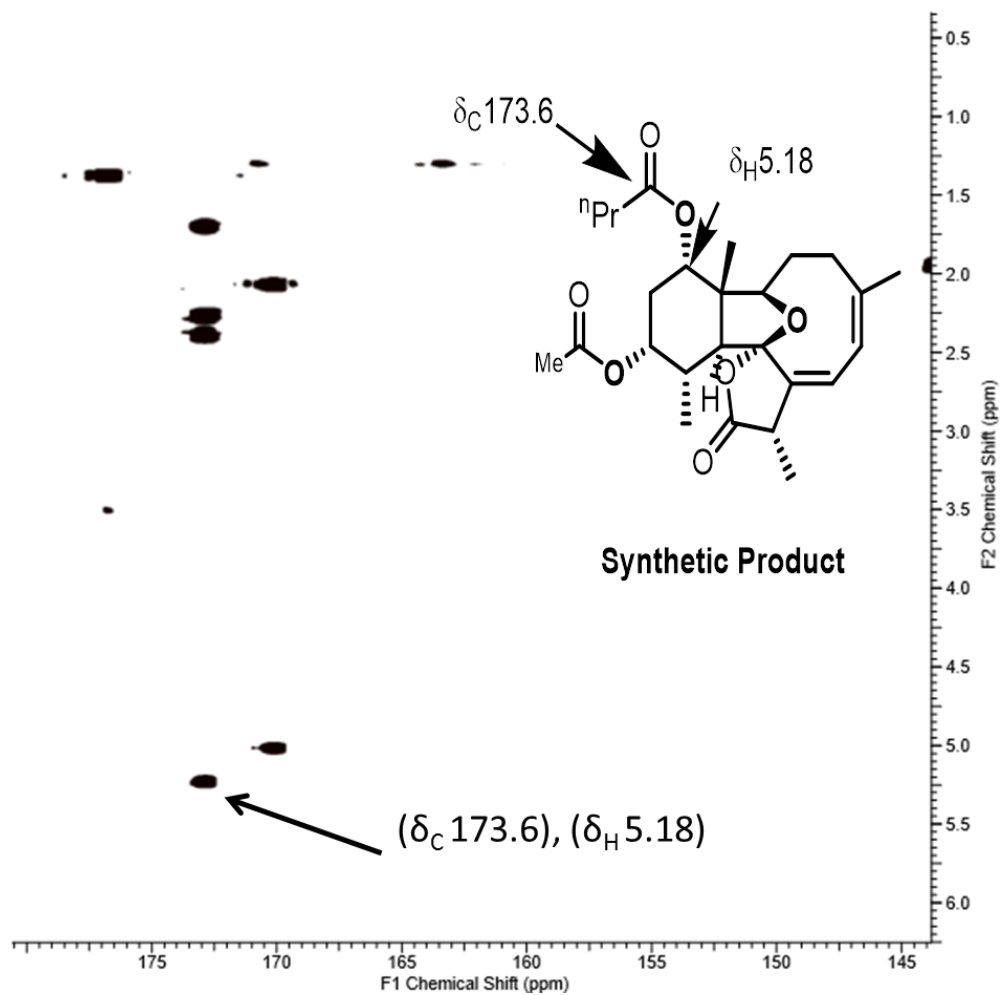


**Figure 55.** gHMBC  $J_{CH3}$  NMR spectrum spiroketal  $\gamma$  lactone (**33**)( $CDCl_3$ , 400 MHz).

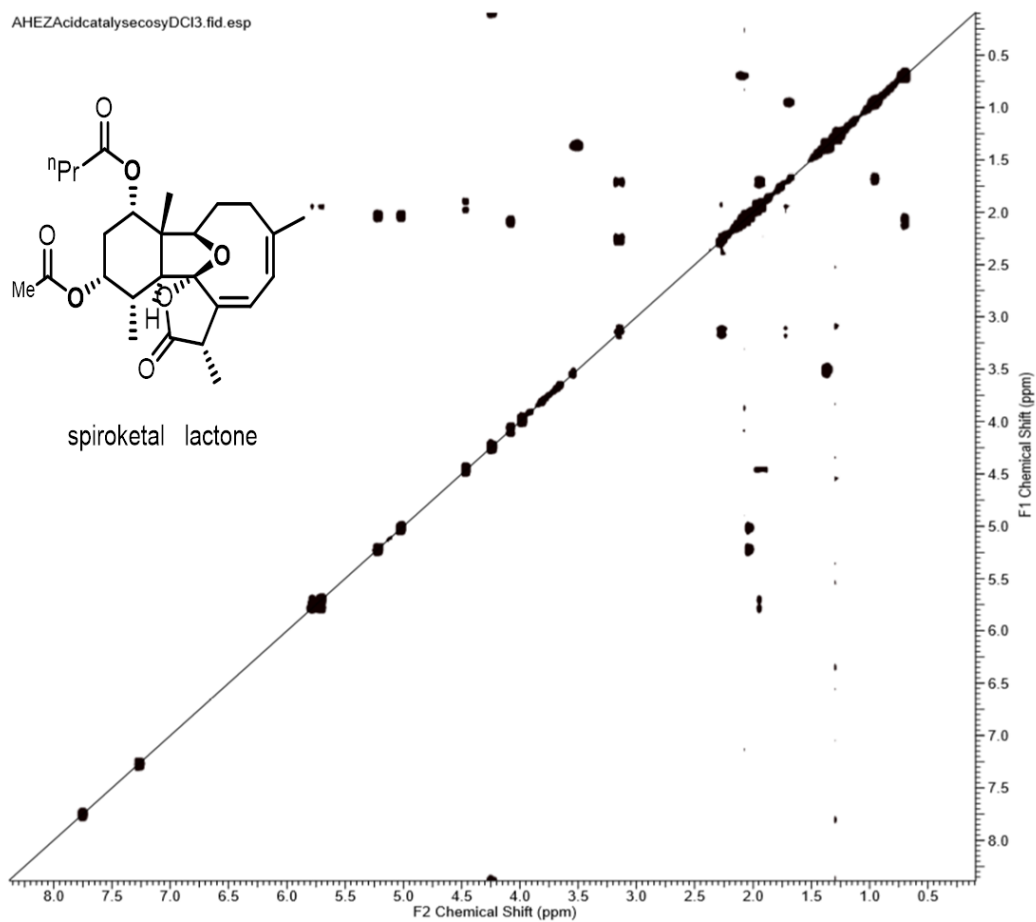


**Figure 56.** gCOSY NMR spectrum of spiroketal  $\gamma$  lactone (**33**)(CDCl<sub>3</sub>, 400 MHz).

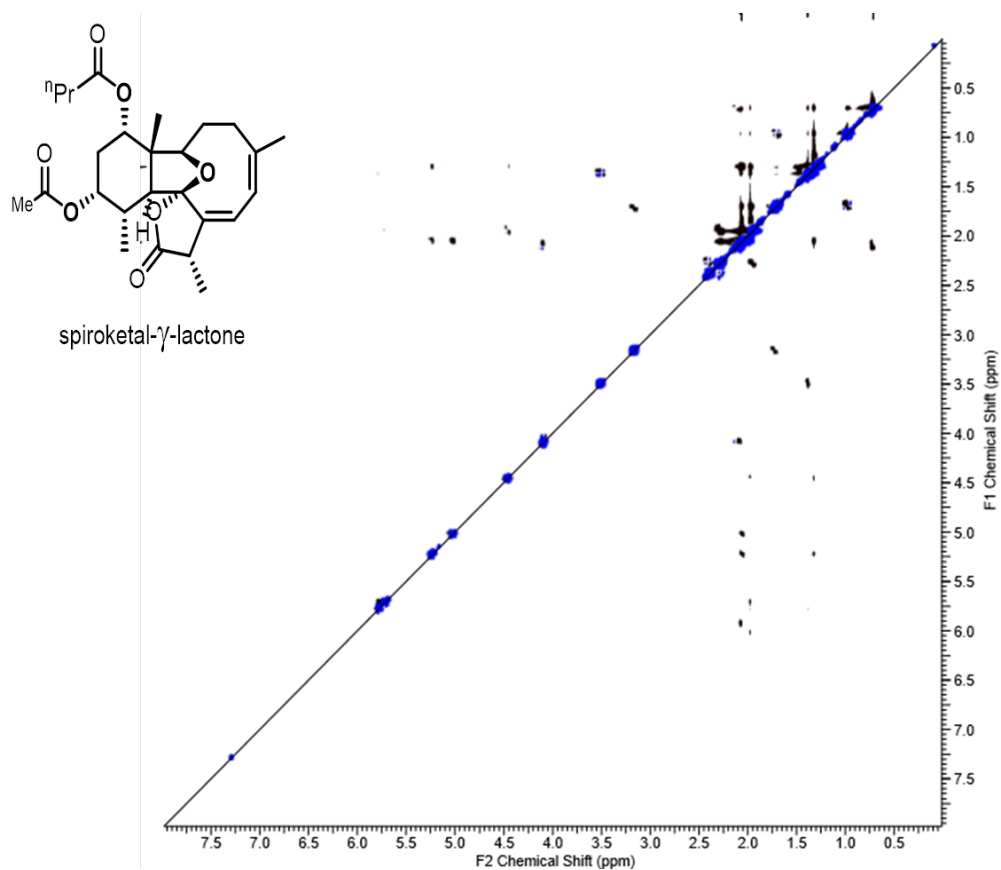


**Figure 57.** gROSY NMR spectrum of spiroketal  $\gamma$  lactone (**33**)(CDCl<sub>3</sub>, 400 MHz).

Time (min)	Proton integration						Sum of peak area			
	Briareolate Ester L		Briareolate Ester G		Briareolate Ester B		Briareolate Ester L	Briareolate Ester G	Briareolate Ester B	Total
	H6	H7	H6	H7	H6	H7				
	$\delta(6.22)$	$\delta(7.68)$	$\delta(6.14)$	$\delta(6.71)$	$\delta(5.60)$	$\delta(5.90)$				
0	1.31	1.22	0	0	0	0	2.53	0	0	2.53
0.5	0.91	1.14	0.2	0.24	0	0	2.05	0.44	0	2.49
1	0.92	0.85	0.28	0.28	0	0	1.77	0.56	0	2.33
3	0.8	0.92	0.47	0.41	0	0	1.72	0.88	0	2.6
5	0.88	0.82	0.55	0.52	0	0	1.7	1.07	0	2.77
7	0.79	0.76	0.67	0.56	0	0	1.55	1.23	0	2.78
10	0.45	0.52	0.68	0.6	0	0	0.97	1.28	0	2.25
15	0.27	0.34	0.46	0.5	0	0	0.61	0.96	0	1.57
20	0.42	0.44	0.65	0.72	0	0	0.86	1.37	0	2.23
30	0.38	0.44	0.61	0.7	0	0	0.82	1.31	0	2.13
Time (min)	% conversion									
	Briareolate Ester L		Briareolate Ester G		Briareolate Ester B		Briareolate Ester L	Briareolate Ester G	Briareolate Ester B	
0	100		0						0	
0.5	82		18						0	
1	76		24						0	
3	66		34						0	
5	61		39						0	
7	56		44						0	
10	43		57						0	
15	39		61						0	
20	39		61						0	
30	38		62						0	

**Table 6.** Table of integrated proton peaks for photochemical reaction in UVC light with Briareolate esters L (**19**). (CD<sub>3</sub>OD, 400 MHz).

Time (min)	Proton integration						Sum of peak area			
	Briareolate Ester L			Briareolate Ester G			Briareolate Ester L	Briareolate Ester G	Briareolate Ester B	Total
	H6	H7	$\delta(7.68)$	H6	H7	$\delta(6.71)$				
	$\delta(6.22)$	$\delta(7.68)$	$\delta(6.14)$	$\delta(6.14)$	$\delta(6.71)$	$\delta(5.60)$				
0	0.7	0.81	0	0	0	0	1.51	0	0	1.51
1	1.28	1.36	0.97	1.01	1.01	0.34	2.64	1.98	0.68	5.3
3	1.04	1.01	0.55	0.52	0.52	0.21	2.05	1.07	0.39	3.51
6	0.92	0.98	0.48	0.51	0.51	0.28	1.9	0.99	0.54	3.43
10	0.97	1.01	0.56	0.52	0.52	0.49	1.98	1.08	0.96	4.02
20	0.86	1	0.51	0.53	0.53	0.77	1.86	1.04	1.49	4.39
30	0.76	0.86	0.54	0.51	0.51	1.28	1.62	1.05	2.57	5.24
40	1.01	1	0.62	0.53	0.53	2.07	2.01	1.15	4.31	7.47
50	1.41	1.44	0.74	0.76	0.76	3.06	2.85	1.5	6.13	10.48

Time (min)	% conversion		
	Briareolate Ester L	Briareolate Ester G	Briareolate Ester B
0	100	0	0
1	50	37	13
3	58	30	11
6	55	29	16
10	49	27	24
20	42	24	34
30	31	20	49
40	27	15	58
50	27	14	58

**Table 7.** Table of integrated proton peaks for photochemical reaction in UVA light with Briareolate esters L (**19**) (CD<sub>3</sub>OD, 400 MHz).

Time   (min)	Proton integration						Sum of peak area			
	Briareolate Ester L		Briareolate Ester G		Briareolate Ester B					
	H6	H7	H6	H7	H6	H7	Briareolate Ester L	Briareolate Ester G	Briareolate Ester B	Total
	$\delta(6.22)$	$\delta(7.68)$	$\delta(6.14)$	$\delta(6.71)$	$\delta(5.60)$	$\delta(5.90)$				
0	0.55	0.55	0.79	0.76	2.98	3.19	1.1	1.55	6.17	8.82
1	0.46	0.57	0.75	0.92	2.33	2.46	1.03	1.67	4.79	7.49
3	0.82	0.82	1.72	1.72	2.38	2.55	1.64	3.44	4.93	10.01
6	1.18	1.4	2.03	2.39	1.78	2.05	2.58	4.42	3.83	10.83
10	1.25	1.2	2.02	2.01	1.14	1.09	2.45	4.03	2.23	8.71
20	0.56	0.56	1.05	0.95	0.15	0.17	1.12	2	0.32	3.44
30	0.88	1	1.52	1.64	0	0	1.88	3.16	0	5.04
40	0.88	1	1.52	1.64	0	0	1.88	3.16	0	5.04
50	0.88	1	1.52	1.64	0	0	1.88	3.16	0	5.04
% conversion										
Time (min)	Briareolate Ester L			Briareolate Ester G			Briareolate Ester B			
	0	12	18					70		
	1	14	22					64		
	3	16	34					49		
	6	24	41					35		
	10	28	46					26		
	20	33	58					9		
	30	37	63					0		
	40	37	63					0		

**Table 8.** Table of integrated proton peaks in UVC light with Briareolate esters B (22) (CD<sub>3</sub>OD, 400 MHz).



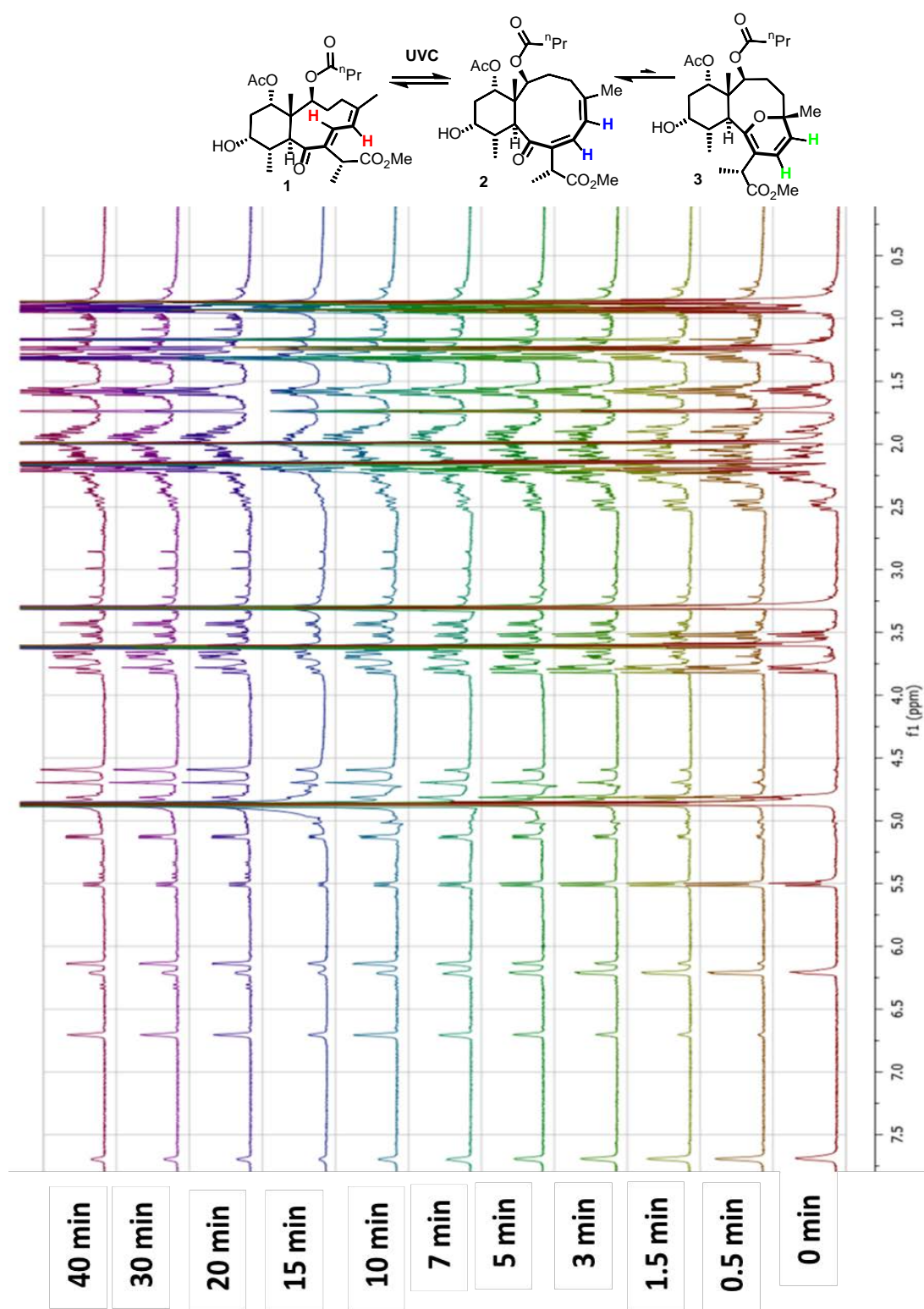


**Figure 58.** Stack of NMR data recorded over time from a photochemical reaction in UVC light with Briareolate esters L(**19**) starting material (CD<sub>3</sub>OD, 400 MHz).

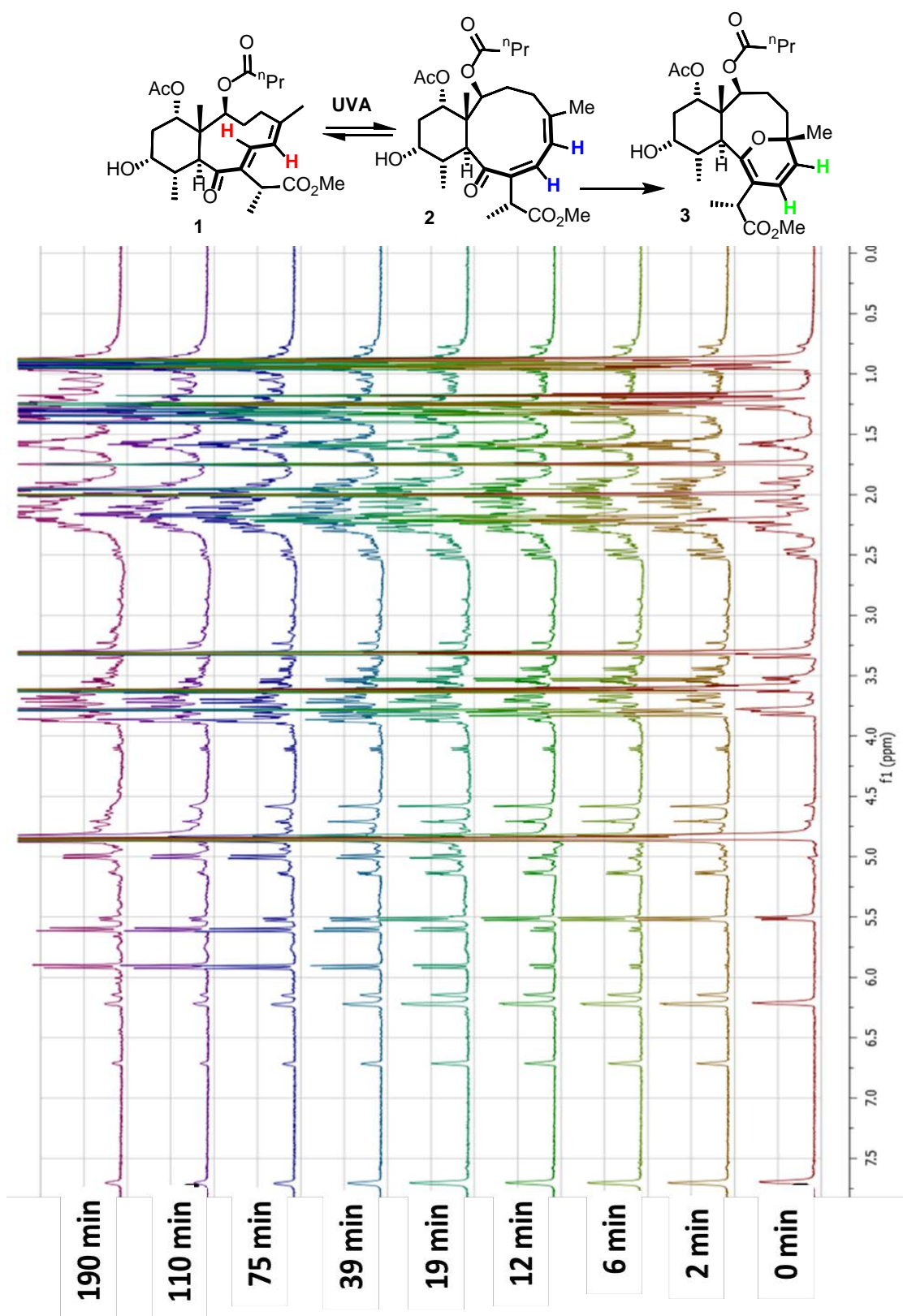


**Figure 59.** Stack of NMR data recorded over time from a photochemical reaction in UVA light with Briareolate esters L (**19**) starting material (CD<sub>3</sub>OD, 400 MHz).

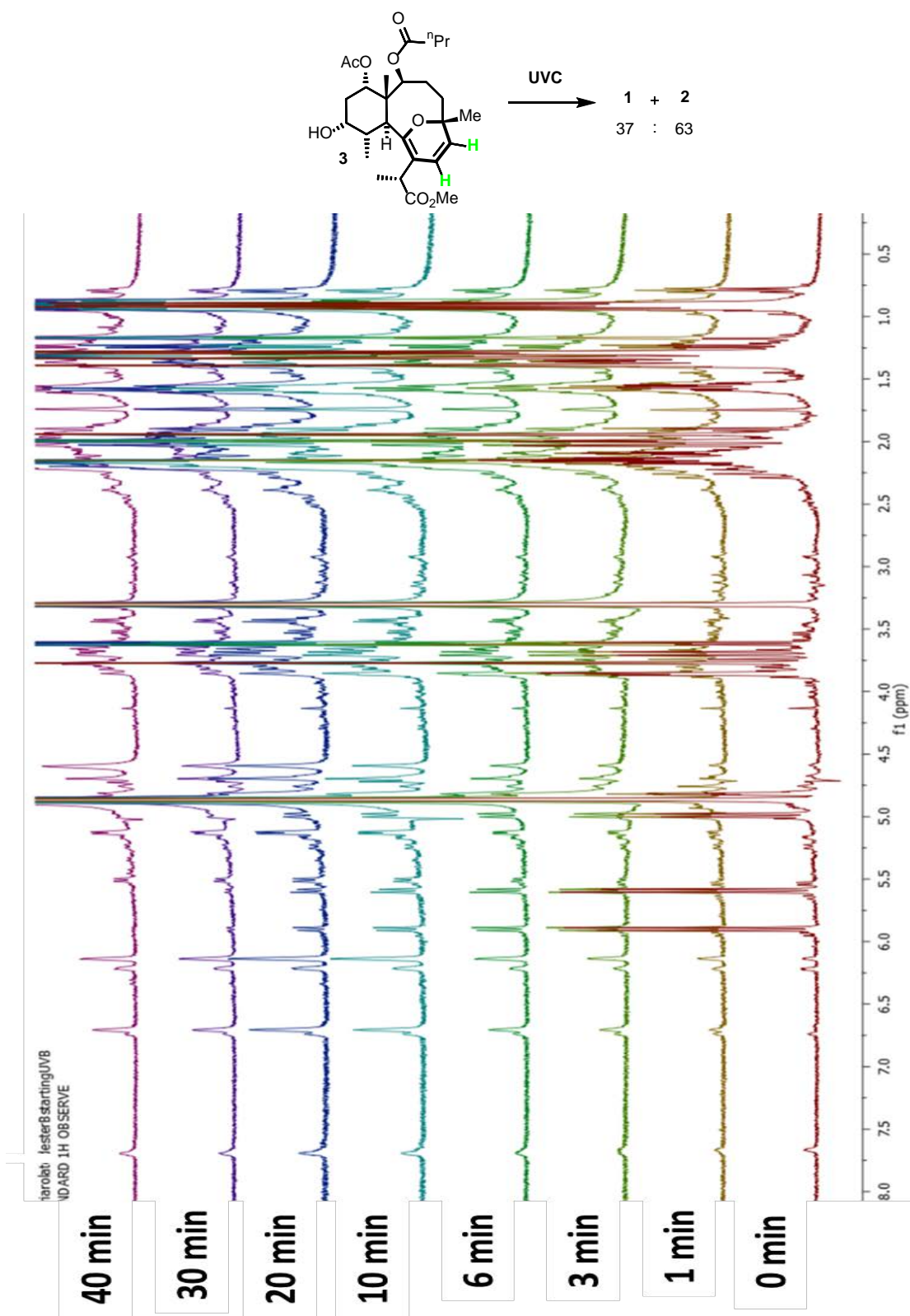


**Figure 60.** Stack of NMR data recorded over time from a photochemical reaction in UVC light with Briareolate esters B (**22**) starting material ( $\text{CD}_3\text{OD}$ , 400 MHz).

## Appendix B

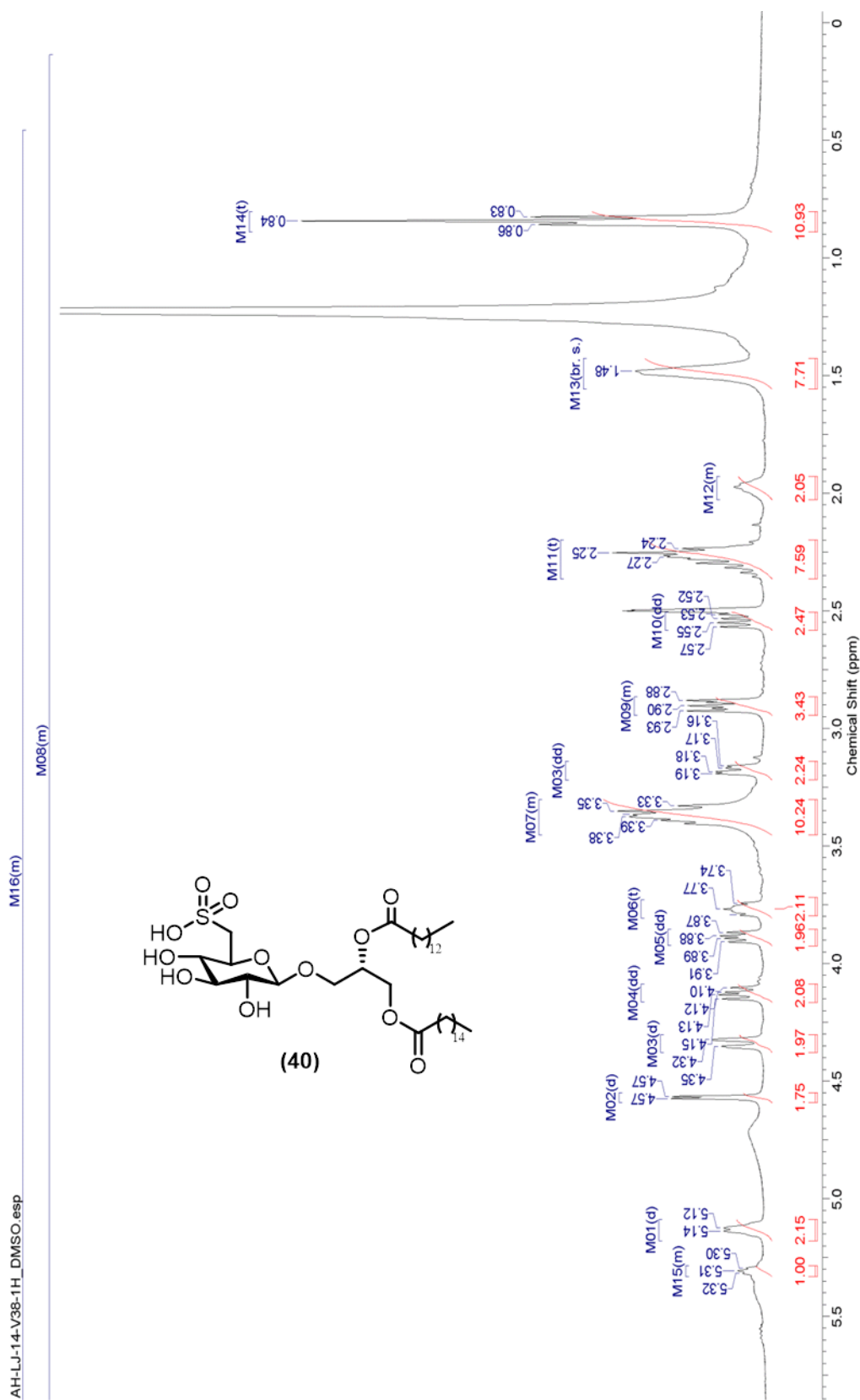


**Figure 61.**  $^1\text{H}$  NMR Spectrum LJ-14-75(**40**) ( $\text{DMSO}-d_6$ ), 400 MHz

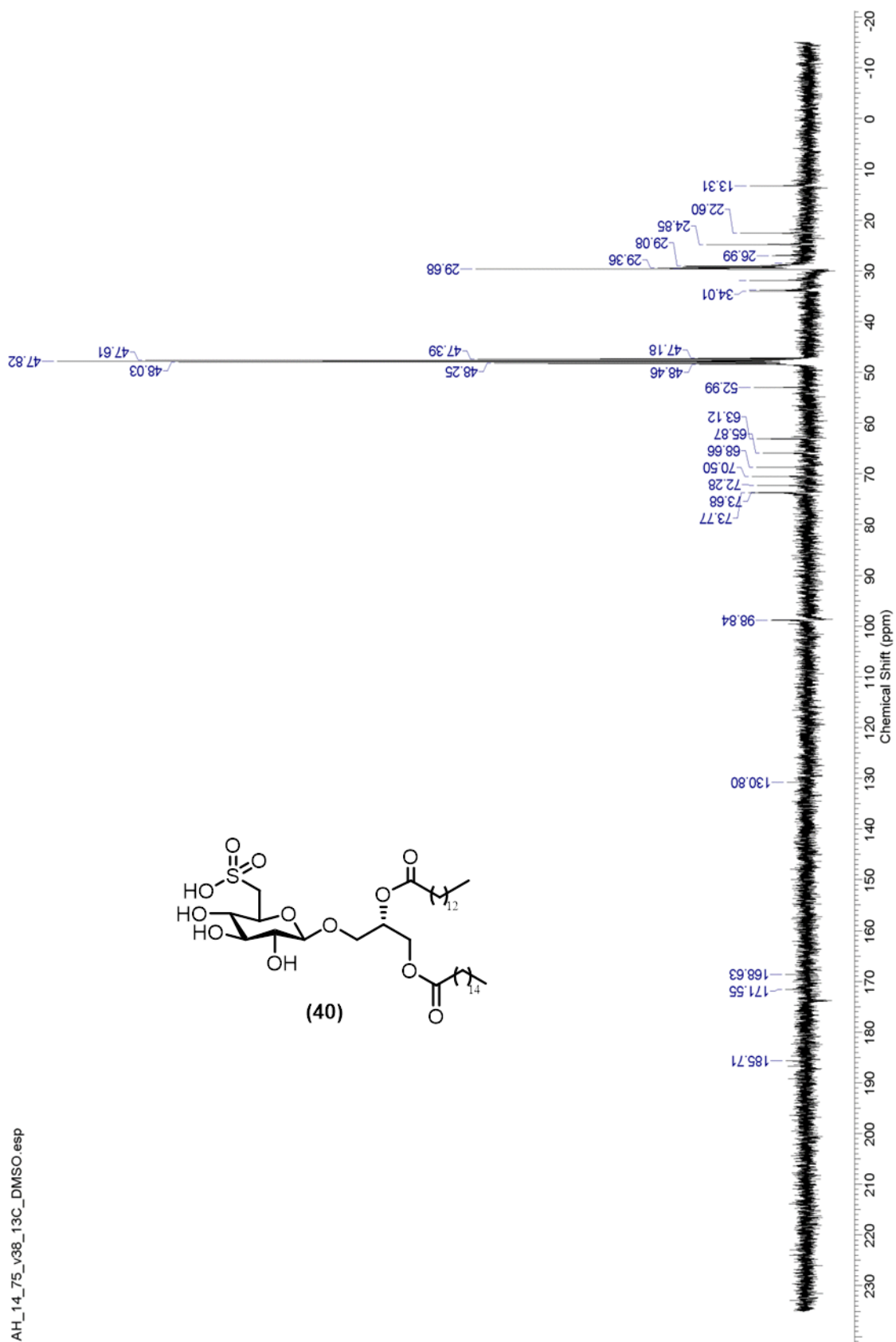


**Figure 62.**  $^{13}\text{C}$  NMR Spectrum LJ-14-75\_V38 (**40**) (DMSO- $\text{D}_6$ ), 100 MHz

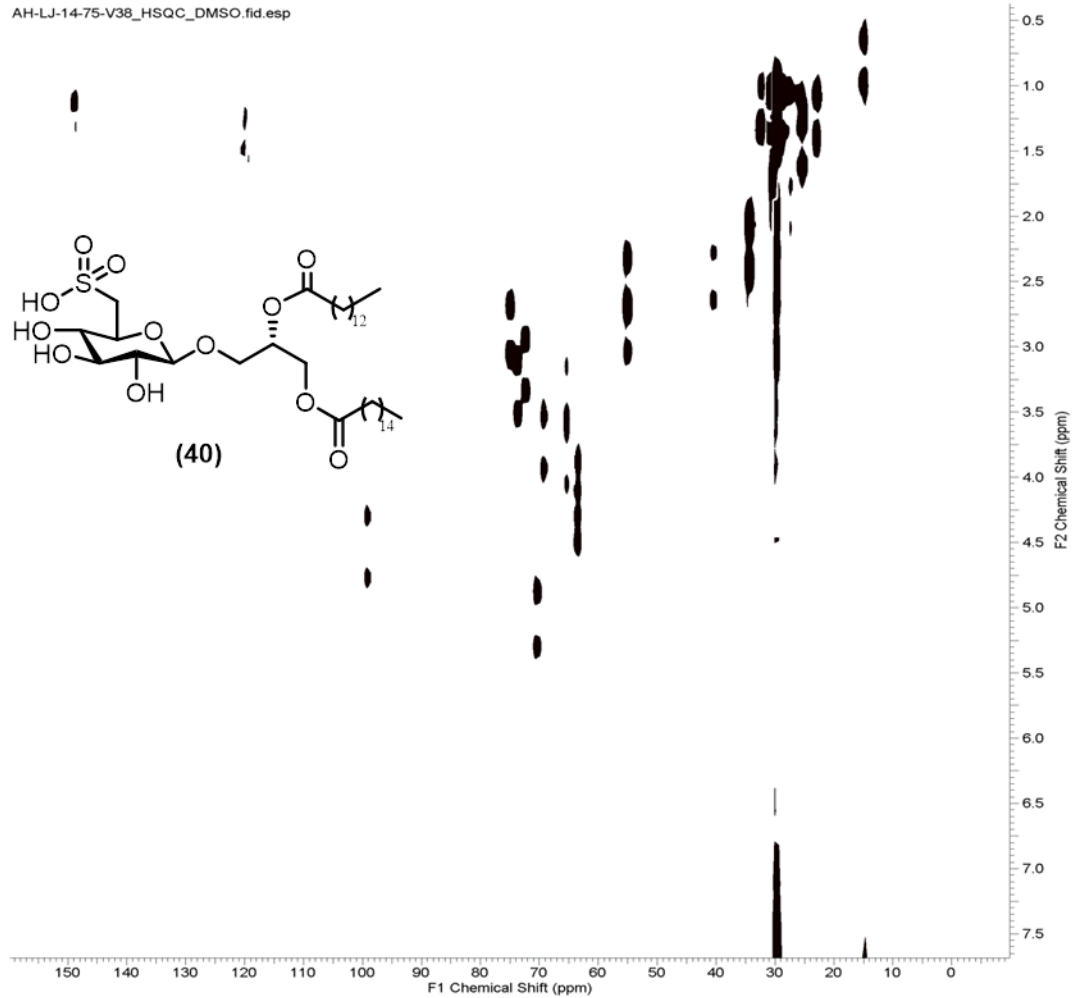


**Figure 63.**gHSQC NMR Spectrum LJ-14-75-V38 (**40**)(DMSO- $\text{D}_6$ ), 400 MHz

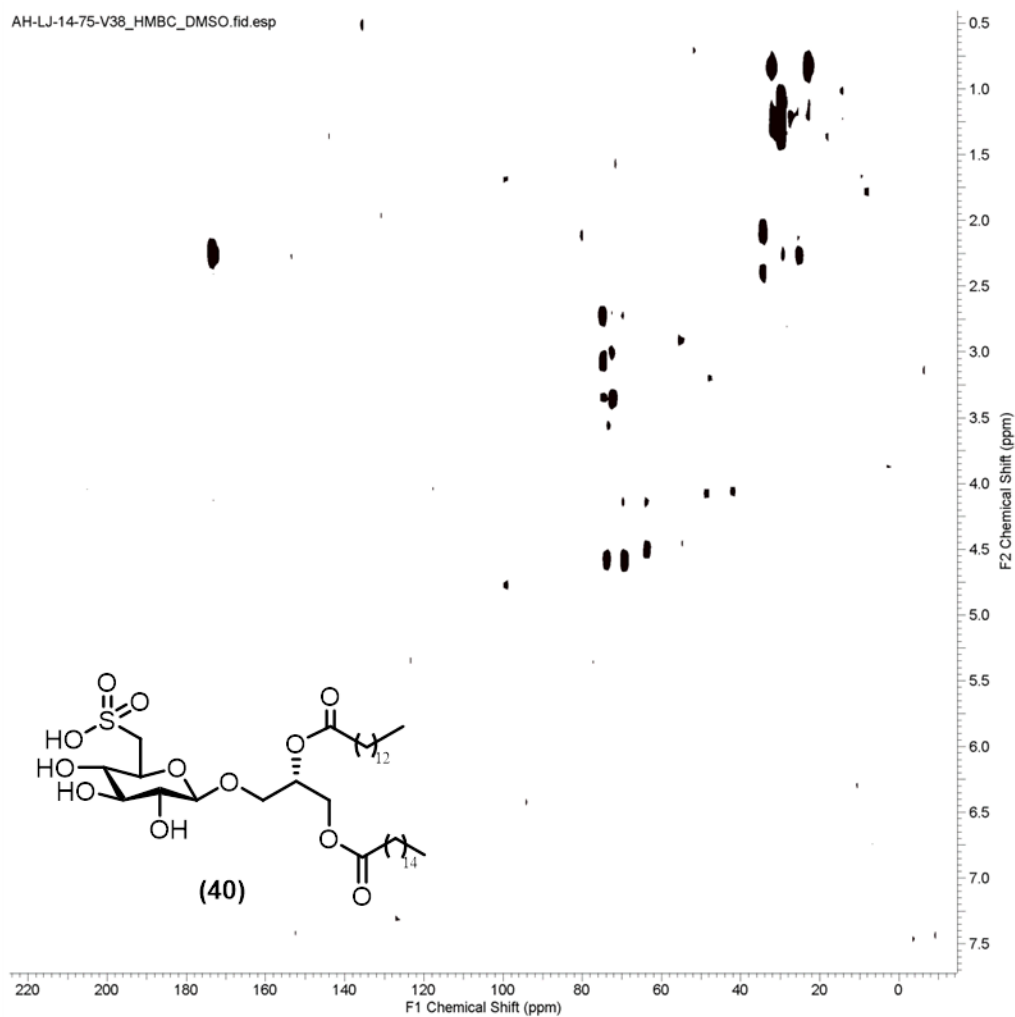


**Figure 64.** gHMBC NMR Spectrum LJ-14-75\_V38(**40**)(DMSO- $\text{D}_6$ ), 400 MHz



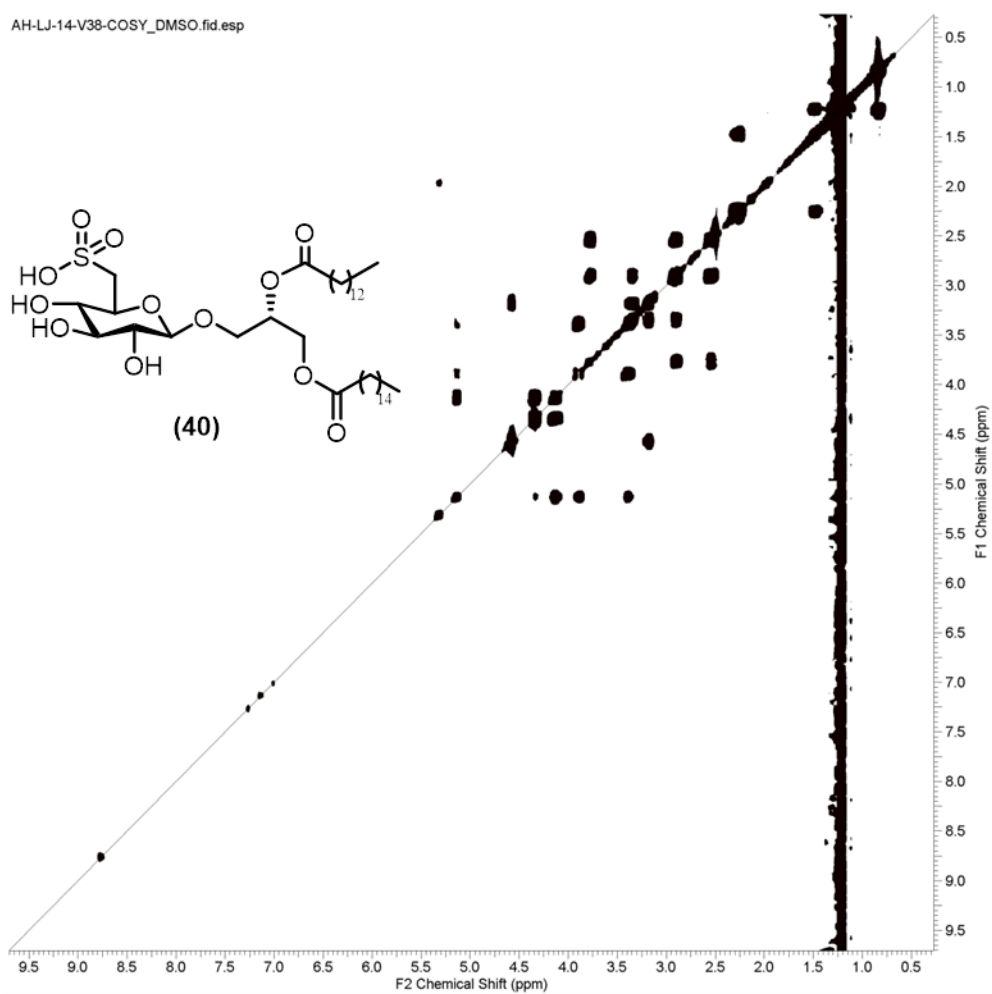


**Figure 65.** gCOSY NMR Spectrum LJ-14-75(40) (DMSO- $\text{D}_6$ ), 400 MHz



## Appendix C

**Pseudopterosin A:** amorphous solid;  $[\alpha]_D^{25}$  -85' (c 0.69, CHCl<sub>3</sub>); UV (MeOH)  $\lambda_{\max}$  = 230 nm ( $\epsilon$  11 200), 278 ( $\epsilon$  2060), 283 ( $\epsilon$  2200); IR (CHCl<sub>3</sub>) 3500, 3030, 2920, 1200 cm<sup>-1</sup>; HRESIMS (positive-ion)  $m/z$  [M + Na]<sup>+</sup> 455.2415 (calcd for C<sub>25</sub>H<sub>36</sub>O<sub>6</sub>Na, 455.2409).

**Pseudopterosin B:** oil  $[\alpha]_D^{25}$  -55.2' (c 2.1, CHCl<sub>3</sub>); UV (MeOH)  $\lambda_{\max}$  = 230-235 nm ( $\epsilon$  6000), 274 ( $\epsilon$  1400), 285 ( $\epsilon$  1600) IR (CHCl<sub>3</sub>) 3500, 3030, 2960, 1745, 1220, 1080, 1040 cm<sup>-1</sup> ESIMS (positive-ion)  $m/z$  492 [M + H<sub>2</sub>O]<sup>+</sup>; HRESIMS (positive-ion)  $m/z$  [M + H]<sup>+</sup> 475.2693 (calcd for C<sub>27</sub>H<sub>39</sub>O<sub>7</sub>, 475.2695).

**Pseudopterosin C:** crystallized  $[\alpha]_D^{25}$  -77' (c 1.09, CHCl<sub>3</sub>); UV (MeOH)  $\lambda_{\max}$  = 229 nm ( $\epsilon$  9600), 275 ( $\epsilon$  1500), 282 ( $\epsilon$  1700); IR (CHCl<sub>3</sub>) 3350-3450, 2920, 1725, 1440, 1370, 1310, 1240, 1070, 1030 cm<sup>-1</sup>; ESIMS (positive-ion)  $m/z$  492 [M + H<sub>2</sub>O]<sup>+</sup>; HRESIMS (positive-ion)  $m/z$  [M + H]<sup>+</sup> 475.2693 (calcd for C<sub>27</sub>H<sub>39</sub>O<sub>7</sub>, 475.2695).

**Pseudopterosin D:** (4). isolated as an oil.  $[\alpha]_D^{25}$  -107.3 (c 0.55, CHCl<sub>3</sub>); UV (MeOH)  $\lambda_{\max}$  230 nm ( $\epsilon$  6500), 272 ( $\epsilon$  3300), 282 (c 3100); IR (CHCl<sub>3</sub>) 3500, 3030, 2960, 1745, 1220 cm<sup>-1</sup>; HRESIMS (positive-ion)  $m/z$  [M + H]<sup>+</sup> 475.2693 (calcd for C<sub>27</sub>H<sub>39</sub>O<sub>7</sub>, 475.2695).

**Pseudopterosin K 2' acetate:** amorphous solid;  $[\alpha]_D^{25}$  -117.6 (c 0.017, CHCl<sub>3</sub>); UV (MeOH)  $\lambda_{\max}$  228 ( $\epsilon$  31232), 277 ( $\epsilon$  5477), 284 ( $\epsilon$  6075) nm; IR (film)  $\nu_{\max}$  3344, 2927, 1745, 1456, 1432, 1374, 1242 cm<sup>-1</sup>; <sup>1</sup>H (CDCl<sub>3</sub>, 500 MHz) and <sup>13</sup>C (CDCl<sub>3</sub>, 125 MHz) NMR spectra, see Table 2; HRESIMS (positive-ion)  $m/z$  [M + Na]<sup>+</sup> 511.2655 (calcd for C<sub>28</sub>H<sub>40</sub>O<sub>7</sub>Na, 511.26717).

**Pseudopterosin K 4' acetate:** amorphous solid;  $[\alpha]_D^{25}$  -130.4 (c 0.046, CHCl<sub>3</sub>); UV (MeOH)  $\lambda_{\max}$  228 ( $\epsilon$  36892), 277 ( $\epsilon$  6197), 284 ( $\epsilon$  6871) nm; IR (film)  $\nu_{\max}$  3395, 2925, 1732, 1431, 1375, 1241 cm<sup>-1</sup>; <sup>1</sup>H (CDCl<sub>3</sub>, 500 MHz) and <sup>13</sup>C (CDCl<sub>3</sub>, 125 MHz) NMR spectra, see Table 2; ESIMS (positive-ion)  $m/z$  489 [M + H]<sup>+</sup>; HRESIMS (positive-ion)  $m/z$  [M + H<sub>2</sub>O]<sup>+</sup> 506.3163 (calcd for C<sub>28</sub>H<sub>42</sub>O<sub>8</sub>, 506.2880).

**Pseudopterosin Iso-A:** amorphous solid;  $[\alpha]_D^{25}$  -130.4 (c 0.046, CHCl<sub>3</sub>); UV (MeOH)  $\lambda_{\max}$  228 ( $\epsilon$  15471), 277 ( $\epsilon$  3413), 284 ( $\epsilon$  3309) nm; IR (film)  $\nu_{\max}$  3365, 2925, 1457, 1312, 1248 cm<sup>-1</sup>; <sup>1</sup>H (CDCl<sub>3</sub>, 500 MHz) and <sup>13</sup>C (CDCl<sub>3</sub>, 125 MHz) NMR spectra, see Table 2; HRESIMS (positive-ion)  $m/z$  [M + Na]<sup>+</sup> 455.2415 (calcd for C<sub>25</sub>H<sub>36</sub>O<sub>6</sub>Na, 455.2409).

**Pseudopterosin Iso-C:** amorphous solid;  $[\alpha]_D^{25}$  -130.4 (c 0.05, CHCl<sub>3</sub>); UV (MeOH)  $\lambda_{\max}$  228 ( $\epsilon$  16003), 277 ( $\epsilon$  4266), 284 ( $\epsilon$  3555) nm; IR (film)  $\nu_{\max}$  3394, 2926, 1732, 1456, 1374, 1236 cm<sup>-1</sup>; <sup>1</sup>H (CDCl<sub>3</sub>, 500 MHz) and <sup>13</sup>C (CDCl<sub>3</sub>, 125 MHz) NMR spectra, see Table 2; ESIMS (positive-ion)  $m/z$  492 [M + H<sub>2</sub>O]<sup>+</sup>; HRESIMS (positive-ion)  $m/z$  [M + H]<sup>+</sup> 475.2693 (calcd for C<sub>27</sub>H<sub>39</sub>O<sub>7</sub>, 475.2695).

**Pseudopterosin Iso-D** : amorphous solid;  $[\alpha]_D^{25} - 133.3$  ( $c$  0.015,  $\text{CHCl}_3$ ); UV (MeOH)  $\lambda_{\text{max}}$  228 ( $\epsilon$  15879), 277 ( $\epsilon$  3126), 284 ( $\epsilon$  3056) nm; IR (film)  $\nu_{\text{max}}$  3394, 2926, 1741, 1456, 1373, 1235  $\text{cm}^{-1}$ ;  $^1\text{H}$  ( $\text{CDCl}_3$ , 500 MHz) and  $^{13}\text{C}$  ( $\text{CDCl}_3$ , 125 MHz) NMR spectra, see Table 2; HRESIMS (positive-ion)  $m/z$   $[\text{M} + \text{H}]^+$  475.2693 (calcd for  $\text{C}_{27}\text{H}_{39}\text{O}_7$ , 475.2695).

## References

- 1) (a) Carroll, S. B., Evo-devo and an expanding evolutionary synthesis: a genetic theory of morphological evolution. *Cell* **2008**, *134* (1), 25-36; (b) Mohammadi, S.; Prasanna, B., Analysis of genetic diversity in crop plants—salient statistical tools and considerations. *Crop Science* **2003**, *43* (4), 1235-1248.
- 2) (a) EUBACTERIA, E., Ribosomal RNA phylogeny and the primary lines of evolutionary descent. *Biol* **1965**, *8*, 357-366; (b) White Jr, L., *The historical roots of our ecologic crisis*. Set: 1967; Vol. 155.
- 3) (a) Butler, M. S., The role of natural product chemistry in drug discovery. *J. Nat. Prod.* **2004**, *67* (12), 2141-2153; (b) Faulkner, D. J., Marine natural products. *Natural Product Reports* **2002**, *19* (1), 1-49; (c) Avise, J. C., *Molecular markers, natural history and evolution*. Springer Science & Business Media: 2012.
- 4) (a) Li, J. W.-H.; Vederas, J. C., Drug discovery and natural products: end of an era or an endless frontier? *Science* **2009**, *325* (5937), 161-165; (b) Shu, Y.-Z., Recent natural products based drug development: a pharmaceutical industry perspective. *J. Nat. Prod.* **1998**, *61* (8), 1053-1071; (c) Newman, D. J.; Cragg, G. M.; Snader, K. M., Natural products as sources of new drugs over the period 1981-2002. *J. Nat. Prod.* **2003**, *66* (7), 1022-1037.
- 5) (a) Newman, D. J.; Cragg, G. M., Natural Products as Sources of New Drugs over the Last 25 Years<sup>1</sup>. *J. Nat. Prod.* **2007**, *70* (3), 461-477; (b) Barnes, P. M.; Bloom, B.; Nahin, R. L.; Statistics, N. C. f. H., *Complementary and alternative medicine use among adults and children: United States, 2007*. US Department of Health and Human Services,

Centers for Disease Control and Prevention, National Center for Health Statistics  
Hyattsville, MD: 2008.

- 6) (a) Newman, D. J.; Cragg, G. M., Natural Products as Sources of New Drugs from 1981 to 2014. *J. Nat. Prod.* **2016**, 79 (3), 629-661; (b) Cristina Campos, H.; Divino da Rocha, M.; Pereira Dias Viegas, F.; Carolina Nicastro, P.; Calve Fossaluzza, P.; Alberto Manssour Fraga, C.; J Barreiro, E.; Viegas, C., The role of natural products in the discovery of new drug candidates for the treatment of neurodegenerative disorders I: Parkinson's disease. *CNS & Neurological Disorders-Drug Targets (Formerly Current Drug Targets-CNS & Neurological Disorders)* **2011**, 10 (2), 239-250; (c) Müller-Kuhrt, L., Putting nature back into drug discovery. *Nat. Biotechnol.* **2003**, 21 (6), 602-602.
- 7) Barnes, P. M.; Powell-Griner, E.; McFann, K.; Nahin, R. L. In *Complementary and alternative medicine use among adults: United States, 2002*, Seminars in Integrative Medicine, Elsevier: 2004; pp 54-71.
- 8) Dewick, P. M., *Medicinal natural products: a biosynthetic approach*. John Wiley & Sons: 2002.
- 9) (a) Carroll, C. B.; Zeissler, M. L.; Hanemann, C. O.; Zajicek, J. P.,  $\Delta^9$ -tetrahydrocannabinol ( $\Delta^9$ -THC) exerts a direct neuroprotective effect in a human cell culture model of Parkinson's disease. *Neuropathology and Applied Neurobiology* **2012**, 38 (6), 535-547; (b) Kalant, H., Medicinal use of cannabis: history and current status. *Pain Research and Management* **2001**, 6 (2), 80-94; (c) Butler, M. S., Natural products to drugs: natural product derived compounds in clinical trials. *Natural Product Reports* **2005**, 22 (2), 162-195.

- 10) elsohly, M. A., Marijuana and the cannabinoids. Steven B. Karch, M., Ed. Humana press: Totowa
- 11) Tramèr, M. R.; Carroll, D.; Campbell, F. A.; Reynolds, D. J. M.; Moore, R. A.; McQuay, H. J., Cannabinoids for control of chemotherapy induced nausea and vomiting: quantitative systematic review. *Bmj* **2001**, 323 (7303), 16.
- 12) Verma, A., *Invertebrates: Protozoa to Echinodermata*. Narosa Publishing House: 2005.
- 13) Rocha, J.; Peixe, L.; Gomes, N. C. M.; Calado, R., Cnidarians as a Source of New Marine Bioactive Compounds—An Overview of the Last Decade and Future Steps for Bioprospecting. *Marine Drugs* **2011**, 9 (10), 1860-1886.
- 14) Newman, D. J.; Cragg, G. M.; Battershill, C. N., Therapeutic agents from the sea: biodiversity, chemo-evolutionary insight and advances to the end of Darwin's 200th year. **2009**.
- 15) Martins, A.; Vieira, H.; Gaspar, H.; Santos, S., Marketed marine natural products in the pharmaceutical and cosmeceutical industries: Tips for success. *Marine Drugs* **2014**, 12 (2), 1066-1101.
- 16) Dias, D. A.; Urban, S.; Roessner, U., A historical overview of natural products in drug discovery. *Metabolites* **2012**, 2 (2), 303-336.
- 17) (a) Ferreira, S., Prostaglandins, aspirin-like drugs and analgesia. *Nature* **1972**, 240 (102), 200-203; (b) Leal, M. C.; Puga, J.; Serôdio, J.; Gomes, N. C.; Calado, R., Trends in the discovery of new marine natural products from invertebrates over the last two decades—where and what are we bioprospecting. *PLoS ONE* **2012**, 7 (1).

- 18)** (a) Molinski, T. F.; Dalisay, D. S.; Lievens, S. L.; Saludes, J. P., Drug development from marine natural products. *Nature Reviews Drug Discovery* **2009**, 8 (1), 69-85; (b) Shetty, N.; Gupta, S., Eribulin drug review. *South Asian journal of cancer* **2014**, 3 (1), 57; (c) Bai, R. L.; Paull, K. D.; Herald, C. L.; Malspeis, L.; Pettit, G. R.; Hamel, E., Halichondrin B and homohalichondrin B, marine natural products binding in the vinca domain of tubulin. Discovery of tubulin-based mechanism of action by analysis of differential cytotoxicity data. *J. Biol. Chem.* **1991**, 266 (24), 15882-15889.
- 19)** Wang, Y.; Habgood, G. J.; Christ, W. J.; Kishi, Y.; Littlefield, B. A.; Yu, M. J., Structure–activity relationships of Halichondrin B analogues: modifications at C.30–C.38. *Bioorg. Med. Chem. Lett.* **2000**, 10 (10), 1029-1032.
- 20)** (a) Coffroth, M. A., Ingestion and incorporation of coral mucus aggregates by a gorgonian soft coral. *Marine ecology progress series. Oldendorf* **1984**, 17 (2), 193-199; (b) Balandrin, M. F.; Klocke, J. A.; Wurtele, E. S.; Bollinger, W. H., Natural plant chemicals: sources of industrial and medicinal materials. *Science* **1985**, 228 (4704), 1154-1160; (c) Williams, G. C., *Adaptation and Natural Selection: A Critique of Some Current Evolutionary Thought: A Critique of Some Current Evolutionary Thought*. Princeton University Press: 2008.
- 21)** (a) Paul A. Steudlera, b., \*, ; Francis J. Schmitza, b.; Ciereszko, L. S., Chemistry of coelenterates. Sterol composition of some predator-prey pairs on coral reefs. *Comparative Biochemistry and Physiology Part B: Comparative Biochemistry* **1977**, 56B, 385-392; (b) Ciereszko, L. S.; Odense, P. H.; Schmidt, R. W., CHEMISTRY OF COELENTERATES. II. OCCURRENCE OF TAUROBETAINE AND CREATINE IN GORGONIANS\*. *Ann. N.Y. Acad. Sci.* **1960**, 90 (3), 920-922; (c) Schmitz, F. J.;

- Lorance, E. D., Chemistry of coelenterates. XXI. Lactones from the gorgonian *Pterogorgia guadalupensis*. *The Journal of Organic Chemistry* **1971**, 36 (5), 719-721; (d) Chen, P.-J. S. a. M.-C., The Heterocyclic Natural Products of Gorgonian Corals of Genus *Briareum* Exclusive of Briarane-type Diterpenoids. *Hetrocycles* **2002**, 57, 1705-1715.
- 22)** (a) Steudler, P. A.; Schmitz, F. J.; Ciereszko, L. S., Chemistry of coelenterates. Sterol composition of some predator-prey pairs on coral reefs. *Comparative Biochemistry and Physiology Part B: Comparative Biochemistry* **1977**, 56 (4), 385-392; (b) Rodríguez, A. D.; Cóbar, O. M., The briarellins, new eunicellin-based diterpenoids from a Caribbean gorgonian, *Briareum asbestinum*. *Tetrahedron* **1995**, 51 (25), 6869-6880.
- 23)** (a) McGarvey, D. J.; Croteau, R., Terpenoid metabolism. *The Plant Cell* **1995**, 7 (7), 1015-1026; (b) Dubey, V. S.; Bhalla, R.; Luthra, R., An overview of the non-mevalonate pathway for terpenoid biosynthesis in plants. *Journal of biosciences* **2003**, 28 (5), 637-646.
- 24)** Dookran, R.; Maharaj, D.; Mootoo, B. S.; Ramsewak, R.; McLean, S.; Reynolds, W. F.; Tinto, W. F., Briarane and asbestinane diterpenes from *Briareum asbestinum*. *Tetrahedron* **1994**, 50 (7), 1983-1992.
- 25)** Stierle, D. B.; Carte, B.; Faulkner, D. J.; Tagle, B.; Clardy, J., The asbestinins, a novel class of diterpenes from the gorgonian *Briareum asbestinum*. *J. Am. Chem. Soc.* **1980**, 102 (15), 5088-5092.
- 26)** Berrue, F.; Kerr, R. G., Diterpenes from gorgonian corals. *Natural Product Reports* **2009**, 26 (5), 681-710.
- 27)** Kennard, O.; Watson, D.; Di Sanseverino, L. R.; Tursch, B.; Bosmans, R.; Djerassi, C., Chemical studies of marine invertebrates. IV. Terpenoids LXII. Eunicellin, a

diterpenoid of the gorgonian Eunicella stricta. X-ray diffraction analysis of Eunicellin dibromide. *Tetrahedron Lett.* **1968**, 9 (24), 2879-2884.

**28)** Paquette\*, P. B. a. L. A., Survey of Oxygenated 2,11-Cyclized Cembranoids of Marine Origin. *Hetrocycles* **1998**, 49 (1998), 531-555.

**29)** Cobar, O. M., Survey of 2, 11-cyclized cembranoids from Caribbean sources. *Natural product research* **2009**, 23 (1), 26-43.

**30)** Stocking, E. M.; Williams, R. M., Chemistry and biology of biosynthetic Diels–Alder reactions. *Angew. Chem. Int. Ed.* **2003**, 42 (27), 3078-3115.

**31)** (a) Bates, R. W.; Pinsa, A.; Kan, X., Synthesis of the Northern hemisphere of the briaranes. *Tetrahedron* **2010**, 66 (33), 6340-6348; (b) Moon, N. G.; Harned, A. M., A Concise Synthetic Route to the Stereotetrad Core of the Briarane Diterpenoids. *Org. Lett.* **2015**, 17 (9), 2218-2221.

**32)** Stichnoth, D.; Kölle, P.; Kimbrough, T. J.; Riedle, E.; de Vivie-Riedle, R.; Trauner, D., Photochemical formation of intricarene. *Nat Commun* **2014**, 5.

**33)** (a) Hoffmann, N., Photochemical reactions as key steps in organic synthesis. *Chem. Rev.* **2008**, 108 (3), 1052-1103; (b) Roche, S. P.; Porco, J. A., Dearomatization strategies in the synthesis of complex natural products. *Angew. Chem. Int. Ed.* **2011**, 50 (18), 4068-4093; (c) Stichnoth, D.; Kölle, P.; Kimbrough, T. J.; Riedle, E.; de Vivie-Riedle, R.; Trauner, D., Photochemical formation of intricarene. *Nature communications* **2014**, 5; (d) Bach, T.; Hehn, J. P., Photochemical reactions as key steps in natural product synthesis. *Angew. Chem. Int. Ed.* **2011**, 50 (5), 1000-1045.

**34)** Lillya, C. P.; Kluge, A. F., Molecular spectra and conformations of conjugated dienones. *The Journal of Organic Chemistry* **1971**, 36 (14), 1977-1988.



- 35)** (a) Houk, K. N.; Gonzalez, J.; Li, Y., Pericyclic reaction transition states: Passions and punctilios, 1935-1995. *Acc. Chem. Res.* **1995**, 28 (2), 81-90; (b) Laschat, S., Pericyclic Reactions in Biological Systems—Does Nature Know About the Diels—Alder Reaction? *Angewandte Chemie International Edition in English* **1996**, 35 (3), 289-291; (c) Nicolaou, K. C.; Snyder, S. A.; Montagnon, T.; Vassilikogiannakis, G., The Diels—Alder reaction in total synthesis. *Angew. Chem. Int. Ed.* **2002**, 41 (10), 1668-1698; (d) Wiest, O.; Houk, K., Density functional theory calculations of pericyclic reaction transition structures. In *Density Functional Theory IV*, Springer: 1996; pp 1-24.
- 36)** (a) Tietze, L. F., Domino reactions in organic synthesis. *Chem. Rev.* **1996**, 96 (1), 115-136; (b) Nicolaou, K.; Montagnon, T.; Snyder, S. A., Tandem reactions, cascade sequences, and biomimetic strategies in total synthesis. *Chem. Commun.* **2003**, (5), 551-564; (c) Thompson, S.; Coyne, A. G.; Knipe, P. C.; Smith, M. D., Asymmetric electrocyclic reactions. *Chem. Soc. Rev.* **2011**, 40 (7), 4217-4231; (d) Vaidya, T.; Eisenberg, R.; Frontier, A. J., Catalytic Nazarov cyclization: the state of the art. *ChemCatChem* **2011**, 3 (10), 1531-1548; (e) Beaudry, C. M.; Malerich, J. P.; Trauner, D., Biosynthetic and Biomimetic Electrocyclizations. *Chemical Reviews* **2005**, 105 (12), 4757-4778.
- 37)** (a) Layton, M. E.; Morales, C. A.; Shair, M. D., Biomimetic synthesis of (-)-Longithorone A. *J. Am. Chem. Soc.* **2002**, 124 (5), 773-775; (b) Munakata, R.; Katakai, H.; Ueki, T.; Kurosaka, J.; Takao, K.-i.; Tadano, K.-i., Total synthesis of (+)-macquarimicin A. *J. Am. Chem. Soc.* **2003**, 125 (48), 14722-14723; (c) Dineen, T. A.; Roush, W. R., Total synthesis of cochleamycin A. *Org. Lett.* **2004**, 6 (12), 2043-2046; (d) Balskus, E. P.; Jacobsen, E. N., Asymmetric catalysis of the transannular Diels-Alder

reaction. *Science* **2007**, *317* (5845), 1736-1740; (e) Marsault, E.; Toró, A.; Nowak, P.; Deslongchamps, P., The transannular Diels–Alder strategy: applications to total synthesis. *Tetrahedron* **2001**, *57* (20), 4243-4260.

**38)** (a) Evans, D. A.; Starr, J. T., A Cascade Cycloaddition Strategy Leading to the Total Synthesis of (–)-FR182877. *Angew. Chem.* **2002**, *114* (10), 1865-1868; (b) Vosburg, D. A.; Vanderwal, C. D.; Sorensen, E. J., A synthesis of (+)-FR182877, featuring tandem transannular Diels-Alder reactions inspired by a postulated biogenesis. *J. Am. Chem. Soc.* **2002**, *124* (17), 4552-4553; (c) Evans, D. A.; Starr, J. T., A cycloaddition cascade approach to the total synthesis of (–)-FR182877. *J. Am. Chem. Soc.* **2003**, *125* (44), 13531-13540; (d) Vanderwal, C. D.; Vosburg, D. A.; Weiler, S.; Sorensen, E. J., An enantioselective synthesis of FR182877 provides a chemical rationalization of its structure and affords multigram quantities of its direct precursor. *J. Am. Chem. Soc.* **2003**, *125* (18), 5393-5407.

**39)** (a) Woodward, R. B.; Hoffmann, R., Stereochemistry of Electrocyclic Reactions. *Journal of the American Chemical Society* **1965**, *87* (2), 395-397; (b) Longuet-Higgins, H.; Abrahamson, E., The electronic mechanism of electrocyclic reactions. *J. Am. Chem. Soc.* **1965**, *87* (9), 2045-2046; (c) Rondan, N. G.; Houk, K., Theory of stereoselection in conrotatory electrocyclic reactions of substituted cyclobutenes. *J. Am. Chem. Soc.* **1985**, *107* (7), 2099-2111.

**40)** Woodward, R. B.; Hoffmann, R., The Conservation of Orbital Symmetry. *Angewandte Chemie International Edition in English* **1969**, *8* (11), 781-853.

**41)** Malerich, J. P.; Maimone, T. J.; Elliott, G. I.; Trauner, D., Biomimetic Synthesis of Antimalarial Naphthoquinones. *J. Am. Chem. Soc.* **2005**, *127* (17), 6276-6283.

**42)** (a) Becker, R. S.; Michl, J., Photochromism of synthetic and naturally occurring 2H-chromenes and 2H-pyrans. *J. Am. Chem. Soc.* **1966**, 88 (24), 5931-5933; (b) Büchi, G.; Yang, N., Light-catalyzed Organic Reactions. VI. 1 The Isomerization of Some Dienones<sup>2</sup>, 3. *J. Am. Chem. Soc.* **1957**, 79 (9), 2318-2323; (c) Balenović, K.; Poje, M., Self-condensation of 1, 3, 4, 6-tetraketones. The electrocyclic reaction of a dienone system derived from the dienolic form. *Tetrahedron Lett.* **1979**, 20 (23), 2175-2178; (d) Peng, W.; Hirabaru, T.; Kawafuchi, H.; Inokuchi, T., Substituent-Controlled Electrocyclization of 2, 4-Dienones: Synthesis of 2, 3, 6-Trisubstituted 2H-Pyran-5-carboxylates and Their Transformations. *Eur. J. Org. Chem.* **2011**, 2011 (28), 5469-5474; (e) Marvell, E. N.; Chadwick, T.; Caple, G.; Gosink, T.; Zimmer, G., Rates of electrocyclic reactions. Conversion of  $\alpha$ -pyrans to cis-dienones. *The Journal of Organic Chemistry* **1972**, 37 (19), 2992-2997; (f) Childs, R. F.; Hine, K. E.; Hung, F. A., Photoisomerization of protonated cyclohex-2-enones. *Can. J. Chem.* **1979**, 57 (12), 1442-1445; (g) Gaudiana, R. A.; Graf, J. F.; Lillya, C. P., Conformational effects and regiospecificity in conjugated dienone photoisomerization. *The Journal of Organic Chemistry* **1979**, 44 (4), 646-648; (h) Kikuchi, O., A classification of the photochemical electrocyclic reactions of heteroatom conjugated systems. *Tetrahedron Lett.* **1981**, 22 (9), 859-862; (i) Maynard, D. F.; Okamura, W. H., 6. pi.-Electrocyclization of 1-Azatrienes to 1, 2-Dihydropyridines. *The Journal of Organic Chemistry* **1995**, 60 (6), 1763-1771; (j) Krasnaya, Z. A., Dienone  $\rightleftharpoons$  2H-pyran valence isomerization.(Review). *Chemistry of Heterocyclic Compounds* **1999**, 35 (11), 1255-1271.

- 43)** Delbaere, S.; Micheau, J.-C.; Frigoli, M.; Vermeersch, G., Unexpected halogen substituent effects on the complex thermal relaxation of naphthopyrans after UV irradiation. *The Journal of Organic Chemistry* **2005**, *70* (13), 5302-5304.
- 44)** (a) Sun, H.; Waraszkiewicz, S.; Erickson, K.; Finer, J.; Clardy, J., Dictyoxepin and Dictyolene, two new diterpenes from the marine alga *Dictyota acutiloba* (Phaeophyta). *J. Am. Chem. Soc.* **1977**, *99* (10), 3516-3517; (b) Pohnert, G.; Boland, W., The oxylipin chemistry of attraction and defense in brown algae and diatoms. *Natural Product Reports* **2002**, *19* (1), 108-122; (c) Nicolaou, K.; Petasis, N.; Zipkin, R.; Uenishi, J., The endiandric acid cascade. Electrocyclizations in organic synthesis. I. Stepwise, stereocontrolled total synthesis of endiandric acids A and B. *J. Am. Chem. Soc.* **1982**, *104* (20), 5555-5557; (d) Derewacz, D. K.; Covington, B. C.; McLean, J. A.; Bachmann, B. O., Mapping Microbial Response Metabolomes for Induced Natural Product Discovery. *ACS Chemical Biology* **2015**, *10* (9), 1998-2006.
- 45)** Olson, B. S.; Trauner, D., Concise synthesis of (')-smenochromene D. *Synlett* **2005**, (4), 700-702.
- 46)** (a) Fritzsche, J., Note sur les carbures d'hydrogène solides, tirés du goudron de houille. *CR Acad. Sci* **1867**, *69*, 1035-1037; (b) Dürr, H.; Bouas-Laurent, H., *Photochromism: molecules and systems: molecules and systems*. Gulf Professional Publishing: 2003.
- 47)** (a) Crano, J. C.; Guglielmetti, R. J., *Organic Photochromic and Thermochromic Compounds: Volume 2: Physicochemical Studies, Biological Applications, and Thermochromism*. Springer Science & Business Media: 1999; Vol. 2; (b) Tamai, N.; Miyasaka, H., Ultrafast dynamics of photochromic systems. *Chem. Rev.* **2000**, *100* (5),

- 1875-1890; (c) Goudjil, K. In *Photochromic ultraviolet protective shield*, 2000; pp 289-298; (d) Kao, Y.-T.; Zhu, X.; Xu, F.; Min, W., Focal switching of photochromic fluorescent proteins enables multiphoton microscopy with superior image contrast. *Biomedical Optics Express* **2012**, *3* (8), 1955-1963; (e) Ercole, F.; Davis, T. P.; Evans, R. A., Photo-responsive systems and biomaterials: photochromic polymers, light-triggered self-assembly, surface modification, fluorescence modulation and beyond. *Polymer Chemistry* **2010**, *1* (1), 37-54; (f) Higham, L. T.; Scott, J. L.; Strauss, C. R., Closing the cavity: reactive and light switchable dienone-ether macrocycles. *CrystEngComm* **2010**, *12* (10), 2803-2808.
- 48)** Scherer, K. M.; Bisby, R. H.; Botchway, S. W.; Hadfield, J. A.; Parker, A. W., Anticancer phototherapy using activation of E-combretastatins by two-photon-induced isomerization. *BIOMEDO* **2014**, *20* (5), 051004-051004.
- 49)** Brown, G. H., *Photochromism*. Wiley-Interscience: 1971; Vol. 3.
- 50)** Santiago, A.; Becker, R. S., Photochromic fulgides. Spectroscopy and mechanism of photoreactions. *J. Am. Chem. Soc.* **1968**, *90* (14), 3654-3658.
- 51)** Hovey, R. J.; Chu, N. Y.; Piusz, P. G.; Fuchsman, C. H., Photochromic compounds. Google Patents: 1982.
- 52)** Wolak, M. A.; Gillespie, N. B.; Thomas, C. J.; Birge, R. R.; Lees, W. J., Optical properties of photochromic fluorinated indolylfulgides. *Journal of Photochemistry and Photobiology A: Chemistry* **2001**, *144* (2), 83-91.
- 53)** Gupta, P.; Sharma, U.; Schulz, T. C.; Sherrer, E. S.; McLean, A. B.; Robins, A. J.; West, L. M., Bioactive Diterpenoid Containing a Reversible “Spring-Loaded” (E,Z)-Dieneone Michael Acceptor. *Org. Lett.* **2011**, *13* (15), 3920-3923.

- 54)** (a) Mootoo, B.; Ramsewak, R.; Sharma, R.; Tinto, W.; Lough, A.; McLean, S.; Reynolds, W.; Yang, J.-P.; Yu, M., Further briareolate esters and briareolides from the Caribbean gorgonian octocoral *Briareum asbestinum*. *Tetrahedron* **1996**, 52 (30), 9953-9962; (b) Maharaj, D.; Mootoo, B. S.; Lough, A. J.; McLean, S.; Reynolds, W. F.; Tinto, W. F., Methyl briareolate, the first briarein diterpene containing a C-19 methyl ester. *Tetrahedron Lett.* **1992**, 33 (50), 7761-7764.
- 55)** Crombie, L.; Redshaw, S. D.; Whiting, D. A., The mechanism of intramolecular 'citrin' bicyclisation of chromens: stereochemistry of a forward (H<sup>+</sup> catalysed) and a related reverse (thermal) process. *J. Chem. Soc., Chem. Commun.* **1979**, (14), 630-631.
- 56)** (a) Feliu, A. L.; Seltzer, S., Synthesis and interconversion of the four isomeric 6-oxo-2, 4-heptadienoic acids. *The Journal of Organic Chemistry* **1985**, 50 (4), 447-451; (b) Seltzer, S.; Lin, M., Maleylacetone cis-trans-isomerase. Mechanism of the interaction of coenzyme glutathione and substrate maleylacetone in the presence and absence of enzyme. *J. Am. Chem. Soc.* **1979**, 101 (11), 3091-3097.
- 57)** (a) Rodríguez, A. D.; Ramírez, C.; Cobar, O. M., Briareins C-L, 10 New Briarane Diterpenoids from the Common Caribbean Gorgonian *Briareum asbestinum*1. *J. Nat. Prod.* **1996**, 59 (1), 15-22; (b) Rodríguez, A. D.; Cobar, O. M.; Martínez, N., Isolation and Structures of Sixteen New Asbestinin Diterpenes from the Caribbean Gorgonian *Briareum asbestinum*. *Journal of Natural Products* **1994**, 57 (12), 1638-1655; (c) Rodríguez, A. D.; Cobar, O. M., Structures and bioactivities of new asbestinin diterpenoids from the caribbean gorgonian octocoral *briareum asbestinum*. *Tetrahedron* **1993**, 49 (2), 319-328.

- 58)** Olson, B. S.; Trauner, D., Concise Synthesis of ( $\pm$ )-Smenochromene D (= Likonide B). *Synlett* **2005**, 2005 (04), 700-702.
- 59)** (a) Methot, J. L.; Roush, W. R., Nucleophilic Phosphine Organocatalysis. *Adv. Synth. Catal.* **2004**, 346 (9-10), 1035-1050; (b) Feliu, A. L.; Smith, K. J.; Seltzer, S., Unique, one-step, double isomerization (2E,4Z  $\rightarrow$  2Z,4E) of 6-oxo-2,4-heptadienoic acid catalyzed by maleylacetone cis-trans isomerase. *J. Am. Chem. Soc.* **1984**, 106 (10), 3046-3047; (c) Marvell, E. N.; Caple, G.; Gosink, T. A.; Zimmer, G., Valence isomerization of a cis-dienone to an  $\alpha$ -pyran. *J. Am. Chem. Soc.* **1966**, 88 (3), 619-620.
- 60)** (a) Swayambunathan, V.; Lim, E., Torsional dynamics of 9-carbonyl substituted anthracenes. *The Journal of Physical Chemistry* **1985**, 89 (19), 3960-3962; (b) Wang, Y.; Liu, Z.; Xu, Y.; Zhang, B., The geometrical change and intramolecular energy transfer upon S<sub>1</sub> $\leftarrow$ S<sub>0</sub> excitation in cyclopentanone. *The Journal of Chemical Physics* **2015**, 143 (6), 064304; (c) Turro, N. J., *Modern molecular photochemistry*. University science books: 1991.
- 61)** (a) Bayani Uttara, Ajay V. Singh, Paolo Zamboni, and R.T Mahajan<sup>1</sup>, Oxidative Stress and Neurodegenerative Diseases: A Review of Upstream and Downstream Antioxidant Therapeutic Options. *Current neuropharmacology* **2009**, 7 (1), 65-74; (b) Lin, M. T.; Beal, M. F., Mitochondrial dysfunction and oxidative stress in neurodegenerative diseases. *Nature* **2006**, 443 (7113), 787-795; (c) Barnham, K. J.; Masters, C. L.; Bush, A. I., Neurodegenerative diseases and oxidative stress. *Nature Reviews Drug Discovery* **2004**, 3 (3), 205-214; (d) Baynes, J. W., Role of Oxidative Stress in Development of Complications in Diabetes. *Diabetes* **1991**, 40 (4), 405-412; (e)

Cheeseman, K. H., Mechanisms and effects of lipid peroxidation. *Molecular Aspects of Medicine* **1993**, 14 (3), 191-197; (f) Berlett, B. S.; Stadtman, E. R., Protein Oxidation in Aging, Disease, and Oxidative Stress. *J. Biol. Chem.* **1997**, 272 (33), 20313-20316; (g) Yakes, F. M.; Van Houten, B., Mitochondrial DNA damage is more extensive and persists longer than nuclear DNA damage in human cells following oxidative stress. *Proceedings of the National Academy of Sciences* **1997**, 94 (2), 514-519.

**62)** (a) Soobrattee, M. A.; Neergheen, V. S.; Luximon-Ramma, A.; Aruoma, O. I.; Bahorun, T., Phenolics as potential antioxidant therapeutic agents: mechanism and actions. *Mutation Research/Fundamental and Molecular Mechanisms of Mutagenesis* **2005**, 579 (1), 200-213; (b) Delanty, N.; Dichter, M. A., Antioxidant therapy in neurologic disease. *Archives of neurology* **2000**, 57 (9), 1265-1270; (c) Cuzzocrea, S.; Riley, D. P.; Caputi, A. P.; Salvemini, D., Antioxidant therapy: a new pharmacological approach in shock, inflammation, and ischemia/reperfusion injury. *Pharmacological reviews* **2001**, 53 (1), 135-159.

**63)** (a) Pulz, O.; Gross, W., Valuable products from biotechnology of microalgae. *Appl. Microbiol. Biotechnol.* **2004**, 65 (6), 635-648; (b) Wijffels, R. H., Potential of sponges and microalgae for marine biotechnology. *Trends Biotechnol.* **2008**, 26 (1), 26-31.

**64)** Takamatsu, S.; Hodges, T. W.; Rajbhandari, I.; Gerwick, W. H.; Hamann, M. T.; Nagle, D. G., Marine Natural Products as Novel Antioxidant Prototypes. *Journal of Natural Products* **2003**, 66 (5), 605-608.



- 65)** Benzie, I. F. F.; Strain, J. J., The Ferric Reducing Ability of Plasma (FRAP) as a Measure of “Antioxidant Power”: The FRAP Assay. *Anal. Biochem.* **1996**, 239 (1), 70-76.
- 66)** (a) Benzie, I. F.; Strain, J., The ferric reducing ability of plasma (FRAP) as a measure of “antioxidant power”: the FRAP assay. *Anal. Biochem.* **1996**, 239 (1), 70-76; (b) Thaipong, K.; Boonprakob, U.; Crosby, K.; Cisneros-Zevallos, L.; Byrne, D. H., Comparison of ABTS, DPPH, FRAP, and ORAC assays for estimating antioxidant activity from guava fruit extracts. *Journal of food composition and analysis* **2006**, 19 (6), 669-675.
- 67)** Cheeseman, K. H.; Slater, T. F., An introduction to free radical biochemistry. *British Medical Bulletin* **1993**, 49 (3), 481-493.
- 68)** Cadenas, E.; Davies, K. J., Mitochondrial free radical generation, oxidative stress, and aging. *Free Radical Biol. Med.* **2000**, 29 (3), 222-230.
- 69)** Weinberg, F.; Hamanaka, R.; Wheaton, W. W.; Weinberg, S.; Joseph, J.; Lopez, M.; Kalyanaraman, B.; Mutlu, G. M.; Budinger, G. S.; Chandel, N. S., Mitochondrial metabolism and ROS generation are essential for Kras-mediated tumorigenicity. *Proceedings of the National Academy of Sciences* **2010**, 107 (19), 8788-8793.
- 70)** (a) Massaad, C. A.; Klann, E., Reactive Oxygen Species in the Regulation of Synaptic Plasticity and Memory. *Antioxidants & Redox Signaling* **2011**, 14 (10), 2013-2054; (b) Gottschalk, W.; Pozzo-Miller, L. D.; Figuero, A.; Lu, B., Presynaptic Modulation of Synaptic Transmission and Plasticity by Brain-Derived Neurotrophic Factor in the Developing Hippocampus. *The Journal of Neuroscience* **1998**, 18 (17), 6830-6839; (c) Apel, K.; Hirt, H., REACTIVE OXYGEN SPECIES: Metabolism,

Oxidative Stress, and Signal Transduction. *Annual Review of Plant Biology* **2004**, 55 (1), 373-399; (d) Halliwell, B., Reactive oxygen species in living systems: Source, biochemistry, and role in human disease. *The American Journal of Medicine* **1991**, 91 (3, Supplement 3), S14-S22.

**71)** (a) Otani, H., Reactive Oxygen Species as Mediators of Signal Transduction in Ischemic Preconditioning. *Antioxidants & Redox Signaling* **2004**, 6 (2), 449-469; (b) Glantz, L.; Avramovich, A.; Trembovler, V.; Gurvitz, V.; Kohen, R.; Eidelman, L. A.; Shohami, E., Ischemic preconditioning increases antioxidants in the brain and peripheral organs after cerebral ischemia. *Experimental Neurology* **2005**, 192 (1), 117-124; (c) Halliwell, B., Reactive Oxygen Species and the Central Nervous System. In *Free Radicals in the Brain*, Packer, L.; Prilipko, L.; Christen, Y., Eds. Springer Berlin Heidelberg: 1992; pp 21-40.

**72)** (a) Halliwell, B., Free radicals and other reactive species in disease. *eLS* **2005**; (b) Metodiewa, D.; Koška, C., Reactive oxygen species and reactive nitrogen species: relevance to cyto (neuro) toxic events and neurologic disorders. An overview. *Neurotoxicity research* **1999**, 1 (3), 197-233; (c) Hensley, K.; Carney, J.; Mattson, M.; Aksenova, M.; Harris, M.; Wu, J.; Floyd, R.; Butterfield, D., A model for beta-amyloid aggregation and neurotoxicity based on free radical generation by the peptide: relevance to Alzheimer disease. *Proceedings of the National Academy of Sciences* **1994**, 91 (8), 3270-3274.

**73)** Uttara, B.; Singh, A. V.; Zamboni, P.; Mahajan, R., Oxidative stress and neurodegenerative diseases: a review of upstream and downstream antioxidant therapeutic options. *Current Neuropharmacology* **2009**, 7 (1), 65.

- 74)** (a) Koppula, S.; Kumar, H.; More, S. V.; Kim, B. W.; Kim, I. S.; Choi, D.-K., Recent advances on the neuroprotective potential of antioxidants in experimental models of Parkinson's disease. *International journal of molecular sciences* **2012**, *13* (8), 10608-10629; (b) Steinberg, D.; Witztum, J. L., Is the oxidative modification hypothesis relevant to human atherosclerosis? Do the antioxidant trials conducted to date refute the hypothesis? *Circulation* **2002**, *105* (17), 2107-2111.
- 75)** Kohen, R.; Nyska, A., Invited review: Oxidation of biological systems: oxidative stress phenomena, antioxidants, redox reactions, and methods for their quantification. *Toxicologic pathology* **2002**, *30* (6), 620-650.
- 76)** Briganti, S.; Picardo, M., Antioxidant activity, lipid peroxidation and skin diseases. What's new. *Journal of the European Academy of Dermatology and Venereology* **2003**, *17* (6), 663-669.
- 77)** (a) Itoh, K.; Chiba, T.; Takahashi, S.; Ishii, T.; Igarashi, K.; Katoh, Y.; Oyake, T.; Hayashi, N.; Satoh, K.; Hatayama, I., An Nrf2/small Maf heterodimer mediates the induction of phase II detoxifying enzyme genes through antioxidant response elements. *Biochem. Biophys. Res. Commun.* **1997**, *236* (2), 313-322; (b) Jaiswal, A. K., Nrf2 signaling in coordinated activation of antioxidant gene expression. *Free Radical Biol. Med.* **2004**, *36* (10), 1199-1207; (c) Halliwell, B., Antioxidant defence mechanisms: From the beginning to the end (of the beginning). *Free Radical Res.* **1999**, *31* (4), 261-272.
- 78)** Larson, R., Antioxidant Mechanisms of Secondary Natural Products. In *Oxidative Stress and Antioxidant Defenses in Biology*, Ahmad, S., Ed. Springer US: 1995; pp 210-237.

- 79)** Giordano, F. J., Oxygen, oxidative stress, hypoxia, and heart failure. *The Journal of clinical investigation* **2005**, *115* (115 (3)), 500-508.
- 80)** (a) AshokKumar, T., Antioxidants: New-generation therapeutic base for treatment of polygenic disorders. *Current science* **2004**, *86*; (b) Moosmann, B.; Behl, C., Antioxidants as treatment for neurodegenerative disorders. *Expert opinion on investigational drugs* **2002**, *11* (10), 1407-1435; (c) Tiwari, A. K., Imbalance in antioxidant defence and human diseases: Multiple approach of natural antioxidants therapy. *CURRENT SCIENCE-BANGALORE*- **2001**, *81* (9), 1179-1187; (d) Floyd, R. A., Antioxidants, oxidative stress, and degenerative neurological disorders. *Experimental Biology and Medicine* **1999**, *222* (3), 236-245.
- 81)** (a) Zhao, C. R.; Gao, Z. H.; Qu, X. J., Nrf2–ARE signaling pathway and natural products for cancer chemoprevention. *Cancer epidemiology* **2010**, *34* (5), 523-533; (b) Quitschke, W. W.; Steinhauß, N.; Rooney, J., The effect of cyclodextrin-solubilized curcuminoids on amyloid plaques in Alzheimer transgenic mice: brain uptake and metabolism after intravenous and subcutaneous injection. *Alzheimers Res Ther* **2013**, *5* (2), 16; (c) Hirohata, M.; Hasegawa, K.; Tsutsumi-Yasuhara, S.; Ohhashi, Y.; Ookoshi, T.; Ono, K.; Yamada, M.; Naiki, H., The anti-amyloidogenic effect is exerted against Alzheimer's  $\beta$ -amyloid fibrils in vitro by preferential and reversible binding of flavonoids to the amyloid fibril structure. *Biochemistry* **2007**, *46* (7), 1888-1899.
- 82)** (a) SHL Kim, D.; Y Kim, J.; Han, Y., Curcuminoids in neurodegenerative diseases. *Recent patents on CNS drug discovery* **2012**, *7* (3), 184-204; (b) Dragicevic, N.; Smith, A.; Lin, X.; Yuan, F.; Copes, N.; Delic, V.; Tan, J.; Cao, C.; Shytle, R. D.; Bradshaw, P. C., Green tea epigallocatechin-3-gallate (EGCG) and other flavonoids

reduce Alzheimer's amyloid-induced mitochondrial dysfunction. *Journal of Alzheimer's Disease* **2011**, 26 (3), 507; (c) Rezai-Zadeh, K.; Douglas Shytle, R.; Bai, Y.; Tian, J.; Hou, H.; Mori, T.; Zeng, J.; Obregon, D.; Town, T.; Tan, J., Flavonoid-mediated presenilin-1 phosphorylation reduces Alzheimer's disease  $\beta$ -amyloid production. *Journal of cellular and molecular medicine* **2009**, 13 (3), 574-588; (d) Yang, F.; Lim, G. P.; Begum, A. N.; Ubeda, O. J.; Simmons, M. R.; Ambegaokar, S. S.; Chen, P. P.; Kaye, R.; Glabe, C. G.; Frautschy, S. A., Curcumin inhibits formation of amyloid  $\beta$  oligomers and fibrils, binds plaques, and reduces amyloid in vivo. *J. Biol. Chem.* **2005**, 280 (7), 5892-5901; (e) Onozuka, H.; Nakajima, A.; Matsuzaki, K.; Shin, R.-W.; Ogino, K.; Saigusa, D.; Tetsu, N.; Yokosuka, A.; Sashida, Y.; Mimaki, Y., Nobiletin, a citrus flavonoid, improves memory impairment and A $\beta$  pathology in a transgenic mouse model of Alzheimer's disease. *J. Pharmacol. Exp. Ther.* **2008**, 326 (3), 739-744; (f) Lim, G. P.; Chu, T.; Yang, F.; Beech, W.; Frautschy, S. A.; Cole, G. M., The curry spice curcumin reduces oxidative damage and amyloid pathology in an Alzheimer transgenic mouse. *The Journal of neuroscience* **2001**, 21 (21), 8370-8377.

**83)** (a) Praticò, D.; Uryu, K.; Leight, S.; Trojanowski, J. Q.; Lee, V. M.-Y., Increased lipid peroxidation precedes amyloid plaque formation in an animal model of Alzheimer amyloidosis. *The Journal of neuroscience* **2001**, 21 (12), 4183-4187; (b) Varadarajan, S.; Yatin, S.; Aksenova, M.; Butterfield, D. A., Review: Alzheimer's amyloid  $\beta$ -peptide-associated free radical oxidative stress and neurotoxicity. *Journal of structural biology* **2000**, 130 (2), 184-208.

**84)** (a) Sano, M.; Ernesto, C.; Thomas, R. G.; Klauber, M. R.; Schafer, K.; Grundman, M.; Woodbury, P.; Growdon, J.; Cotman, C. W.; Pfeiffer, E.; Schneider, L.

S.; Thal, L. J., A Controlled Trial of Selegiline, Alpha-Tocopherol, or Both as Treatment for Alzheimer's Disease. *New England Journal of Medicine* **1997**, 336 (17), 1216-1222; (b) Petersen, R. C.; Thomas, R. G.; Grundman, M.; Bennett, D.; Doody, R.; Ferris, S.; Galasko, D.; Jin, S.; Kaye, J.; Levey, A.; Pfeiffer, E.; Sano, M.; van Dyck, C. H.; Thal, L. J., Vitamin E and Donepezil for the Treatment of Mild Cognitive Impairment. *New England Journal of Medicine* **2005**, 352 (23), 2379-2388.

**85)** (a) Sinha, K.; Chaudhary, G.; Gupta, Y. K., Protective effect of resveratrol against oxidative stress in middle cerebral artery occlusion model of stroke in rats. *Life Sci.* **2002**, 71 (6), 655-665; (b) Sharma, M.; Gupta, Y., Chronic treatment with trans resveratrol prevents intracerebroventricular streptozotocin induced cognitive impairment and oxidative stress in rats. *Life Sci.* **2002**, 71 (21), 2489-2498; (c) Ngoungoure, V. L. N.; Schluesener, J.; Moundipa, P. F.; Schluesener, H., Natural polyphenols binding to amyloid: A broad class of compounds to treat different human amyloid diseases. *Molecular nutrition & food research* **2015**, 59 (1), 8-20.

**86)** (a) Simonian, N.; Coyle, J., Oxidative stress in neurodegenerative diseases. *Annu. Rev. Pharmacool. Toxicol.* **1996**, 36 (1), 83-106; (b) Halliwell, B.; Gutteridge, J. M., *Free radicals in biology and medicine*. Oxford university press Oxford: 1999; Vol. 3; (c) Emerit, J.; Edeas, M.; Bricaire, F., Neurodegenerative diseases and oxidative stress. *Biomedicine & pharmacotherapy* **2004**, 58 (1), 39-46.

**87)** Thies, W.; Bleiler, L., 2011 Alzheimer's disease facts and figures. *Alzheimer's & Dementia: The Journal of the Alzheimer's Association* **2011**, 7 (2), 208-244.

**88)** (a) Barnes, D. E.; Yaffe, K., The projected effect of risk factor reduction on Alzheimer's disease prevalence. *The Lancet Neurology* **2011**, 10 (9), 819-828; (b)

Ramírez, B. G.; Blázquez, C.; del Pulgar, T. G.; Guzmán, M.; de Ceballos, M. L., Prevention of Alzheimer's disease pathology by cannabinoids: neuroprotection mediated by blockade of microglial activation. *The Journal of Neuroscience* **2005**, 25 (8), 1904-1913.

**89)** Lucie Cahlí'kova', K. i. M. k., Nina Benes 'ova', Jakub Chlebek, Anna Hos 't 'a'lkova' and Lubom'ır Opletal, *Natural Compounds (Small Molecules) as Potential and Real Drugs of Alzheimer's Disease: A Critical Review*. elsevier: Vol. 1.

**90)** Clyburn, L. D.; Stones, M. J.; Hadjistavropoulos, T.; Tuokko, H., Predicting caregiver burden and depression in Alzheimer's disease. *Journals Of Gerontology Series B* **2000**, 55 (1), S2-S13.

**91)** (a) Karsten, U.; Franklin, L. A.; Lüning, K.; Wiencke, C., Natural ultraviolet radiation and photosynthetically active radiation induce formation of mycosporine-like amino acids in the marine macroalga *Chondrus crispus* (Rhodophyta). *Planta* **1998**, 205 (2), 257-262; (b) Sunda, W.; Kieber, D.; Kiene, R.; Huntsman, S., An antioxidant function for DMSP and DMS in marine algae. *Nature* **2002**, 418 (6895), 317-320.

**92)** Benzie, I. F., Evolution of antioxidant defence mechanisms. *European journal of nutrition* **2000**, 39 (2), 53-61.

**93)** Dunlap, W.; Llewellyn, L.; Doyle, J.; Yamamoto, Y., A Microtiter Plate Assay for Screening Antioxidant Activity in Extracts of Marine Organisms. *Mar. Biotechnol.* **2003**, 5 (3), 294-301.

**94)** De la Coba, F.; Aguilera, J.; Figueroa, F.; De Gálvez, M.; Herrera, E., Antioxidant activity of mycosporine-like amino acids isolated from three red macroalgae and one marine lichen. *J. Appl. Phycol.* **2009**, 21 (2), 161-169.

- 95)** (a) Dunlap, W. C.; Shick, J. M., REVIEW—ULTRAVIOLET RADIATION-ABSORBING MYCOSPORINE-LIKE AMINO ACIDS IN CORAL REEF ORGANISMS: A BIOCHEMICAL AND ENVIRONMENTAL PERSPECTIVE. *Journal of Phycology* **1998**, *34* (3), 418-430; (b) Townsend, B. E. Identification of marine antioxidants. University of Georgia, 2008; (c) Lysek, N.; Kinscherf, R.; Claus, R.; Lindel, T., L-5-Hydroxytryptophan: Antioxidant and Anti-Apoptotic Principle of the Intertidal Sponge *Hymeniacidon heliophila*. *Zeitschrift für Naturforschung C* **2003**, *58* (7-8), 568-572.
- 96)** Niki, E., Assessment of antioxidant capacity in vitro and in vivo. *Free Radical Biol. Med.* **2010**, *49* (4), 503-515.
- 97)** (a) Schins, R. P.; Derhaag, T. J.; De Jong, J.; Bast, A.; Borm, P. J., Serum total radical-trapping antioxidant parameter (TRAP) in coal workers. *Clin. Chem.* **1994**, *40* (7), 1470-1472; (b) Wootton-Beard, P. C.; Moran, A.; Ryan, L., Stability of the total antioxidant capacity and total polyphenol content of 23 commercially available vegetable juices before and after in vitro digestion measured by FRAP, DPPH, ABTS and Folin–Ciocalteu methods. *Food Research International* **2011**, *44* (1), 217-224.
- 98)** (a) Prior, R. L.; Wu, X.; Schaich, K., Standardized methods for the determination of antioxidant capacity and phenolics in foods and dietary supplements. *J. Agric. Food. Chem.* **2005**, *53* (10), 4290-4302; (b) Whitehead, T.; Thorpe, G.; Maxwell, S., Enhanced chemiluminescent assay for antioxidant capacity in biological fluids. *Anal. Chim. Acta* **1992**, *266* (2), 265-277.
- 99)** Cao, G.; Alessio, H. M.; Cutler, R. G., Oxygen-radical absorbance capacity assay for antioxidants. *Free Radical Biol. Med.* **1993**, *14* (3), 303-311.



- 100)** van den Berg, R.; Haenen, G. R.; van den Berg, H.; Bast, A., Applicability of an improved Trolox equivalent antioxidant capacity (TEAC) assay for evaluation of antioxidant capacity measurements of mixtures. *Food Chem.* **1999**, *66* (4), 511-517.
- 101)** Roy, S.; Plowman, S.; Rotblat, B.; Prior, I. A.; Muncke, C.; Grainger, S.; Parton, R. G.; Henis, Y. I.; Kloog, Y.; Hancock, J. F., Individual palmitoyl residues serve distinct roles in H-ras trafficking, microlocalization, and signaling. *Molecular and cellular biology* **2005**, *25* (15), 6722-6733.
- 102)** (a) Mydlarz, L. D.; Jacobs, R. S., An inducible release of reactive oxygen radicals in four species of gorgonian corals. *Marine and Freshwater Behaviour and Physiology* **2006**, *39* (2), 143-152; (b) Mydlarz, L. D.; Jacobs, R. S., Comparison of an inducible oxidative burst in free-living and symbiotic dinoflagellates reveals properties of the pseudopterosins. *Phytochemistry* **2004**, *65* (24), 3231-3241.
- 103)** Slemmer, J. E.; Shacka, J. J.; Sweeney, M.; Weber, J. T., Antioxidants and free radical scavengers for the treatment of stroke, traumatic brain injury and aging. *Current medicinal chemistry* **2008**, *15* (4), 404-414.
- 104)** (a) Look, S. A.; Fenical, W.; Jacobs, R. S.; Clardy, J., The pseudopterosins: anti-inflammatory and analgesic natural products from the sea whip *Pseudopterogorgia elisabethae*. *Proceedings of the National Academy of Sciences* **1986**, *83* (17), 6238-6240; (b) Look, S. A.; Fenical, W.; Matsumoto, G. K.; Clardy, J., The pseudopterosins: a new class of antiinflammatory and analgesic diterpene pentosides from the marine sea whip *Pseudopterogorgia elisabethae* (Octocorallia). *The Journal of Organic Chemistry* **1986**, *51* (26), 5140-5145; (c) Fenical, W., Marine soft corals of the genus *Pseudopterogorgia*: a resource for novel anti-inflammatory diterpenoids. *J. Nat. Prod.* **1987**, *50* (6), 1001-1008;

- (d) Roussis, V.; Wu, Z.; Fenical, W.; Strobel, S. A.; Van Duyne, G. D.; Clardy, J., New anti-inflammatory pseudopterosins from the marine octocoral *Pseudoptero-gorgia elisabethae*. *The Journal of Organic Chemistry* **1990**, *55* (16), 4916-4922; (e) Dayan, N.; Grove, G.; Sivalenka, R., Anti-inflammatory activity of Pseudopterosins by laser doppler blood flow evaluation. *International Journal of Cosmetic Science* **2009**, *31* (6), 480-480; (f) Ata, A.; Kerr, R. G.; Moya, C. E.; Jacobs, R. S., Identification of anti-inflammatory diterpenes from the marine gorgonian *Pseudoptero-gorgia elisabethae*. *Tetrahedron* **2003**, *59* (23), 4215-4222.
- 105)** Rodríguez, I. I.; Shi, Y.-P.; García, O. J.; Rodríguez, A. D.; Mayer, A. M. S.; Sánchez, J. A.; Ortega-Barria, E.; González, J., New Pseudopterosin and seco-Pseudopterosin Diterpene Glycosides from Two Colombian Isolates of *Pseudoptero-gorgia elisabethae* and Their Diverse Biological Activities. *J. Nat. Prod.* **2004**, *67* (10), 1672-1680.
- 106)** (a) Ata, A.; Win, H. Y.; Holt, D.; Holloway, P.; Segstro, E. P.; Jayatilake, G. S., New Antibacterial Diterpenes from *Pseudoptero-gorgia elisabethae*. *Helv. Chim. Acta* **2004**, *87* (5), 1090-1098; (b) Mayer, A. M. S.; Glaser, K. B.; Cuevas, C.; Jacobs, R. S.; Kem, W.; Little, R. D.; McIntosh, J. M.; Newman, D. J.; Potts, B. C.; Shuster, D. E., The odyssey of marine pharmaceuticals: a current pipeline perspective. *Trends in Pharmacological Sciences* **2010**, *31* (6), 255-265.
- 107)** Correa, H.; Aristizabal, F.; Duque, C.; Kerr, R., Cytotoxic and antimicrobial activity of pseudopterosins and seco-pseudopterosins isolated from the octocoral *Pseudoptero-gorgia elisabethae* of San Andres and Providencia Islands (Southwest Caribbean Sea). *Marine Drugs* **2011**, *9* (3), 334-344.

- 108)** (a) Newman, D. J.; Cragg, G. M., Marine Natural Products and Related Compounds in Clinical and Advanced Preclinical Trials†. *J. Nat. Prod.* **2004**, 67 (8), 1216-1238; (b) Moya, C. E.; Jacobs, R. S., Pseudopterosin A inhibits phagocytosis and alters intracellular calcium turnover in a pertussis toxin sensitive site in *Tetrahymena thermophila*. *Comparative Biochemistry and Physiology Part C: Toxicology & Pharmacology* **2006**, 143 (4), 436-443.
- 109)** (a) Haefner, B., Drugs from the deep: marine natural products as drug candidates. *Drug Discovery Today* **2003**, 8 (12), 536-544; (b) Newman, D. J.; Cragg, G. M., Marine natural products and related compounds in clinical and advanced preclinical trials. *J. Nat. Prod.* **2004**, 67 (8), 1216-1238.
- 110)** (a) Thornton, R. S.; Kerr, R. G., Induction of pseudopterosin biosynthesis in the gorgonian *Pseudopteroorgia elisabethae*. *J. Chem. Ecol.* **2002**, 28 (10), 2083-2090; (b) Harrowven, D. C.; Tyte, M. J., Total synthesis of (±)-pseudopterosin A–F and K–L aglycone. *Tetrahedron Lett.* **2004**, 45 (10), 2089-2091; (c) Pomponi, S. A., The bioprocess–technological potential of the sea. *J. Biotechnol.* **1999**, 70 (1), 5-13.
- 111)** Look, S. A.; Fenical, W., The seco-pseudopterosins, new anti-inflammatory diterpene-glycosides from a caribbean gorgonian octocoral of the genus *pseudopteroorgia*. *Tetrahedron* **1987**, 43 (15), 3363-3370.
- 112)** Mayer, A. M.; Rodríguez, A. D.; Berlinck, R. G.; Hamann, M. T., Marine pharmacology in 2003–4: Marine compounds with anthelmintic antibacterial, anticoagulant, antifungal, anti-inflammatory, antimalarial, antiplatelet, antiprotozoal, antituberculosis, and antiviral activities; affecting the cardiovascular, immune and nervous systems, and other miscellaneous mechanisms of action. *Comparative*

*Biochemistry and Physiology Part C: Toxicology & Pharmacology* **2007**, 145 (4), 553-581.

**113)** Santiago-Vázquez, L. Z.; Brück, T. B.; Brück, W. M.; Duque-Alarcon, A. P.; McCarthy, P. J.; Kerr, R. G., The diversity of the bacterial communities associated with the azooxanthellate hexacoral *Cirrhipathes lutkeni*. *The ISME journal* **2007**, 1 (7), 654-659.

**114)** Pretsch, E.; Bühlmann, P.; Affolter, C.; Pretsch, E.; Bhühlmann, P.; Affolter, C., *Structure determination of organic compounds*. Springer: 2009; Vol. 13.

**115)** Gupta, P.; Yadav, D. K.; Siripurapu, K. B.; Palit, G.; Maurya, R., Constituents of *Ocimum sanctum* with Antistress Activity §. *J. Nat. Prod.* **2007**, 70 (9), 1410-1416.

**116)** Dai, J. Q.; Zhu, Q. X.; Zhao, C. Y.; Yang, L.; Li, Y., Glyceroglycolipids from *Serratula strangulata*. *Phytochemistry* **2001**, 58 (8), 1305-1309.

**117)** (a) He, Z.-D.; Ma, C.-Y.; Tan, G. T.; Sydara, K.; Tamez, P.; Southavong, B.; Bouamanivong, S.; Soejarto, D. D.; Pezzuto, J. M.; Fong, H. H., Rourinoside and rouremin, antimalarial constituents from *Rourea minor*. *Phytochemistry* **2006**, 67 (13), 1378-1384; (b) Andersen, R. J.; Taglialatela-Scafati, O., Avrainvilloside, a 6-deoxy-6-aminoglucoglycerolipid from the green alga *Avrainvillea nigricans*. *J. Nat. Prod.* **2005**, 68 (9), 1428-1430.

**118)** (a) Cantillo-Ciau, Z.; Moo-Puc, R.; Quijano, L.; Freile-Pelegrín, Y., The tropical brown alga *Lobophora variegata*: A source of antiprotozoal compounds. *Marine Drugs* **2010**, 8 (4), 1292-1304; (b) Plouguerné, E.; da Gama, B. A.; Pereira, R. C.; Barreto-Bergter, E., Glycolipids from seaweeds and their potential biotechnological applications. *Frontiers in cellular and infection microbiology* **2014**, 4.

- 119)** Kocienski, P. J.; Pontiroli, A.; Qun, L., Enantiospecific syntheses of pseudopterosin aglycones. Part 2. Synthesis of pseudopterosin K-L aglycone and pseudopterosin A-F aglycone via a B[ $\rightarrow$ ]BA[ $\rightarrow$ ]BAC annulation strategy. *J. Chem. Soc., Perkin Trans. I* **2001**, (19), 2356-2366.
- 120)** Berru , F.; McCulloch, M. W. B.; Kerr, R. G., Marine diterpene glycosides. *Biorg. Med. Chem.* **2011**, 19 (22), 6702-6719.
- 121)** Marchetti, M.; Resnick, L.; Gamliel, E.; Kesaraju, S.; Weissbach, H.; Binner, D., Sulindac enhances the killing of cancer cells exposed to oxidative stress. *PLoS ONE* **2009**, 4 (6), e5804.
- 122)** Rodr guez, I. I.; Shi, Y.-P.; Garc a, O. J.; Rodr guez, A. D.; Mayer, A. M.; S nchez, J. A.; Ortega-Barria, E.; Gonz lez, J., New Pseudopterosin and s eco-Pseudopterosin Diterpene Glycosides from Two Colombian Isolates of Pseudopterogorgia elisabethae and Their Diverse Biological Activities. *J. Nat. Prod.* **2004**, 67 (10), 1672-1680.
- 123)** (a) Sugimoto, K.; Sato, N.; Tsuzuki, M., Utilization of a chloroplast membrane sulfolipid as a major internal sulfur source for protein synthesis in the early phase of sulfur starvation in *Chlamydomonas reinhardtii*. *FEBS Lett.* **2007**, 581 (23), 4519-4522;  
(b) Honke, K., Biosynthesis and biological function of sulfoglycolipids. *Proceedings of the Japan Academy. Series B, Physical and Biological Sciences* **2013**, 89 (4), 129-138.
- 124)** Tang, H.-f.; Yi, Y.-h.; Yao, X.-s., Studies on the Chemical Constituents from Marine Brown Algae *Sargassum carpophyllum*. *Chinese Journal of Marine Drugs* **2002**, 21 (6), 11-15.

**125)** Banskota, A. H.; Stefanova, R.; Sperker, S.; Lall, S. P.; Craigie, J. S.; Hafting, J. T.; Critchley, A. T., Polar lipids from the marine macroalga *Palmaria palmata* inhibit lipopolysaccharide-induced nitric oxide production in RAW264.7 macrophage cells. *Phytochemistry* **2014**, *101*, 101-108.

Natural Product Studies of Marine Organisms from the Western Atlantic Ocean

by

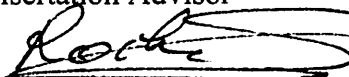
Andrew James Hall

This dissertation was prepared under the direction of the candidate's dissertation advisor, Dr. Lyndon West, Department of Chemistry and Biochemistry, and has been approved by the members of his supervisory committee. It was submitted to the faculty of the Charles E. Schmidt College of Science and was accepted in partial fulfillment of the requirements for the degree of Doctor of Philosophy.

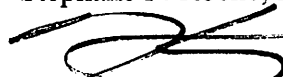
SUPERVISORY COMMITTEE:



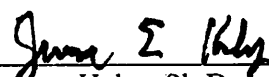
Lyndon West, Ph.D.  
Dissertation Advisor



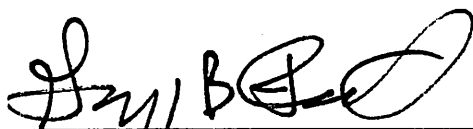
Stéphane P. Roche, Ph.D.



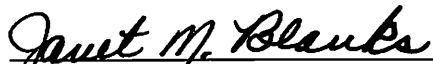
Ken Dawson-Scully, Ph.D.



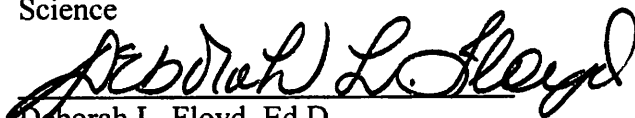
Jerome Haky, Ph.D.



Gregg B. Fields, Ph.D.  
Chair, Department of Chemistry and  
Biochemistry



Janet M. Blanks, Ph.D.  
Interim Dean, Charles E. Schmidt College of  
Science



Deborah L. Floyd, Ed.D.  
Dean, Graduate College

07/20/2016  
Date